GRADO EN INGENIERÍA EN TECNOLOGÍAS INDUSTRIALES

TRABAJO FIN DE GRADO

CONTROL AND SIMULATIONS OF A POWER SUPPLY FOR NANOSATELLITES

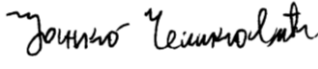Autor: Alejandro Redondo Lázaro

Supervisor: Janko Čeliković

Madrid

Declaro, bajo mi responsabilidad, que el Proyecto presentado con el título

"CONTROL AND SIMULATIONS OF A POWER SUPPLY FOR NANOSATELLITES"

en la ETS de Ingeniería - ICAI de la Universidad Pontificia Comillas en el

curso académico 2019/2020 es de mi autoría, original e inédito y

no ha sido presentado con anterioridad a otros efectos.

El Proyecto no es plagio de otro, ni total ni parcialmente y la información que ha sido

tomada de otros documentos está debidamente referenciada.

Fdo.:   Fecha: 24/ 08/ 2020

ALEJANDRO REDONDO

Autorizada la entrega del proyecto

EL DIRECTOR DEL PROYECTO

Fdo.   Fecha: 27/ 08/2020

Janko Celikovic

COMILLAS
UNIVERSIDAD PONTIFICIA
ICAI

BACHELOR'S DEGREE IN ENGINEERING FOR INDUSTRIAL TECHNOLOGIES

BACHELOR'S DEGREE PROJECT

CONTROL AND SIMULATIONS OF A POWER SUPPLY FOR NANOSATELLITES

Author: Alejandro Redondo Lázaro

Director: Janko Čeliković

Madrid

Acknowledgements

CONTROL Y SIMULACIONES DE UNA FUENTE DE ALIMENTACIÓN PARA UN NANOSATÉLITE

Autor: Redondo Lázaro, Alejandro.

Director: Čeliković, Janko.

Entidad Colaboradora: ICAI – Universidad Pontificia Comillas

RESUMEN DEL PROYECTO

En este trabajo se ha desarrollado el control y las simulaciones de la fuente de alimentación del nanosatélite diseñado por el equipo de la Universidad de Colorado Boulder en el 2020 International Future Energy Challenge (IFEC). Los resultados obtenidos son satisfactorios y presentan un buen punto de partida de cara a las pruebas experimentales de dicha fuente de alimentación.

Palabras clave: Control MPPT, Regulador de carga de Batería, Regulador PID, MATLAB/Simulink, Modelaje de paneles fotovoltaicos, Fuente de alimentación, Nanosatélite

1. Introducción

Este proyecto está ligado al International Future Energy Challenge de 2020. En esta edición, el proyecto consistía en diseñar una fuente alimentación para un nanosatélite con una serie especificaciones y características definidas por los organizadores. Dichas especificaciones se resumen en la figura que se muestra a continuación. Para más información se puede acceder a la página web de la competición [1].
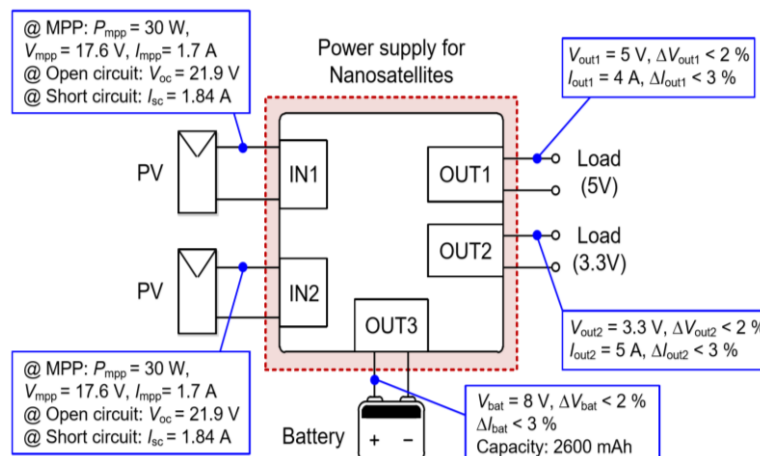

Figura 1.1 Especificaciones y características de la fuente de alimentación [2]

Con respecto a las funcionalidades del control, la fuente de alimentación ha de tener un control que sea capaz de seguir el punto de máxima potencia de los paneles fotovoltaicos, un control que sea capaz de regular la potencia suministrada a las cargas cuando la batería se asume desconectada de dicho sistema, y un control que permita seguir el voltaje de referencia en ambas cargas.

La topología escogida por todos los miembros del equipo para su desarrollo se muestra en la siguiente figura. Consta de dos convertidores CC reductores a ambas entradas de los paneles fotovoltaicos y otros dos convertidores CC reductores a cada carga. Todos ellos conectado mediante un bus común donde se conectará la batería.
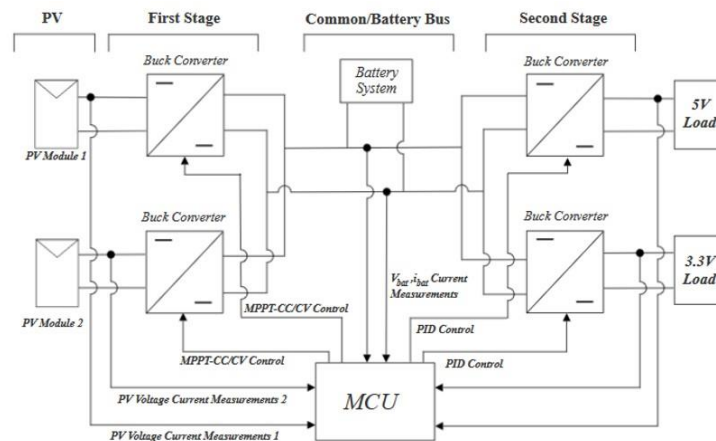
Figura 1.2 Topología de la Fuente de alimentación

2. Definición del proyecto

Este proyecto es el resultado de realizar una parte del trabajo requerido para el diseño de la fuente de alimentación descrita en la Figura 1.2. Se diseñará el control de seguimiento del punto máximo de potencia de los paneles fotovoltaicos (control MPPT), el control que regula la tensión en el bus común y que protege la batería de sobretensión cuando está conectada, y el control PID de los convertidores conectados a las cargas. Adicionalmente, se incluirá un diseño realizado para el cálculo de los valores que el convertir CC a la entrada de la fuente de alimentación han de tener para que la oscilación especificada por los organizadores en el bus de la batería sea alcanzable.

Por otro lado, se diseñará e implementará el modelo completo de la fuente de alimentación en MATLAB para poder realizar simulaciones del modelo completo previamente a las pruebas experimentales.

3. Resultados y Conclusiones

Los valores obtenidos para el diseño final de los parámetros de los controles pueden considerarse muy buen punto de partida por los resultados obtenidos tras las simulaciones. Se puede concluir que el bucle del control MPPT control debe estar entre

los 100 y los 500 Hz y el valor de perturbación entre los 0.002 y 0.008. Por otro lado, el valor óptimo hallado para el parámetro que define el control que regula la tensión y protege la batería, es de 0.0038. Con relación al regulador PID, los valores óptimos hallados de las simulaciones son: para PID de la carga de 5V, Ki_5=0.0287, Kp_5=1.4883, Kd_5=6.2574 y para el PID de la carga de 3.3V, Ki_3.3=0.0344, Kp_3.3=1.7510, Kd_3.3=6.0285. Dichos valores fueron optimizados para una frecuencia de bucle del control MPPT de 200 Hz y un valor de perturbación de 0.004, ya que para estos valores el control MPPT alcanzaba una un punto óptimo de operación.

Los resultados obtenidos y el modelo de MATLAB usado se muestran a continuación.
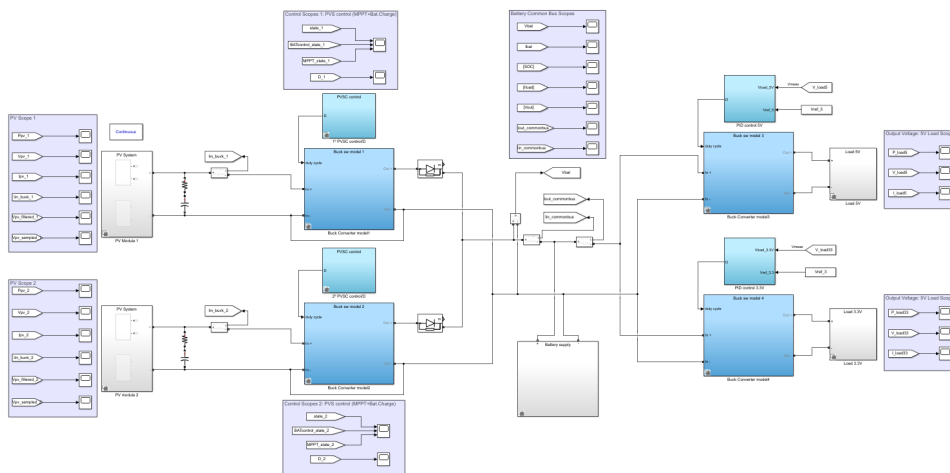
Figura 3.1 Fuente de alimentación modelada en MATLAB/Simulink

Las siguientes figuras muestran los MATLAB scopes de la tensión en ambas cargas.
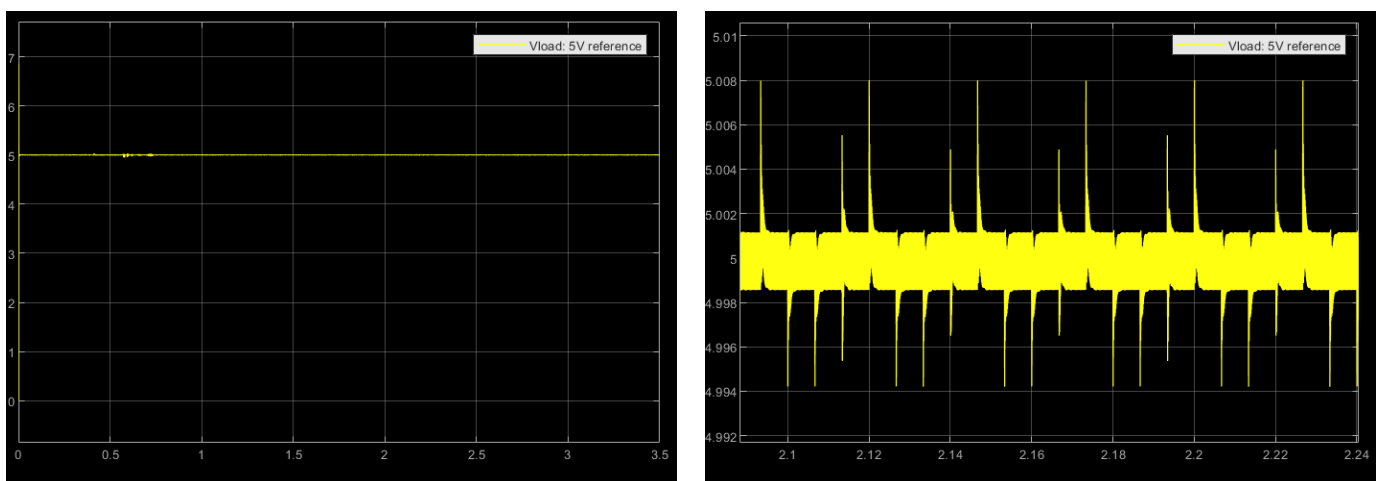
Figura 3.2 MATLAB scopes de la tensión para la carga de 5V
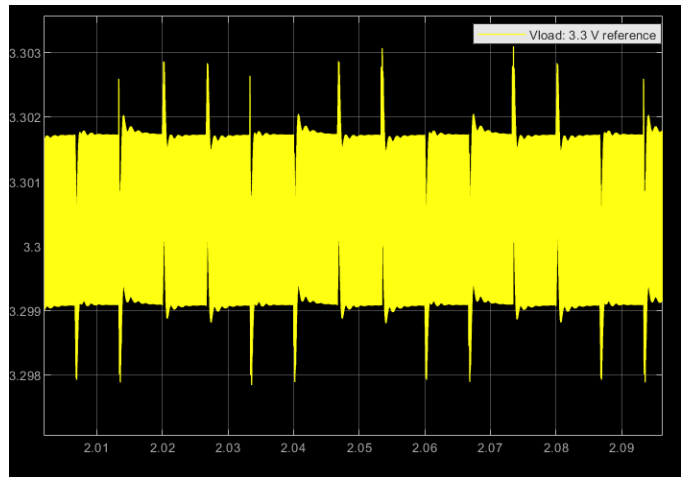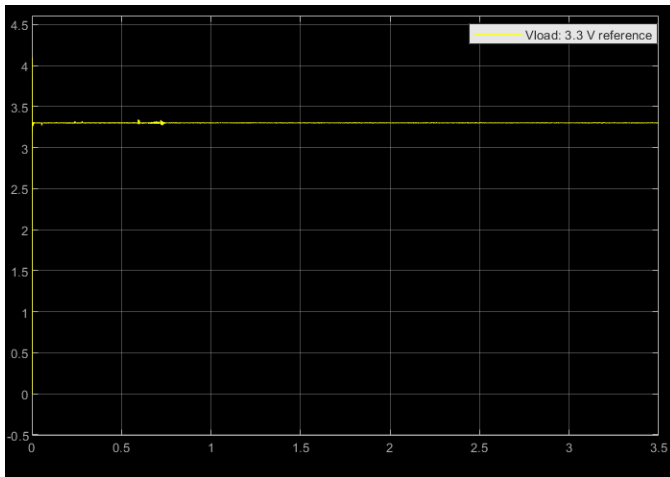
Figura 3.3 MATLAB scopes de la tensión para la carga de 3.3V

Por otro lado, se muestra el mando y la potencia extraída de uno de los paneles fotovoltaicos.
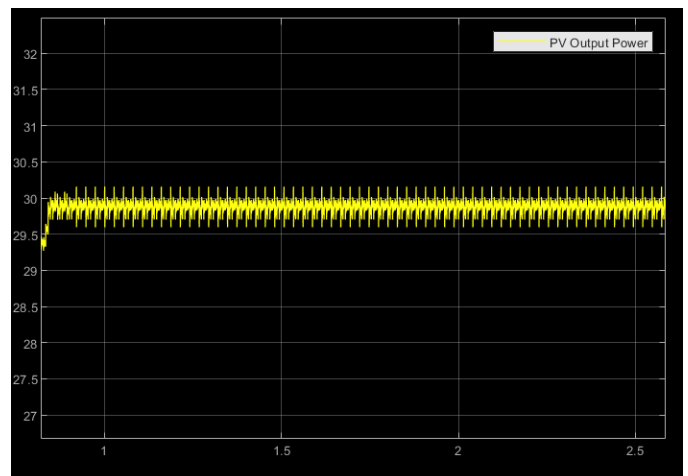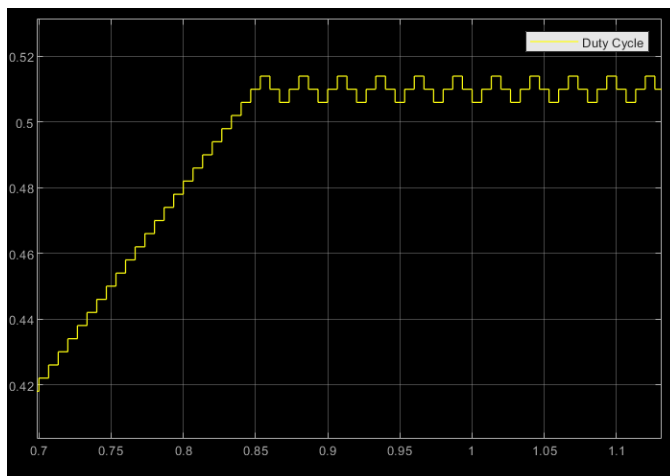
Figura 3.4 MATLAB scopes del mando y la potencia extraída de sistema fotovoltaico

4. Referencias

[1] IEEE International Future Energy Challenge (2020). *IFEC 2020 - Power Supply for Nano Satellites*. http://energychallenge.weebly.com/ifec-2020.html

[2] IEEE International Future Energy Challenge (2020). *IFEC 2020 - Power Supply for Nano Satellites : Preliminary Specifications*. http://energychallenge.weebly.com/uploads/6/4/2/8/6428791/editor/ifec2020-blockdiagram.png?1574586039

[3]   Phaesun. (2016). *Solar Modules Sun Plus*. https://docs-emea.rs-online.com/webdocs/171c/0900766b8171c20b.pdf

[4]   Samsung SDI Co.,Ltd. (2009, May). *Specification of Product for Lithium-ion Rechargeable Cell Model : ICR18650-26F*. https://www.batteryspace.com/prod-specs/ICR18650-26F.pdf

[5]   The 2020 International Future Energy Challenge (IFEC2020). (2020, July 13). *Request for Proposals (RFP)*. http://energychallenge.weeby.com/uploads/6/4/2/8/6428791/ifec_2020_rfp_13_july_2020.pdf

[6]   Xiao, W. (2017). *Photovoltaic power system: Modeling, design, and control*. John Wiley & Sons Ltd.

[7]   Kalyan Kumar, K., Bhaskar, R., Hemanth, K. (2014*). Implementation of MPPT Algorithm for Solar Photovoltaic Cell by Comparing Short-circuit Method and Incremental Conductance Method.* Procedia Technology. https://doi.org/10.1016/j.protcy.2013.12.553

[8]   Keim, R. (2018, June 13). *How to Choose the Frequency of Your Switching Regulator*. ALL ABOUT CIRCUITS. https://www.allaboutcircuits.com/technical-articles/how-to-choose-the-frequency-of-your-switching-regulator/

[9]   Erickson, R. W., Maksimović, D. (2001). *Fundamentals of Power Electronics*. Norwell, Mass: Kluwer Academic.

[10]   Kemet. *Ceramic capacitors KEMET C1210C106K5RACTU*. https://www.digikey.com/product-detail/en/kemet/C1210C106K5RACTU/399-11629-1-ND/4918885

[11]   Würth Elektronik. *Fixed inductors Würth Elektronik 74435574700*. https://www.digikey.com/product-detail/en/w-rth-elektronik/74435574700/732-2179-1-ND/2175694

[12]   Kemet. *Ceramic capacitors KEMET C1210X225K1RAC7800*. https://www.digikey.com/product-detail/en/kemet/C1210X225K1RAC7800/399-16357-1-ND/7652885

[13]   Femia, M., Petrone, G., Spagnuolo, G., Vitelli, M. (2013). *PowerElectronics and Control Techniques for Maximum Energy Harvesting in Photovoltaic Systems.* CRC Press Taylor & Francis Group.

[14]   Rezaee, A. (2016). *Parameter estimation of solar photovoltaic (PV) cells: A Review. Elsevier*. https://doi.org/10.1016/j.rser.2016.03.049

[15]   Anandhraj, P. Mohana, K. (2019, June 1). *Extraction of Solar PV Module Parameters Using Back Search Optimization Algorithm.* Springer. https://doi-org.colorado.idm.oclc.org/10.1007/978-981-13-6772-4_113

[16]   Cubas, J., Pindado, S., De Manuel, C. (2014, March 14). *Explicit Expressions for Solar Panel Equivalent Circuit Parameters Based on Analytical Formulation and the Lambert W-Function.* Instituto Universitario de Microgravedad "Ignacio Da Riva" (IDR/UPM). Escuela Técnica Superior de Ingeniería Aeronáutica y del Espacio (ETSIAE). Universidad Politécnica Madrid.

[17]   Cubas, J., Pindado, S., Farrahi, A. (2013). *New Method for Analytical Photovoltaic Parameter Extraction. ICRERA 2013.* Instituto Universitario de Microgravedad "Ignacio Da Riva" (IDR/UPM). Escuela Técnica Superior de Ingeniería Aeronáutica y del Espacio (ETSIAE). Universidad Politécnica Madrid.

[18]   Yatimi, H., Aroudam, E. (2014). *Renewable Energy in the Service of Mankind Vol II.* In A. Sayigh (Ed). *Select Topics from the World Renewable Energy Congress WREC 2014. Evaluation of the Characteristics of the PV Module Considering Effects of Real Climatic Conditions* (pp. 459-467). Springer. https://link.springer.com/book/10.1007/978-3-319-18215-5

[19]   *Petrone, G., Spagnuolo G., Ramos-Paja, C.A., Spagnuolo, G., Vitelli, M., Xiao, W. (2017, Mar 20). Photovoltaic Sources Modeling.* IEEE Press.

[20]   Gradella Villalba, M., Ruppert Filho, E. (2008, Oct 10). *Dynamic analysis of the input-controlled buck converter fed by a photovoltaic array.* University of Campinas - UNICAMP - Brazil (Original work published 2007, Sep 3). http://dx.doi.org/10.1590/S0103-17592008000400009

[21]   Villalba G.M., Ruppert, E. (2009). *Analysis and Simulation of the P&O MPPT Algortithm using a Linearized PV Array Model.* 35th Annual Conference of IEEE Industrial Electronics, Porto, 2009, pp. 231-236, doi: 10.1109/IECON.2009.5414780.

[22]   Gradella, M., Gama de Siqueira, T., Ruppert, E. (2010, Jan 27). *Voltage Regulation of Photovoltaic Arrays: Small-Signal Analysis and Control Design.* IET Power Electronics (Original work published 2008, Dec 16).

[23]   Pandey, S. Kumar Jena, P. (2017, June). *A Review on Maximum Power Point Tracking Techniques for Photovoltaic Systems.* International Research Journal of Engineering and Technology (IRJET) Volume 4 Issue 6.

[24]   Eltamaly, A.M., Abdelaziz, A.Y. (2020). *Modern Maximum Power Point Tracking Techniques for Photovoltaic Energy Systems.* Springer. https://doi.org/10.1007/978-3-030-05578-3

[25]   MazenAbdel-Salam, M.,Mohamed-Tharwat,E., Goda,M. (2018). *An improved perturb-and-observe based MPPT method for PV systems under varying irradiation levels.* Elsevier. https://doi.org/10.1016/j.solener.2018.06.080

[26]   Wolfram MathWorld. (n.d.). *Extreme Value Theorem.* https://mathworld.wolfram.com/ExtremeValueTheorem.html

[27]   Corradini, L., Maksimovic´,D., Mattavelli, P., Zane, R. (2015). *Digital Control of High-Frecuency Switched-Mode Power Converters.* IEEE Press.

[28]   Pagola, F.L. (2006). *Regulación Automática*. Universidad Pontificia Comillas de Madrid.

[29]   Deng, W., Gehan A. J. Amaratunga, G.A.J. (2014, Oct 16). *Limits of Incremental Conductance for Determining the Maximum Power Point under Rapidly Changing Irradiance and an Alternative Technique based on Fast Scanning. IEEE. 40th Photovoltaic Specialist Conference (PVSC), Denver, CO, 2014, pp. 3690-3694, doi: 10.1109/PVSC.2014.6924908.*

[30]   United Nations Office for Outer Space Affairs. (2015). *Space Supporting the Sustainable Development Goals.* United Nations. https://www.unoosa.org/oosa/en/ourwork/space4sdgs/index.html

[31]   Zivkovic, O. (2019, Dec 5). *A new generation of 'hyper' satellites to prevent a climate catastrophe.* DW Made for Minds. https://www.dw.com/en/a-new-generation-of-hyper-satellites-to-prevent-a-climate-catastrophe/a-51535184

[32]   Välimäki, M. (2017, Jul). *Los satélites finlandeses Aalto nos saludan desde el espacio.* This is Finland. https://finland.fi/es/neegocios-amp-innovacion/los-satelites-finlandeses-aalto-nos-saludan-desde-el-espacio/

CONTROL AND SIMULATIONS OF A POWER SUPPLY FOR NANOSATELLITES

Author: Redondo Lázaro, Alejandro.

Supervisor: Čeliković, Janko.

Collaborating Entity: ICAI – Comillas Pontifical University

ABSTRACT

In this Project, the control and simulations of the nanosatellite´s power supply designed by the University of Colorado Boulder team for the 2020 International future Energy Challenge (IFEC), have been developed. The results obtained have been satisfactory and present a good starting point towards the experimental tests for such power supply.

Keywords: MPPT control, Battery Charge control, PID compensator, MATLAB/Simulink, PV modelling, Power Supply, Nanosatellite.

1. Introduction

This Project is linked to the 2020 International Future Energy Challenge. This year´s edition consisted of designing a power supply for a nanosatellite with a series of specifications and characteristics defined by the organizers. Such specifications are summarized in the next shown figure. For more information, the official competition´s website can be accessed [1].

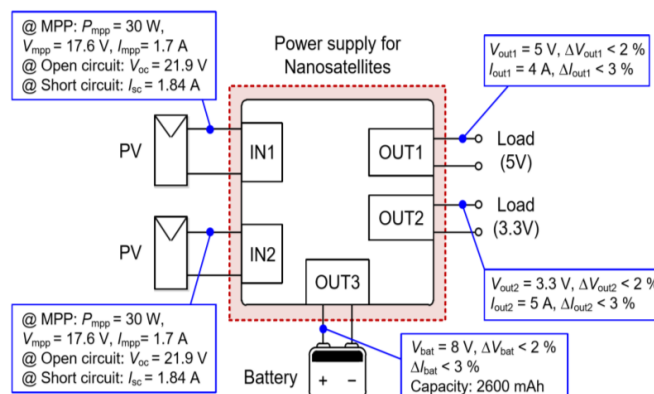*Figure 1.1 Specifications and characteristics of the power supply [2]*

In regards to the control´s functionalities, the power supply must have a control that is able to track the PV module´s maximum power point, a control that is able to regulate the power supplied to the loads when the battery is assumed to be disconnected to such system, and a control that is able to follow the reference voltage in both loads.

The topology agreed by all the team member's consensus consists of two power stages. A first stage where the power converters interface the PV's to a common bus and a second stage where the power converters interface each different load to the common bus.
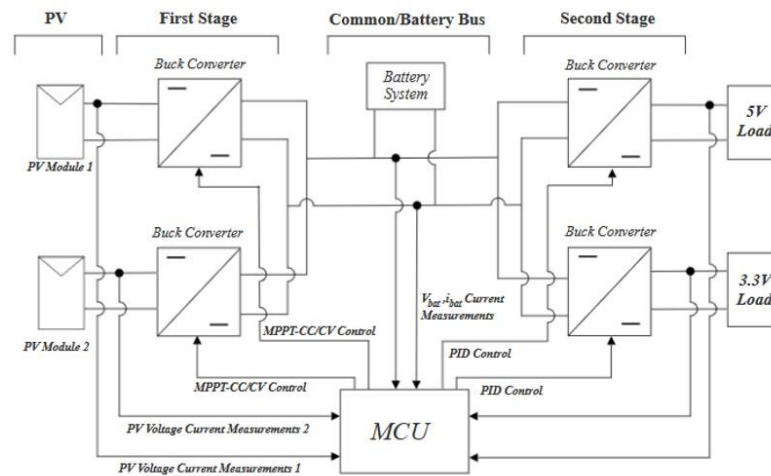

Figure 1.2 Power supply topology

2. Project definition

This Bachelor thesis is the result of carrying out a part of the project previously described. I will be the main responsible of the control and the simulations of the power supply and will be contributing in other parts of the project as needed.

The objectives are set within three main aspects. The Hardware design, the Control design, and the Simulations. First, regarding the Hardware design, the objectives are to design the PV link and the LC filter. The PV link includes the design of the input capacitance required between the PV modules and the output buck converters to attenuate the converter switching at the PV input terminals. The LC filter of the input buck includes the design of the required LC values to achieve the ripple requirements. Secondly, in relation to the Control Design, the objective is to develop the MPPT control, the Battery Charge Control where from its parts (voltage and current protection parts), only the voltage protection part will be designed but both will be implemented in the simulation model, and to design the Output Bucks PID compensator. Finally, towards Simulations, the objective is to verify if the previous control design works as expected to consequently implement the power supply full model and be able to simulate its behaviour before experimental testing.

3. Results and Conclusions

The values obtained for the control´s parameters final design can be considered a good starting point due to the results achieved after the simulations. It can be concluded that the MPPT control´s loop must be between 100 and 500 Hz and the perturbation value should be between 0.002 and 0.008. On the other hand, the optimal value found

for the parameter that defines the control that regulates the tension and that protects the battery is 0.0038. In relation to the PID regulator, the optimal simulations values found are: for the 5V charge PID, Ki_5=0.0287, Kp_5=1.4883, Kd_5=6.2574 and for the 3.3.V charge PID, Ki_3.3=0.0344, Kp_3.3=1.7510, Kd_3.3=6.0285. Such values were optimized for a 200 Hz MPPT control frequency loop and a perturbation value of 0.004, as for these values, the MPPT control reached an optimal operation point.

The results obtained and the MATLAB model used are shown next.
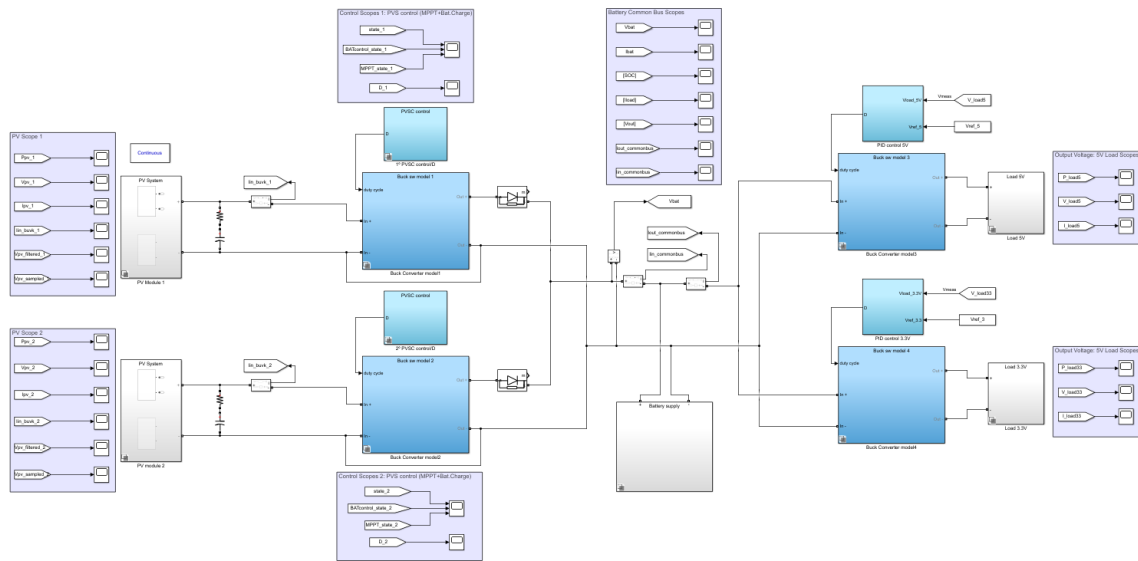
Figure 3.3 Power supply MATLAB/Simulink model

The following figures show the MATLAB voltage measurements scopes for both charges.
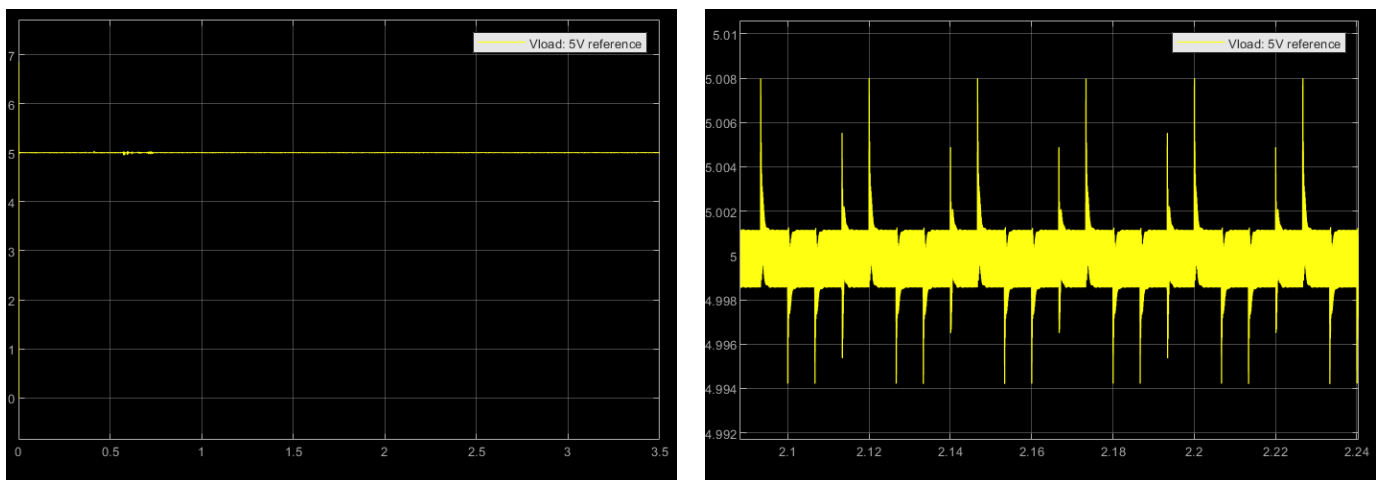
Figure 3.2 MATLAB scopes of 5V load voltage measurement
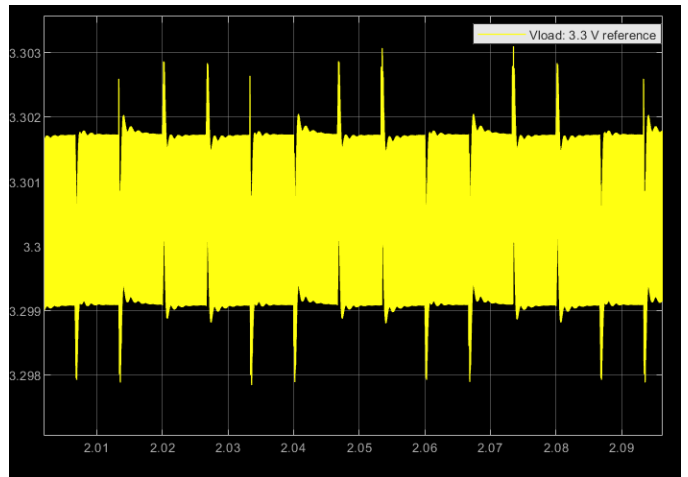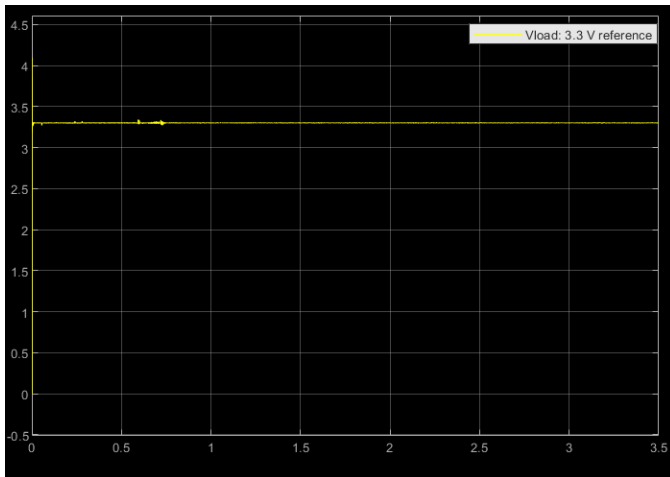
Figure 3.3 MATLAB scopes of 3.3V load voltage measurement

On another hand, the duty cycle and power extracted for one of the photovoltaic panels is shown
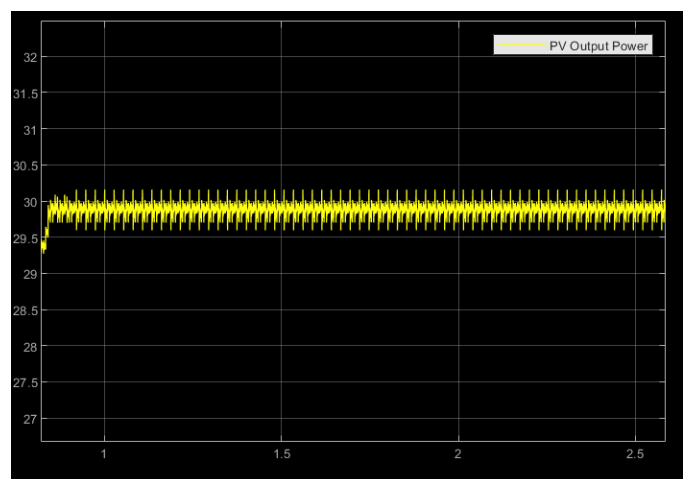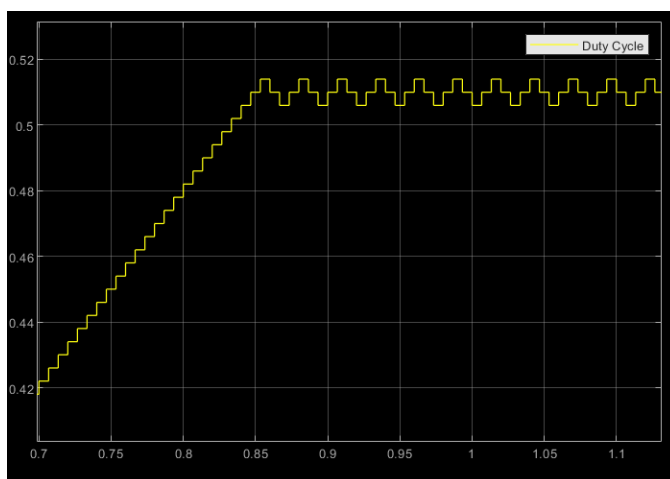
Figure 3.4 MATLAB scopes: duty cycle value and the power extracted from the PV's

4. Bibliography

[1]   IEEE International Future Energy Challenge (2020). *IFEC 2020 - Power Supply for Nano Satellites*. http://energychallenge.weebly.com/ifec-2020.html

[2]   IEEE International Future Energy Challenge (2020). *IFEC 2020 - Power Supply for Nano Satellites : Preliminary Specifications*. http://energychallenge.weebly.com/uploads/6/4/2/8/6428791/editor/ifec2020-blockdiagram.png?1574586039

[3] Phaesun. (2016). *Solar Modules Sun Plus.* https://docs-emea.rs-online.com/webdocs/171c/0900766b8171c20b.pdf

[4] Samsung SDI Co.,Ltd. (2009, May). *Specification of Product for Lithium-ion Rechargeable Cell Model : ICR18650-26F*. https://www.batteryspace.com/prod-specs/ICR18650-26F.pdf

[5] The 2020 International Future Energy Challenge (IFEC2020). (2020, July 13). *Request for Proposals (RFP).* http://energychallenge.weeby.com/uploads/6/4/2/8/6428791/ifec_2020_rfp_13_july_2020.pdf

[6] Xiao, W. (2017). *Photovoltaic power system: Modeling, design, and control.* John Wiley & Sons Ltd.

[7] Kalyan Kumar, K., Bhaskar, R., Hemanth, K. (2014*). Implementation of MPPT Algorithm for Solar Photovoltaic Cell by Comparing Short-circuit Method and Incremental Conductance Method.* Procedia Technology. https://doi.org/10.1016/j.protcy.2013.12.553

[8] Keim, R. (2018, June 13). *How to Choose the Frequency of Your Switching Regulator*. ALL ABOUT CIRCUITS. https://www.allaboutcircuits.com/technical-articles/how-to-choose-the-frequency-of-your-switching-regulator/

[9] Erickson, R. W., Maksimović, D. (2001). *Fundamentals of Power Electronics.* Norwell, Mass: Kluwer Academic.

[10] Kemet. *Ceramic capacitors KEMET C1210C106K5RACTU.* https://www.digikey.com/product-detail/en/kemet/C1210C106K5RACTU/399-11629-1-ND/4918885

[11] Würth Elektronik. *Fixed inductors Würth Elektronik 74435574700.* https://www.digikey.com/product-detail/en/w-rth-elektronik/74435574700/732-2179-1-ND/2175694

[12] Kemet. *Ceramic capacitors KEMET C1210X225K1RAC7800.* https://www.digikey.com/product-detail/en/kemet/C1210X225K1RAC7800/399-16357-1-ND/7652885

[13] Femia, M., Petrone, G., Spagnuolo, G., Vitelli, M. (2013). *PowerElectronics and Control Techniques for Maximum Energy Harvesting in Photovoltaic Systems.* CRC Press Taylor & Francis Group.

[14] Rezaee, A. (2016). *Parameter estimation of solar photovoltaic (PV) cells: A Review. Elsevier.* https://doi.org/10.1016/j.rser.2016.03.049

[15] Anandhraj, P. Mohana, K. (2019, June 1). *Extraction of Solar PV Module Parameters Using Back Search Optimization Algorithm.* Springer. https://doi-org.colorado.idm.oclc.org/10.1007/978-981-13-6772-4_113

[16] Cubas, J., Pindado, S., De Manuel, C. (2014, March 14). *Explicit Expressions for Solar Panel Equivalent Circuit Parameters Based on Analytical Formulation and the Lambert W-Function.* Instituto Universitario de Microgravedad "Ignacio Da Riva" (IDR/UPM). Escuela Técnica Superior de Ingeniería Aeronáutica y del Espacio (ETSIAE). Universidad Politécnica Madrid.

[17] Cubas, J., Pindado, S., Farrahi, A. (2013). *New Method for Analytical Photovoltaic Parameter Extraction. ICRERA 2013.* Instituto Universitario de Microgravedad "Ignacio Da Riva" (IDR/UPM). Escuela Técnica Superior de Ingeniería Aeronáutica y del Espacio (ETSIAE). Universidad Politécnica Madrid.

[18] Yatimi, H., Aroudam, E. (2014). *Renewable Energy in the Service of Mankind Vol II.* In A. Sayigh (Ed). *Select Topics from the World Renewable Energy Congress WREC 2014. Evaluation of the Characteristics of the PV Module Considering Effects of Real Climatic Conditions* (pp. 459-467). Springer. https://link.springer.com/book/10.1007/978-3-319-18215-5

[19] *Petrone, G., Spagnuolo G., Ramos-Paja, C.A., Spagnuolo, G., Vitelli, M., Xiao, W. (2017, Mar 20). Photovoltaic Sources Modeling.* IEEE Press.

[20] Gradella Villalba, M., Ruppert Filho, E. (2008, Oct 10). *Dynamic analysis of the input-controlled buck converter fed by a photovoltaic array.* University of Campinas - UNICAMP - Brazil (Original work published 2007, Sep 3). http://dx.doi.org/10.1590/S0103-17592008000400009

[21] Villalba G.M., Ruppert, E. (2009). *Analysis and Simulation of the P&O MPPT Algortithm using a Linearized PV Array Model.* 35th Annual Conference of IEEE Industrial Electronics, Porto, 2009, pp. 231-236, doi: 10.1109/IECON.2009.5414780.

[22] Gradella, M., Gama de Siqueira, T., Ruppert, E. (2010, Jan 27). *Voltage Regulation of Photovoltaic Arrays: Small-Signal Analysis and Control Design.* IET Power Electronics (Original work published 2008, Dec 16).

[23] Pandey, S. Kumar Jena, P. (2017, June). *A Review on Maximum Power Point Tracking Techniques for Photovoltaic Systems.* International Research Journal of Engineering and Technology (IRJET) Volume 4 Issue 6.

[24] Eltamaly, A.M., Abdelaziz, A.Y. (2020). *Modern Maximum Power Point Tracking Techniques for Photovoltaic Energy Systems.* Springer. https://doi.org/10.1007/978-3-030-05578-3

[25] MazenAbdel-Salam, M.,Mohamed-Tharwat,E., Goda,M. (2018). *An improved perturb-and-observe based MPPT method for PV systems under varying irradiation levels.* Elsevier. https://doi.org/10.1016/j.solener.2018.06.080

[26] Wolfram MathWorld. (n.d.). *Extreme Value Theorem.* https://mathworld.wolfram.com/ExtremeValueTheorem.html

[27] Corradini, L., Maksimovic´,D., Mattavelli, P., Zane, R. (2015). *Digital Control of High-Frecuency Switched-Mode Power Converters.* IEEE Press.

[28] Pagola, F.L. (2006). *Regulación Automática*. Universidad Pontificia Comillas de Madrid.

[29] Deng, W., Gehan A. J. Amaratunga, G.A.J. (2014, Oct 16). *Limits of Incremental Conductance for Determining the Maximum Power Point under Rapidly Changing Irradiance and an Alternative Technique based on Fast Scanning. IEEE. 40th Photovoltaic Specialist Conference (PVSC), Denver, CO, 2014, pp. 3690-3694, doi: 10.1109/PVSC.2014.6924908.*

[30] United Nations Office for Outer Space Affairs. (2015). *Space Supporting the Sustainable Development Goals.* United Nations. https://www.unoosa.org/oosa/en/ourwork/space4sdgs/index.html

[31] Zivkovic, O. (2019, Dec 5). *A new generation of 'hyper' satellites to prevent a climate catastrophe.* DW Made for Minds. https://www.dw.com/en/a-new-generation-of-hyper-satellites-to-prevent-a-climate-catastrophe/a-51535184

[32] Välimäki, M. (2017, Jul). *Los satélites finlandeses Aalto nos saludan desde el espacio.* This is Finland. https://finland.fi/es/neegocios-amp-innovacion/los-satelites-finlandeses-aalto-nos-saludan-desde-el-espacio/

Table of contents

LIST OF FIGURES

LIST OF TABLES

Chapter 1. INTRODUCTION

This project origins from the "Introduction to Power Electronics" Class from the University of Colorado Boulder. The professor Dragan Maksimović fomented the creation of a team to participate in the *"2020 International Future Energy Challenge (IFEC)"* in representation of the University of Colorado Boulder.

From professor Dragan Maksimović's proposal, a team of 6 members led by Janko Čeliković was born. Janko Čeliković who completed his bachelors and masters engineering degree in the University of Belgrade and that in the present is carrying out his doctorate through the University of Colorado Boulder, had the opportunity of participating in one of such competition´s past editions when he was a bachelor's degree student. His team turned out to be one of the best of their edition. He was the one who proposed the idea of creating a team and participating in "IFEC 2020" competition to Dragan with those students interested in "Power Electronics" so they could benefit from a unique experience such as he did during his edition.

The "IFEC" is an international competition that promotes innovation, conservation, and the efficient use of electrical energy. Such competition is oriented towards undergraduate students that belong to an engineering program with the intention of putting into practice the theoretical knowledge acquired throughout the degree. The IFEC sponsors consist of the Institute of Electrical and Electronics Engineers (IEEE) Power Electronics Society (PELS), Power & Energy Society (PES), Industry Application Society (IAS) and Power Sources Manufacturers Association (PSMA) [1].

This year's edition topic consists in developing a "*Power Supply for Nanosatellites*". The nanosatellites industry is growing rapidly, especially in recent years. Its costs are decreasing, and its production period is becoming shorter. Its applications are very extensive as they include global tracking, internet of things, remote sensing, defense and security,

electronic equipment testing. All these characteristics are favouring the investment and expansion of the nanosatellite industry [1].

1.1 POWER SUPPLY REQUIREMENTS AND SPECIFICATIONS

Throughout this section the global power supply specifications will be explained, including the input and output characteristics, performance targets, control functions, and test profile of the power supply. All the information explained in this section and additional information regarding the competition can be found at [1].

1.1.1 INPUTS AND OUTPUTS CHARACTERISTICS

The power supply consists of two inputs and three outputs. The inputs are two solar PV panels mounted on the nanosatellite surface and the outputs are two different load types and a battery (energy storage system). In the next image we can see the inputs and outputs specifications that the power supply will have.
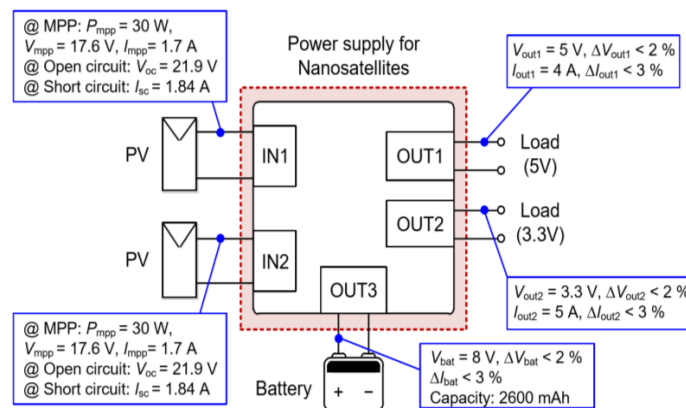
Figure 1.1 Specifications of the inputs and outputs of the power supply [2]

1.1.1.1 PV 1 AND PV2: SOLAR PV MODULES

Both PV solar panels are equivalent, and their main characteristics are shown in the next table. Additional information can be found in PV modules datasheet [3].

10

Technical Data	Sun Plus 30
Maximum power (Pmax)	30 W
Voltage at MPP (Vmpp)	17.6 V
Current at MPP (Impp)	1.7 A
Short circuit current (Isc)	1.84 A

Table 1.1 Solar PV panels characteristics

1.1.1.2 LOAD 1: 5 V DC LOAD

Load characteristics: $V_{load1} = +5\ V$ @ $I_{load1} = 4\ A$.

Voltage ripple requirement at load side: $\Delta V_{load1} < 2\%$ @ $100\%\ load$.

Current ripple requirement at load side: $\Delta I_{load1} < 3\%$ @ $100\%\ load$.

1.1.1.3 LOAD 2: 3.3 V DC LOAD

Load characteristics: $V_{load2} = +3.3\ V$ @ $I_{load2} = 5\ A$.

Voltage ripple requirement at load side: $\Delta V_{load2} < 2\%$ @ $100\%\ load$.

Current ripple requirement at load side: $\Delta I_{load2} < 3\%$ @ $100\%\ load$.

1.1.1.4 BATTERY

The battery characteristics are shown in the next figure. Additional information can be found in [4].

Technical Data	Battery
Battery voltage	8 V
Nominal Capacity	2600 mAh
Under voltage detection	1600 µs
Over current detection	580 µs (max 1400 µs)

Table 1.2 Battery characteristics

Voltage ripple requirement at the battery (discharging): $\Delta V_{bat} < 2\%$ @ $100\%\ load$.

11

Current ripple requirement at the battery (charging): $\Delta I_{Bat} < 3\%$ @ $100\%\ load$.

1.1.2   PERFORMANCE TARGETS

The overall performance targets are based on power consumption, weight, and dimensions. The next table shows the performance target for each specific characteristic.

Performance targets	
Total power consumption by the converters	< 5 W
Weight (not including PV panels and batteries)	< 200g
Dimension (not including PV panels and batteries)	< 90 x 96 x25 mm
Cooling system	No forced-air or liquid cooling

Table 1.3 Performance targets of the power supply

1.1.3   CONTROL FUNCTIONS

The power supply has to be able to operate in three different modes. The next table shows the different operating modes.

Mode	*PV panels state*	*Battery state*	*Loads state*
1º	Active	Inactive	Active
2º	Active	Active	Active
3º	Inactive	Active	Active

Table 1.4 Operating modes of the power supply

In the first mode all the power is supplied by the PV panels as the battery is in the inactive state. To meet the load demand, the control should regulate the PV modules power output. In the second mode, both the PV panels and the battery are in the active state. The control should regulate the PV to operate at its maximum power point. If the available power

12

is greater than the load demands, the battery will be charged with the power surplus, if the opposite occurs the battery will be discharged to meet the power shortage. In the third mode, the PV panels are supposed to be in the inactive state and all the power is being supplied by the battery.

1.1.4 TEST PROFILE

The control modes will be tested under the following test profile. The testing will be done on the final prototype and will last a total of 20 minutes, divided into three operating modes as follows: 5 minutes in control mode 1, 6 minutes in control mode two and the last 9 minutes in control mode three. This can be illustrated in the following graphs.
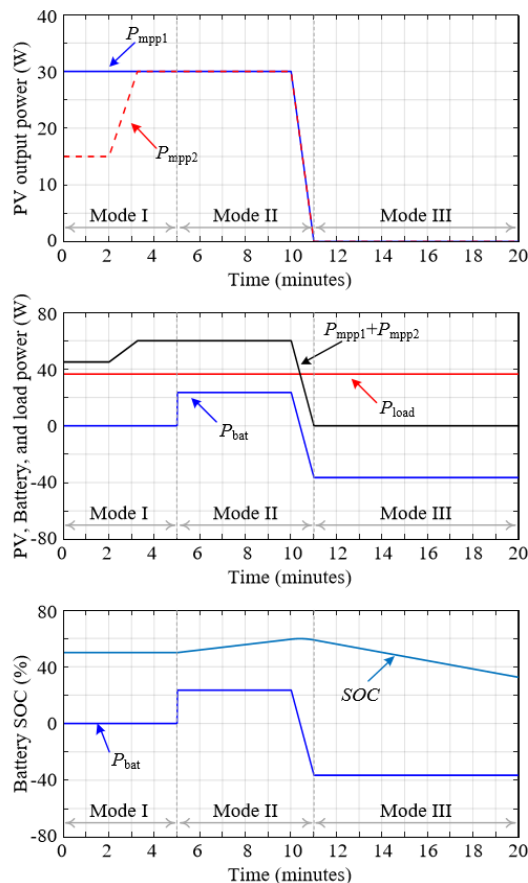
Figure 1.2 Testing profile that will be applied to the final prototype [5]

1.2 *POWER SUPPLY TOPOLOGY SELECTED*

The topology agreed by all the team member's consensus consists of two power stages. A first stage where the power converters interface the PV's to a common bus and a second stage where the power converters interface each different load to the common bus.

The first stage is used to regulate the PV panels available power. The PV side converter (PVSC) will be controlled to track the maximum power point of the PV panels or to limit the voltage common bus to the maximum battery voltage. The topology proposed for the first stage can bear a resemblance to a bidirectional battery charger/discharger, where the PVSC is used to interface the common bus, in which the battery is connected, and the PV module [6]. The topology selected for the PVSC, is based on the input and output voltage of the converter. The input and output voltage respectively are the PV voltage at the maximum power point and the battery voltage. From the simulations of the PV modules carried out in the fourth chapter, it can be appreciated how in figures 4.10 and 4.11, the PV voltage at the MPP under all the different input conditions tested, does not go below the nominal battery voltage (8V). Therefore, as there is no need to boost or to step up the input voltage, the dc-dc buck converter was chosen to be the PVSC. The buck converter will then be controlled by the maximum power point tracking (MPPT) algorithm and the battery controller. The control will adjust the duty cycle in order to extract the maximum power available from the PV or to limit the voltage and current at the battery terminals, as already explained.

The second stage power converters will also be buck converters, as the power at the common bus or battery bus will always be higher than the loads reference voltage, hence we require a step-down topology. Each buck converter will be controlled with a PID controller in order to track the load's reference voltage, 5 and 3.3 volts.

The following figure shows the power supply topology design.
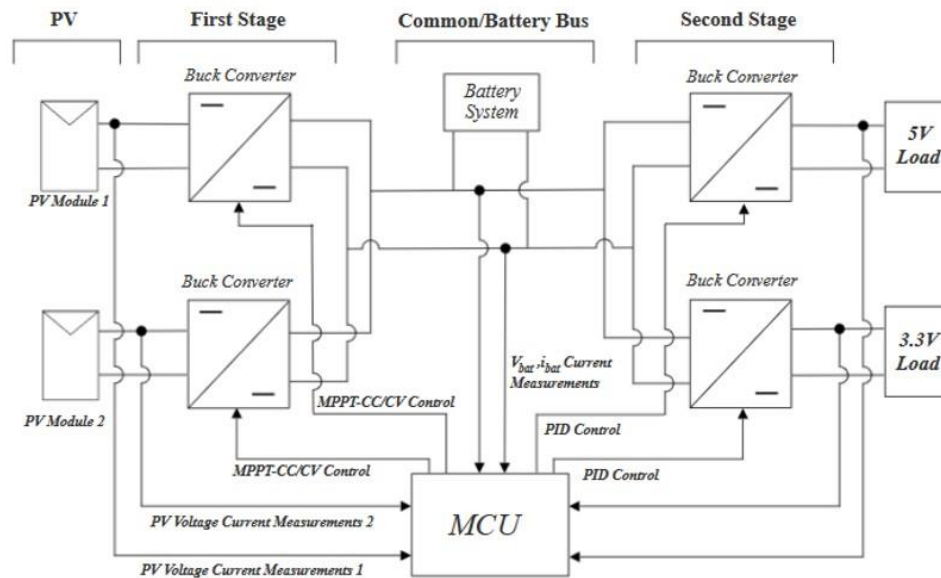
Figure 1.3 Power supply topology

The power supply control functionalities will be carried out in software through an MCU. This allows more flexibility in the design of the MPPT algorithm and its implementation, as some MPPT control algorithms (i.e. Incremental Conductance) cannot be implemented in an analog domain [7]. Furthermore, it eases the PID implementation, as the PID circuits and voltage references could be avoided reducing the weight of the power supply.

1.2.1 SWITCHING TOPOLOGY

The switching topology of the Buck converter is covered in the following sections. It can be divided into, the switching frequency and the switch realization.

1.2.1.1 SWITCHING FREQUENCY

When selecting the switching frequency, the following characteristics should be considered as there is a tradeoff between: board space, efficiency, and ripple magnitudes.

Higher switching frequencies lead to less board space, as the passive components of the converter can reduce its size, and lower ripple magnitudes. However, it increases the losses at the converter lowering its efficiency [8] [9]. The decision of the switching frequency was 100 kHz and was based on the previous characteristics mentioned and from the team member's experience. At this frequency with a proper design the project specifications can be achieved, if the switching frequency was higher the power supply could become lossy and problems related with noise could appear.

1.2.1.2 SWITCHING REALIZATION

To decide how to implement the switching function of the converter, the following will need to be considered. As already discussed, the power supply will be tested under three operating modes, two of them include the charging and discharging of a battery. The inductor current when the battery is being charged will be positive. However, when it is being discharged it will turn negative. To ensure that the converter operates in continuous conduction mode (CCM) in all three operating modes without the need of additional control strategies, the converter's switching will be emulated with a current-bidirectional two-quadrant switch, allowing the inductor current to be of both polarities. It will be implemented with the use of two MOSFETs, the MOSFET that replaces the diode will be operated as a synchronous rectifier, meaning that, when the diode should be conducting, the MOSFET will be controlled to be in "on state" and when the diode should be in reverse biased mode, the MOSFET will be controlled to be in the "off state". An additional advantage besides being able to conduct current in both directions, is the ability to decrease conduction losses, as the "on resistance" (R_{on}) of the MOSFET could be chosen to be very low, reducing the switching losses and improving its efficiency [9]. However, choosing a very low R_{on} could affect the size of the converter, the lower the "on resistance" the bigger its size. Hence, the tradeoff between efficiency and size in selecting the MOSFETs will need to be considered as the project specifications limit the power supply size. This analysis was evaluated by the PCB and hardware.

16

Chapter 2. PROJECT CHARACTERISTICS

2.1 MOTIVATION

This Bachelor thesis is the result of carrying out a part of the project previously described. I will be the main responsible of the control and the simulations of the power supply and will be contributing in other parts of the project as needed.

2.2 OBJECTIVES

The objectives are set within three main aspects. The Hardware design, the Control design, and the Simulations. First, regarding the Hardware design, the objectives are to design the PV link and the LC filter. The PV link includes the design of the input capacitance required between the PV modules and the output buck converters to attenuate the converter switching at the PV input terminals. The LC filter of the input buck includes the design of the required LC values to achieve the ripple requirements. Secondly, in relation to the Control Design, the objective is to develop the MPPT control, the Battery Charge Control where from its parts (voltage and current protection parts), only the voltage protection part will be designed but both will be implemented in the simulation model, and to design the Output Bucks PID compensator. Finally, towards Simulations, the objective is to verify if the previous control design works as expected to consequently implement the power supply full model and be able to simulate its behaviour before experimental testing.

2.3 *METHODOLOGY*

To obtain the objectives stated, the following methodology will be used.

For the LC filter´s design, first the inductance value to subsequently determine the capacitance value will be designed, as the capacitance value is affected by the inductance value. Its values will be calculated through two derived equations in [9]. Consequently, through an input buck converter simulation, a verification will take place to observe if the ripple requirements can be achieved. Moreover, the PV link input capacitance design will be based on a frequency response analysis.

In regard to the MPPT´s control design. Firstly, the different types and actual methods that exist will be studied to subsequently choose the most suitable one for the development of the global project. Once selected, the parameters that define how it should be applied will be designed. Such MPPT methods will be the Perturb and Observe (P&O) and IncCond (IncCond) methods. As it will be seen in Chapter 5, such methods are based on different algorithms but the parameters than characterize them are the same, perturbation frequency (f_{MPPT}) and the perturbation size step (Δd). Since the MPTT is not a linear control, the design will be based on a time domain analysis. This will permit that both parameters can be designed independently.

For the voltage protection part of the battery charge control and the PID control of the output, as they are going to be implemented in software, the method used for their design will be the same. The method used will be based on the bilinear transformation, that consists of mapping the plant and compensator transfer functions in the z-domain into an equivalent continuous time domain (p-domain) in order to be able to apply the basic continuous time control theory used for analog control design. Once the parameters are calculated, they will be mapped again into the z-domain.

2.4 THESIS STRUCTURE

The main body of this thesis project presents the following structure. It is formed by 5 chapters, in which one of them is dedicated to the hardware design and the rest to the control and simulations of the Power supply. Moreover, a small summary for each chapter of the thesis can be found.

In Chapter 3, the LC filter of the Buck converter is designed to meet the competition's specification's output and current ripple requirements. Furthermore, the input capacitance value needed to attenuate the converter switching at the PV input terminals will be designed.

In Chapter 4, the photovoltaic panels that will be the power converter´s inputs will be modeled and simulated. The model used for the final simulations and its linearized version that will be needed for the design of the MPPT control parameters will be developed.

In Chapter 5, the controls that the power supply will have will be modeled and designed. These include, the MPTT control, the Battery Charge control and the PID compensators of the Output Buck

In Chapter 6, all results obtained in the previous chapters will be verified within a simulated environment (MATLAB). All the necessary operating modes that specify the competition´s test cases explained in Chapter 1 will be simulated. Additionally, the entire power supply model will also be included as it will be very useful to simulate the whole power supply behaviour before testing the power supply experimentally.

Finally, in Chapter 7, the conclusions obtained for this thesis project will be presented.

Chapter 3. HARDWARE DESIGN

Throughout this chapter, the LC filter of the input buck converter and the input capacitance at the PV link will be designed.

3.1 LOW PASS FILTER DESIGN

The design of the input buck converter parameters will be based on the performance targets and competition specifications that have to be achieved. The next sections will specifically cover the design of the LC filter values.

3.1.1 INDUCTANCE VALUE DESIGN

In order to select the proper inductor value, a steady state analysis of the Buck converter was done. The basic techniques used for this analysis can be found in [9].

The equivalent circuit of the buck converter when its switch is in position 1, is shown in the next figure.
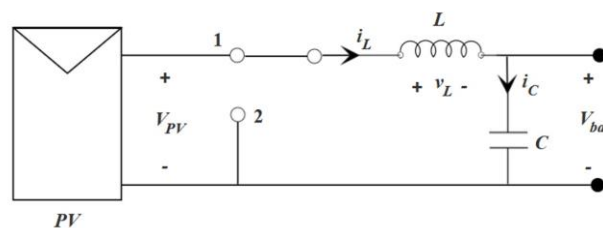
Figure 3.1 PVS Input buck converter at position 1

The inductor voltage equation for the switch in position 1 is:

$$v_L = v_{PV} - v_{bat} \qquad (3.1)$$

Applying the small-ripple approximation (SRA) to the capacitor voltage (v_{bat}):

$$v_L \approx V_{PV} - V_{bat} \qquad (3.2)$$

Solving for the inductor current slope:

$$v_L = L * \frac{di_L}{dt} \approx V_{PV} - V_{bat} \rightarrow i_L = \frac{V_{PV} - V_{bat}}{L} \qquad (3.3)$$

The equivalent circuit of the buck converter when the switch is in position 2, is shown in the next figure.
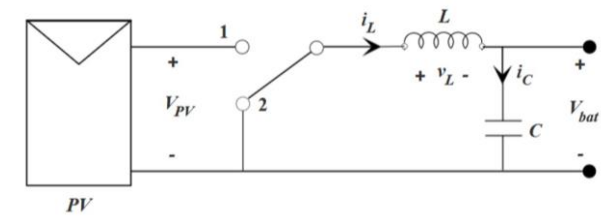
Figure 3.2 PVS Input buck converter at position 2

The inductor voltage equation for the switch in position 2 is:

$$v_L = -v_{bat} \qquad (3.4)$$

Applying the small-ripple approximation (SRA) to the capacitor voltage (v_{bat}):

$$v_L \approx -V_{bat} \qquad (3.5)$$

Solving for the inductor current slope:

$$v_L = L * \frac{di_L}{dt} \approx -V_{bat} \rightarrow i_L = \frac{-V_{bat}}{L} \qquad (3.6)$$

From the previous equations derived when the circuit is in position 1 and 2 the inductor voltage and current waveforms can be sketched.
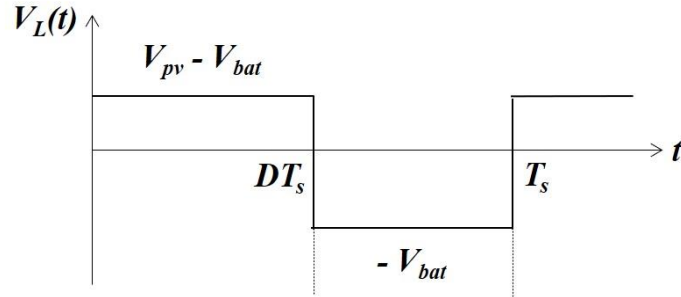
Figure 3.3 Input buck converter inductor voltage waveform
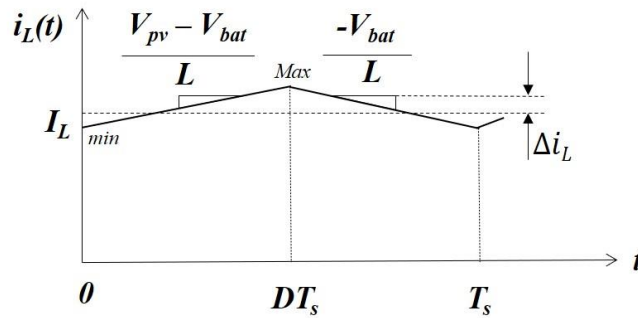
Figure 3.4 Input buck converter inductor current waveform

From Figure 3.4, the next equation can be derived:

$$slope = \frac{V_{PV} - V_{bat}}{L} = \frac{2 * \Delta i_L (\, ripple = I_{L_{DC}} \, to \, I_{max/min})}{D * Ts} \qquad (3.7)$$

Solving for the inductance value in Eq. (3.7):

$$L = \frac{V_{PV} - V_{bat}}{2 * \Delta i_L} * D * Ts \qquad (3.8)$$

Eq. (3.8) expresses the inductance as a function of the inductor current ripple. This equation will be used to determine the required inductance vale in order to meet the desired inductor current ripple, usually assumed to be between 10-20% of the DC inductor current

[9]. The selected inductor ripple will affect the output voltage ripple. Therefore, it is preferable to select a lower and achievable inductor current ripple than a higher one.

Furthermore, the duty cycle and DC inductor current values will be calculated as follows. The duty cycle will be calculated applying the inductor volt-second balance principle (VSB). This principle states that the average inductor voltage over a period is zero in steady state. Therefore, the area under the inductor voltage waveform of Figure 3.3 will be equal to zero:

$$< v_L > = 0 \rightarrow (V_{PV} - V_{bat}) * D * Ts + (-V_{bat}) * (1 - D) * Ts = 0$$

$$(V_{PV} - V_{bat}) * D + (-V_{bat}) * D' = 0$$

(3.9)

$$M_{ideal}(D) = \frac{V_{bat}}{V_{PV}} = D$$

(3.10)

The PV voltage at the maximum power pint (MPP) and for standard test conditions (STC) is 17.6 V and the battery bus voltage will be about 8 V. Substituting these values into Eq. (3.10), the duty cycle expected for MPP operating conditions will be equal to:

$$D = \frac{V_{bat}}{V_{PV}} = \frac{17.6}{8} \approx 0.4545$$

(3.11)

To calculate the expected DC inductor current, the next calculations were carried out. Assuming lossless components:

$$P_{in} = P_{out} \rightarrow P_{PV@MPP} = P_{out}$$

(3.12)

Then:

$$V_{MPP} * I_{MPP} = V_{bat} * I_{out}$$

(3.13)

In steady state the average capacitor current is zero (capacitor charge balance principle), hence the output current for the buck converter topology will be equal to the inductor current:

$$I_{out} = I_L \qquad (3.14)$$

Substituting Eq. (3.14) in Eq. (3.13) and solving for the DC inductor current (I_L), a reasonable approximation of the DC inductor current for nominal operating conditions can be obtained:

$$I_L = \frac{V_{MPP} * I_{MPP}}{V_{bat}} = \frac{17.6 * 1.7}{8} = 3.74 \, A \qquad (3.15)$$

Knowing the expected duty cycle and DC inductor current of the converter, the value of the inductance to achieve a specific ripple can be calculated using Eq. (3.8). The next table was built to calculate the inductance value required for different inductor ripple ratings.

(%)	10	11	12	13	15	16	18	20
ΔIL	0.37	0.41	0.45	0.49	0.56	0.6	0.67	0.75
L (µH)	58.3	53	48.6	44.9	38.9	36.5	32.4	29.2

Table 3.1 Inductance values for different inductor ripple ratings

From the table above, it can be observed how depending on the inductor ripple set the inductance value required changes, it goes from $30 \, to \, 60\mu H$. As explained before, the inductor current ripple will affect the output ripple, hence the inductance value should be preferable between $45 \, to \, 60\mu H$.

The hardware team based on this analysis, the one carried out in Section 5.2.1, and other considerations, ended up choosing the following inductor. The 47µH Shielded Wirewound Inductor 6.8A 33.5mOhm Nonstandard (Würth Elektronik 74435574700) [11].

3.1.2   CAPACITANCE VALUE DESIGN

To select the capacitor value, the following considerations must be taken into account. The voltage ripple at the battery during discharging has to be lower than 2% and the current ripple at the battery charging has to be lower than 3%. In order to meet this requirement, the capacitor will have to be carefully chosen.

The next equation can be used to determine the minimum capacitor value to obtain the output voltage ripple specified. It is important to mention that the equation does not include the additional ripple introduced by the equivalent series resistance (ESR) of the capacitor. The derivation of this expression can be found in [9] and it is based on the total charge contained in a capacitor.

$$\Delta v = \frac{\Delta i_L}{8 * C * fs} \rightarrow \quad C = \frac{\Delta i_L}{8 * \Delta v * fs} \qquad (3.16)$$

The current ripple of Eq. (3.16) will be recalculated using the final inductor value selected by the hardware team, $L = 47\mu F$.

$$\Delta i_L = \frac{17.6 - 8}{2 * 47E - 6} * 0.4545 * \frac{1}{100E3} = 0.4642 \qquad (3.17)$$

The voltage ripple will be specified to be 2% of the output common bus voltage reference. Hence, substituting the values calculated in Eq. (3.17) into Eq. (3.16), lead to the following minimum capacitance required:

$$C_{min} = \frac{0.4642}{8 * 0.08 * 100E3} = 7.253 \text{ μF} \qquad (3.18)$$

With this capacitance value assuming lossless capacitor, the voltage output ripple requirement at the battery bus should be achieved. However, this does not account for the battery current ripple.

A simulation with the parameters designed ($L = 47\mu H$ and $C = 7.253\ \mu F$) was done to verify the voltage and the current output ripple at the battery bus. The MATLAB model used is shown in the next figure.
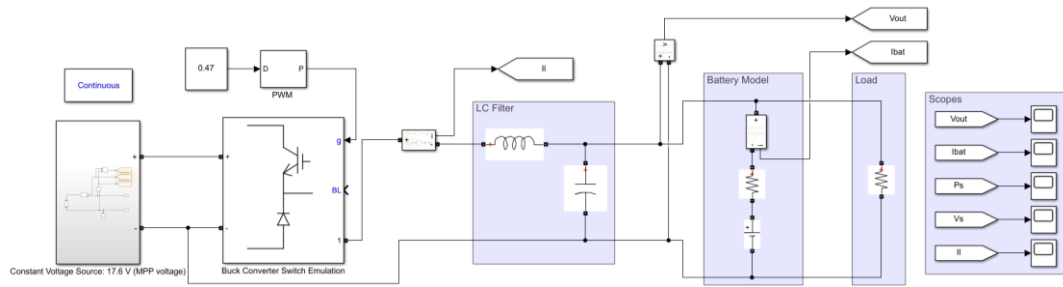
Figure 3.5 Simulink model used to verify parameters design

The following figure shows the output bus voltage and the battery current waveforms zoomed.
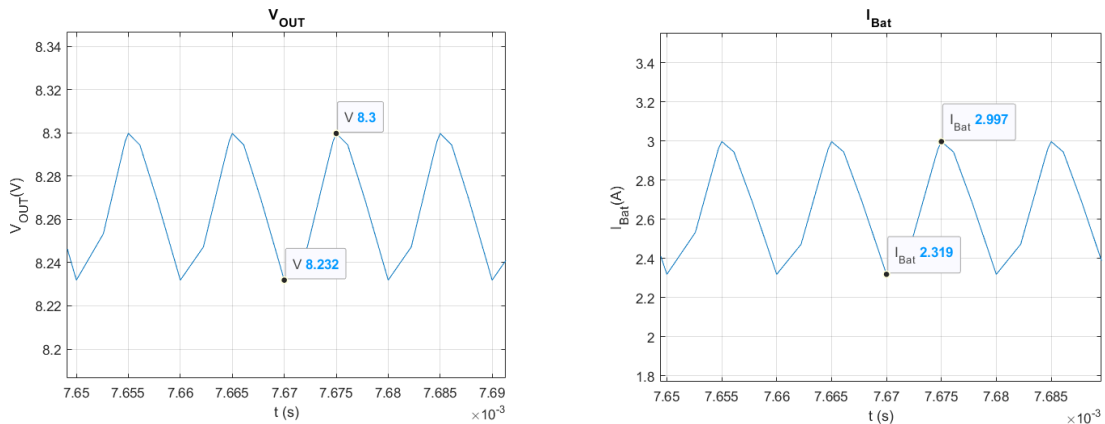
Figure 3.6 Output voltage and battery current waveforms (L=47µH, C=7.253 µF)

It can be appreciated how the output voltage ripple is lower than 2%. On the contrary, the battery current ripple is higher than 3%. Therefore, the capacitance value should de higher in order to meet the current battery ripple requirements. A different approach was carried out to account for the battery current ripple.

The next figure represents a small signal model of the Buck converter output, it will be useful to calculate the transfer function in Laplace domain of $\frac{\hat{i}_{bat}}{\hat{i}_L}$, and evaluate the filtering action of the capacitor.
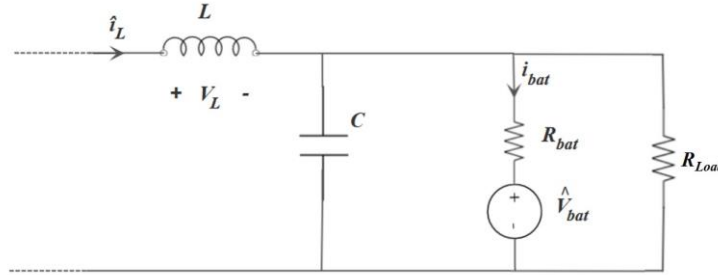
Figure 3.7 Small signal model of the PV side buck converter output

To model the transfer function $\hat{v}_{bat}$ will be set to zero. Figure 3.7 can be modified and simplified as follows. The capacitor ESR can be considered negligible for this analysis, as the ESR will only affect at high frequencies. Moreover, the $(R_{bat}//R_{load})$ can be approximated to R_{bat} as $R_{bat} \ll R_{load}$. Hence, leading to the following figure.
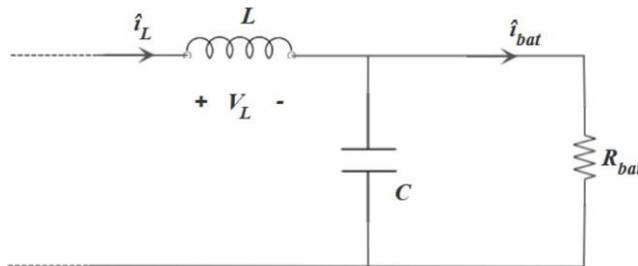
Figure 3.8 Small signal model of the PV side buck converter output

To obtain the transfer function the current divider rule was applied:

$$\frac{\hat{i}_{bat}}{\hat{i}_L} = \left(\frac{\frac{1}{s*C}}{R_{bat} + \frac{1}{s*C}} \right) = \left(\frac{1}{s*C*R_{bat} + 1} \right) \qquad (3.19)$$

27

Eq. (3.19) is a single pole transfer function where the corner frequency is equal to:

$$f_{o_{\frac{i_{bat}}{i_L}}} = \frac{1}{2 * \pi * R_{bat} * C} \qquad (3.20)$$

Substituting the LC parameters previously calculated:

$$f_{o_{\frac{i_{bat}}{i_L}}} = \frac{1}{2 * \pi * 0.1 * 7.253\mu} = 219.4 kHz \qquad (3.21)$$

The bandwidth is too high, it should be at least 10 times lower than $100 kHz$ to correctly filter out the inductor current. Therefore, the previous capacitance value designed was not enough to meet the battery current ripple requirements.

The next table presents capacitors values for different corner frequencies, all at least 10 times lower than the switching frequency.

f_o (Hz)	10000	9000	8500	8000	7000
C (μF)	159.15	176.84	187.24	198.94	227.36

Table 3.2 Capacitor values for different resonant frequencies

Simulations were carried out in order to verify the battery ripple. It should be considered that the model does not account for losses and does not represent the total topology but gives a good approximation to estimate the capacitor value required to meet the project's specifications. In the next figure, it can be appreciated how both ripple specifications are met. Hence, a reasonable capacitor value between the MPPT buck converters and the battery bus should be around 180 to 220 µF.
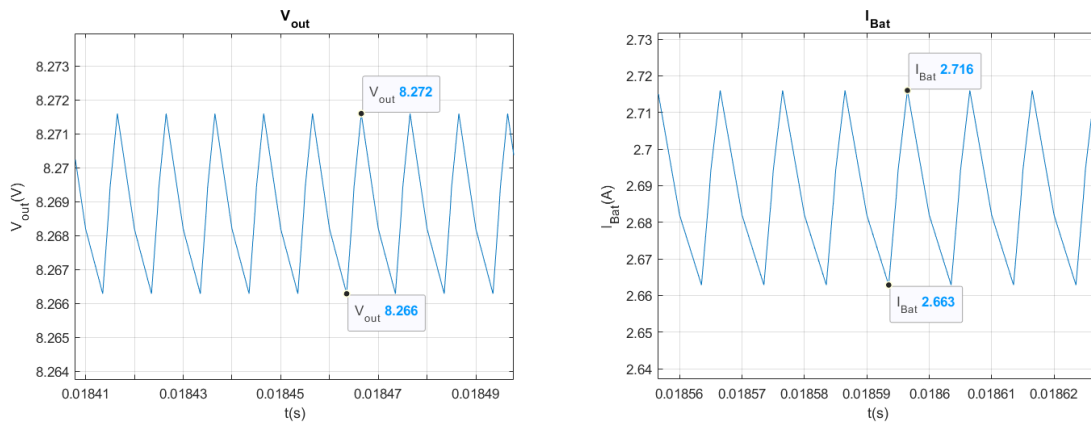
Figure 3.9 Output voltage and battery current waveforms (L=47µH, C=180µF)

The hardware team based on this analysis, the one carried out in Section 5.2.1, and other considerations, ended up choosing the following capacitance value (200 µF). Achieved with, 20x10µF ±10% 50V Ceramic Capacitor X7R 1210 (KEMET C1210C106K5RACTU) [10].

3.2   PV LINK

The input current at the buck converter is always pulsing. Therefore, a filter action will be needed in order to correctly track and extract the maximum power available from the PV modules. The PV link between the PV panels and the PVSC will then be a bank of capacitors. The design of the input capacitance value will be based on a similar approach to the previous one used for designing the capacitance of the LC filter. In the next figure, we can see the PV linear equivalent circuit modeled in Section 4.4 emulating the behaviour of the PV at the MPP, and the input bank of capacitors.
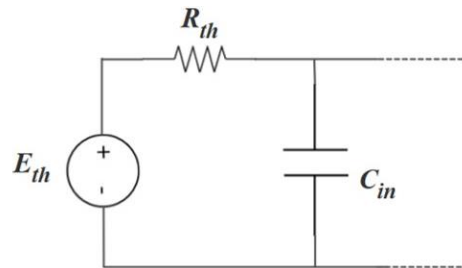
Figure 3.10 PV equivalent linear circuit and input capacitance

From Figure 3.10, we can calculate the transfer function between the PV voltage and the converter input voltage in Laplace domain:

$$\frac{V_{in}}{E_{th}} = \frac{1}{1 + s * R_{th} * C_{in}}$$

(3.22)

The corner frequency will then be defined as:

$$f_{o_{\frac{V_{in}}{E_{th}}}} = \frac{1}{2 * \pi * R_{th} * C_{in}}$$

(3.23)

Its value should be at least 1000 times lower than the switching frequency, as not having a constant voltage at the PV terminals, the MPPT tracking control could be affected by reducing considerably its efficiency. The next table presents input capacitors values for different corner frequencies.

f_o (Hz)	40	50	70	80	100
C (µF)	430.31	344.25	245.89	215.15	172.12

Table 3.3 Input capacitor values for different resonant frequencies

A reasonable value for the input capacitance could be around 200 µF, this value should be enough to attenuate the converter switching at the PV input terminals. The input capacitance should be within that range. The hardware team based on this analysis, ended up choosing the following capacitance value (192.2 µF). Achieved with, 19x10µF ±10% 50V Ceramic

Capacitor X7R 1210 (KEMET C1210C106K5RACTU) [10] + 2.2µF ±10% 100V Ceramic Capacitor X7R 1210 (KEMET C1210X225K1RAC7800) [12].

The next table shows a summary of the Input Buck inductance and capacitance values of the LC filter and the capacitance at the PV link bus. These values will be used in the MATLAB models for simulating the power supply control behaviour.

Circuit parameters	Values
C_{out}	$20x10µF$
$ESR - C_{out}$	$(13.621m\Omega)/20$
L	$47µH$
R_L	$33.5\ m\Omega$
C_{PVlink}	$19x10µF + 2.2µF$
$ESR - C_{PVlink}$	$\approx (13.621m\Omega)/20$

Table 3.4 First stage components values summary

Chapter 4. PV MODELING AND SIMULATION

The power supply will have two identical Photovoltaic (PV) modules as inputs. Therefore, its correct modeling will be necessary for two main purposes. The first one is associated to the design and testing of the Maximum Power Point Tracking (MPPT) Control and the second is related with the simulation of the power supply under the test cases specified by the competition. Throughout this chapter different modeling approaches and their mathematical explanation will be developed. This is due to the way the IFEC 2020 organization shared the information regarding the PV modules. At first only some relevant parameters were shared leading to the first modeling approach. But once the datasheet was provided, a more relevant proposition was carried out. Moreover, a linear model will be described, as needed in other sections.

4.1 PV MODEL TYPES

The PV modeling will be approached through an equivalent circuit as it presents many advantages to its implementation in simulation environments (MATLAB, LTSpice, PLECS,...) [13]. There are distinct types of equivalent circuits that model the PV module behaviour, within the most common ones, we find the single diode model (SDM) and the double diode model (DDM), respectively Figure 4.1 and Figure 4.2. Both can be simplified and adjusted according to the level of accuracy required.
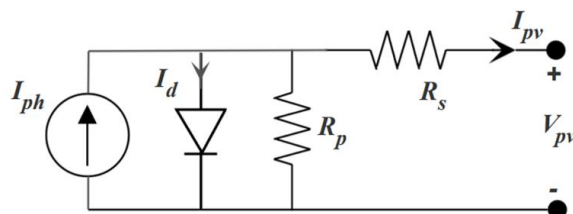
Figure 4.1 Equivalent circuit of single diode model (SDM)

32
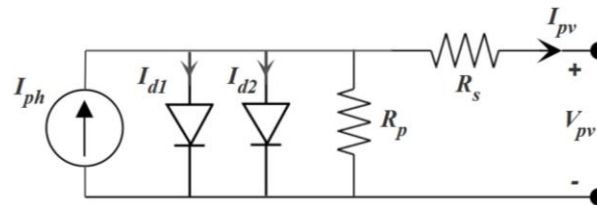
Figure 4.2 Equivalent circuit of double diode model (DDM)

Each of them presents a tradeoff between how precise the model is and how easy it is to be implemented. Its difficulty comes as a function of the unknown parameters to be estimated, the more parameters to be assessed the harder and complex the modeling of the PV module will be [14]. Hence, to correctly represent the I-V characteristic curve of the PV modules, both the model and its parameters must be taken into account, as a very complex model with a poor parameter estimation will lead to a bad representation of the PV module behaviour.

The parameters of the PV model chosen can be estimated based on datasheet information, on experimental I-V data or a combination of both. The information available of the PV will help determine the model and method to extract its parameters [15].

The SDM will be used to model and simulate both PV modules, as its level of accuracy and complexity are enough for the purpose of this research [16] [17]. Consecutively, the different equivalent circuits of the SDM will be presented, within the SDM we can encounter four different approaches. The first one represents an ideal version of the SDM (ISDM), the next two are simplified versions: the ISDM with a series resistance (SDM_Rs) and the ISDM with a shunt resistance (SDM_Rp) [14]. And lastly, the complete SDM, shown in the figure 4.1.

Successively, the I-V characteristic equation of the ISDM, SDM_Rs and the complete SDM will be derived, with an additional focus on the ideal model to explain its derivation process.

4.1.1 *Ideal Single Diode Model (ISDM)*

The ISDM is the most simplified version of the SDM and it is just composed of an ideal current source in parallel with an ideal diode, as shown in Figure 4.3. This model is not accurate enough to use in simulations. However, it is very convenient to understand how the I-V relationship of the ISDM is derived, as the SDM_Rs and SDM will follow the same process but with additional circuit components.
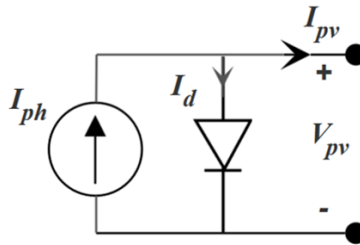
Figure 4.3 Equivalent circuit of ideal single diode model (ISDM)

The output PV current I_{PV} is found by applying Kirchhoff's law:

$$I_{pv} = I_{ph} - I_d \qquad (4.1)$$

where I_{ph} represents the photo-induced or photo-generated current and I_d represents the current through the diode, defined by the Shockley equation:

$$I_d = I_o * \left(e^{\left(\frac{q*V_d}{a*N_s*K*T} \right)} - 1 \right) \qquad (4.2)$$

where I_o (A) is the diode reverse saturation current, V_d (V) is the voltage across the diode, a is the diode ideality factor, N_s is the number of PV cells connected in series (assumed to be 1 if considering just one PV cell), q (C) is the electron charge constant, K $\left(\frac{J}{K} \right)$ is the Boltzmann constant and T (K) is the temperature of the solar cell.

34

The Shockley equation can be further simplified with the use of the following variables. The parameters a and N_s can be grouped as:

$$a_m = a * N_s \tag{4.3}$$

and q, K and T can be grouped in a new variable called thermal voltage V_t, defined as:

$$V_t = \frac{K * T}{q} \tag{4.4}$$

Substituting Eq. (4.3) and Eq. (4.4) in Eq. (4.2), and considering for this particular equivalent circuit that the voltage across the diode is equal to the output PV voltage, the Shockley equation will be expressed as:

$$I_d = I_o * \left(e^{\left(\frac{V_{pv}}{a_m * Vt}\right)} - 1 \right) \tag{4.5}$$

Finally, the I/V characteristic of the ISDM is obtained by substituting Eq. (4.5) into Eq. (4.1):

$$I_{pv} = I_{ph} - I_o * \left(e^{\left(\frac{V_{pv}}{a_m * Vt}\right)} - 1 \right) \tag{4.6}$$

This equivalent circuit contains only 3 unknown parameters (Iph, I_o, a) and is the easiest way to model a PV panel, with the disadvantage of its lack of accuracy.

4.1.2 *ISDM with a Series Resistance*

This model presents an additional component in comparison to the previous one explained. It considers some losses with the addition of a series resistance to the ISDM, as shown in Figure 4.4.
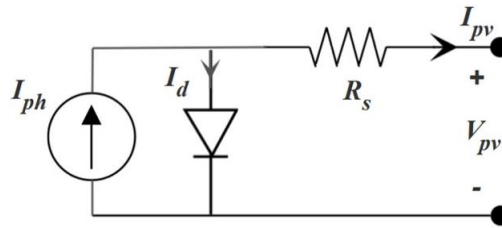
Figure 4.4 Equivalent circuit of the ISDM with series resistance

The mathematical modeling follows the same procedure as the ideal case. However, the addition of Rs will change the I/V characteristic of the ideal model to a more accurate version of it, as including Rs, the losses by the semiconductor material and bad contacts within the PV cell will be taken into account [16] [18].

In this version, the voltage across the diode will change to:

$$V_d = V_{pv} + I_{pv} * R_s \qquad (4.7)$$

leading to the following I/V characteristic:

$$I_{pv} = I_{ph} - I_0 * \left(e^{\left(\frac{V_{pv} + I_{pv} * R_s}{a_m * V_t} \right)} - 1 \right) \qquad (4.8)$$

This model includes an additional parameter, Rs. Therefore, the unknown parameters will increase to 4 (I_{ph}, I_o, a, R_s).

4.1.3 *SINGLE DIODE MODEL (SDM)*

The equivalent circuit has already been shown in Figure 4.1. This circuit with the addition of the shunt resistance, also includes losses related to the surface effects and to the non-ideality of the semiconductor junction of the PV [18].

For this circuit, the output current will slightly change as some current will flow into the shunt branch. Applying Kirchhoff's law:

$$I_{PV} = I_{ph} - I_d - I_{Rp} \qquad\qquad (4.9)$$

The new term I_{Rp}, can be calculated as:

$$I_{Rp} = \frac{V_d}{R_p} = \frac{V_{pv} + I_{pv} * R_s}{R_p} \qquad\qquad (4.10)$$

Substituting in Eq. (4.9) the expressions of I_d and I_{Rp}, we find the I/V characteristic equation for the SDM:

$$I_{PV} = I_{ph} - I_o * \left(e^{\left(\frac{V_{pv} + I_{pv} * R_s}{a_m * V_t}\right)} - 1 \right) - \frac{V_{pv} + I_{pv} * R_s}{R_p} \qquad\qquad (4.11)$$

In this case, with the addition of R_p, the number of unknown variables increases to 5 $(I_{ph}, I_o, a, R_s, R_p)$.

4.2 FIRST MODELING APPROACH

Due to the non-linear nature of the I-V characteristic of PV panel, identifying the unknown parameters of the selected model can be a challenging task. In general, depending on the accuracy required and the information available from the PV panel, two strategies can be carried out: the use of numerical methods to solve the nonlinear system of equations to find the exact solution or simplified methods where reasonable approximations are assumed in order to get explicit equations of the unknown parameters [19]. Other approaches exist where both methods are combined. As already mentioned, this project follows the guidelines of a global competition. Initially, the only data available from the PV modules were the most representative points of the I-V curve at the standard test condition (STC): operation in open-circuit $(0, V_{OC,STC} = 21.9\,V)$ and in short-circuit $(I_{SC,STC} = 1.84\,A, 0)$ conditions, and operation at the maximum power point $(I_{MPP,STC} = 1.7\,A, V_{MPP,STC} = 17.6\,V)$.

From the information given and knowing that the full datasheet was going to be provided, the ISDM with series resistance was chosen as a first approach for the PV simulations. With reasonable approximations the ISDM with Rs circuit presents a fast and comfortable way of obtaining the unknown parameters of the circuit model. To obtain them, the following procedure was done. Applying the boundary conditions at Eq. (4.8), the following four equations are obtained:

- Short circuit equation $(0, I_{sc})$:

$$I_{sc} = I_{ph} - I_o * \left(e^{\left(\frac{I_{sc}*R_S}{a_m*V_t} \right)} - 1 \right) \qquad (4.12)$$

where:

$$I_{ph} \gg I_o * \left(e^{\left(\frac{I_{sc}*R_S}{a_m*V_t} \right)} - 1 \right) \qquad (4.13)$$

Hence the photocurrent can be approximated to the short circuit current:

$$I_{sc} \approx I_{ph} \qquad (4.14)$$

- Open circuit equation $(V_{oc}, 0)$:

$$0 = I_{ph} - I_o * \left(e^{\left(\frac{V_{oc}}{a_m*V_t} \right)} - 1 \right) \qquad (4.15)$$

- Maximum power point equation (V_{mpp}, I_{mpp}):

$$I_{mpp} = I_{ph} - I_o * \left(e^{\left(\frac{V_{mpp}+I_{mpp}*R_S}{a_m*V_t} \right)} - 1 \right) \qquad (4.16)$$

- At the maximum power point:

$$\frac{dP_{PV}}{dV_{PV}}\Big|_{V_{mpp}, I_{mpp}} = 0 \tag{4.17}$$

The equation of power output can be obtained by multiplying the PV voltage on both sides of Eq. (4.8):

$$P_{PV} = V_{PV} * I_{PV} = V_{PV} * \left(I_{ph} - I_o * \left(e^{\left(\frac{V + I * R_S}{a_m * V_t}\right)} - 1 \right) \right)$$

$$P_{PV} = V_{PV} * I_{ph} - V_{PV} * I_o * \left(e^{\left(\frac{V + I * R_S}{am * V_t}\right)} - 1 \right) \tag{4.18}$$

Applying Eq. (4.17) to Eq. (4.18):

$$\frac{dP_{PV}}{dV_{PV}}\Big|_{@MPP} = I_{ph} - I_o * \left(e^{\left(\frac{V_{mpp} + I_{mpp} * R_S}{a_m * V_t}\right)} - 1 \right) - \frac{V_{mpp} * I_o * \left(e^{\left(\frac{V_{mpp} + I_{mpp} * R_S}{a_m * V_t}\right)} - 1 \right)}{a_m * V_t} = 0 \tag{4.19}$$

From this system of equations, it is possible to find the parameters of the equivalent circuit for the single diode with Rs. The system was solved using MATLAB (Appendix A.1). The values obtained were the following: $I_{ph} = 1.84\ A$, $I_o = 0.00000050447$, $a_m = 56.442$, $R_s = 0.33323\ \Omega$

Successively, the equivalent circuit of the single diode with R_s of Figure 4.4, was implemented in Simulink with the values just obtained. To incorporate the parameter "a_m", that accounts for the ideality factor times the number of PV cells in series shown in Eq. (4.3), the following arrangement was done. The ideality factor was assumed to be 1, leading to 56 cells in series. The values were introduced in the diode block parameters in Simulink in the resulting manner, as seen in Figure 4.5. This procedure was done, as the information available did not provide the total number of cells in series of the PV module.

Diode model:	Exponential	▼
Parameterization:	Use parameters IS and N	▼
Saturation current, IS:	Io	A ⌄
Emission coefficient, N:	1	
Ohmic resistance, RS:	0	Ohm ⌄
Measurement temperature:	25	degC ⌄
Number of series diodes:	am	
Number of parallel diodes:	1	

Figure 4.5 Diode Simulink block parameters

The next figures show both, the model implemented in Simulink and the results obtained from its simulations.
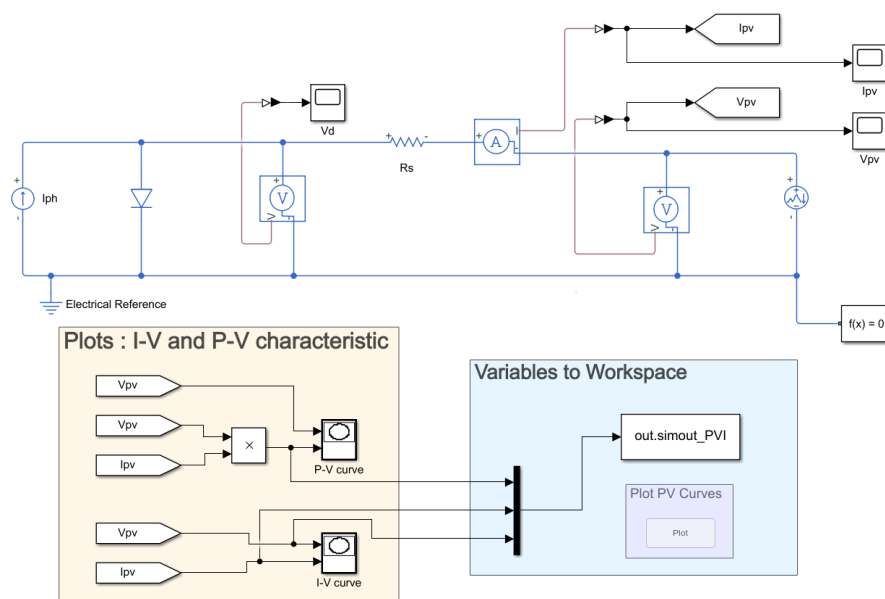
Figure 4.6 Equivalent circuit of ISD with series resistance implemented in Simulink

The results obtained from its simulation are displayed below.
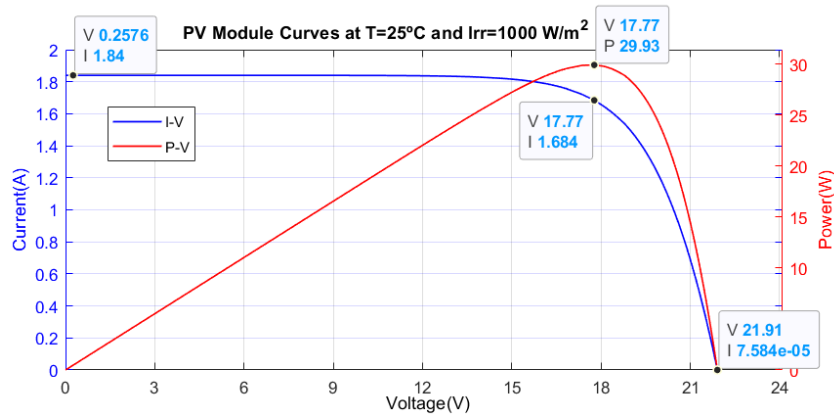
Figure 4.7 Characteristic curves of the PV module

In Figure 4.7, it can be appreciated how the blue line represents the I-V characteristic and how the red line represents the P-V characteristic, including some data tips with the most significant values. Both curves present a good representation of the I-V characteristic of the PV module and a good first approach to start designing the MPPT control.

The modeling and simulation of the PV module were done at its standard test condition (STC), assuming the PV inputs, irradiance and temperature were $1000 \ W/m^2$ and 25ºC, respectively. From the SDM equations derived above, the parameters were assumed independently of the environmental conditions applied on the PV panel. In real life applications, in which this is not the case, any change on the PV inputs will significantly affect the PV module behaviour, hence needing to modify the value of the model parameters. In order to reproduce the test cases specified by the competition, the PV model will need to include the irradiance and temperature dependence so that the PV modules can be simulated in any environmental condition. This was considered in the second approach.

4.3 *SECOND MODELING APPROACH*

Once the access to the full datasheet was provided, an already defined block in MATLAB was used to model the PV modules. The block is based on the equivalent circuit of the SDM and can represent the behaviour of the PV module under any atmospheric condition. In the next table, we can see the technical data provided of the PV module.

Technical Data	*Sun Plus 30*
Maximum power (Pmax)	30 W
Voltage at MPP (Vmpp)	17.6 V
Current at MPP (Impp)	1.7 A
Short circuit current (Isc)	1.84 A
Open circuit voltage (Voc)	21.9 V
Temperature coefficient of Voc	-0.33%
Temperature coefficient of Isc	0.05%
Number of series cells (Ns)	36 x mono

Table 4.1 PV datasheet parameters

The data was introduced in the MATLAB block as follows.
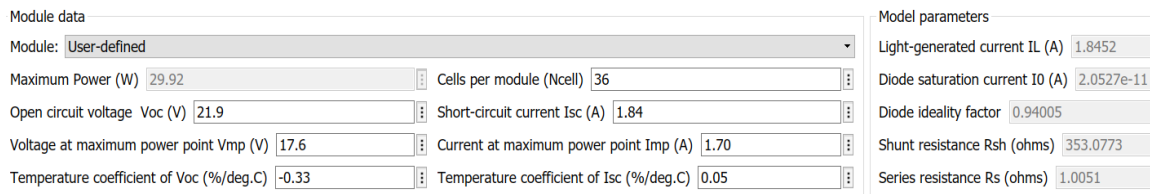
Figure 4.8 PV Simulink block parameters

In Figure 4.8, we can appreciate how once the values are introduced, the model gives you the equivalent circuit values of the SDM: $I_{ph} = IL$, $I_o = I0$, a, $R_p = R_{sh}$ and $R_s = R_{sh}$.

With this block other conditions were tested apart from the STC. In the next figures we can see the PV module block where for different input values (Irradiance and temperature) the I-V and P-V characteristics were simulated.
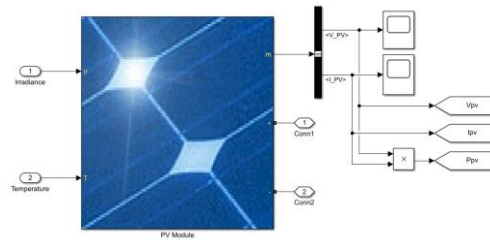
Figure 4.9 PV array Simulink predefined block
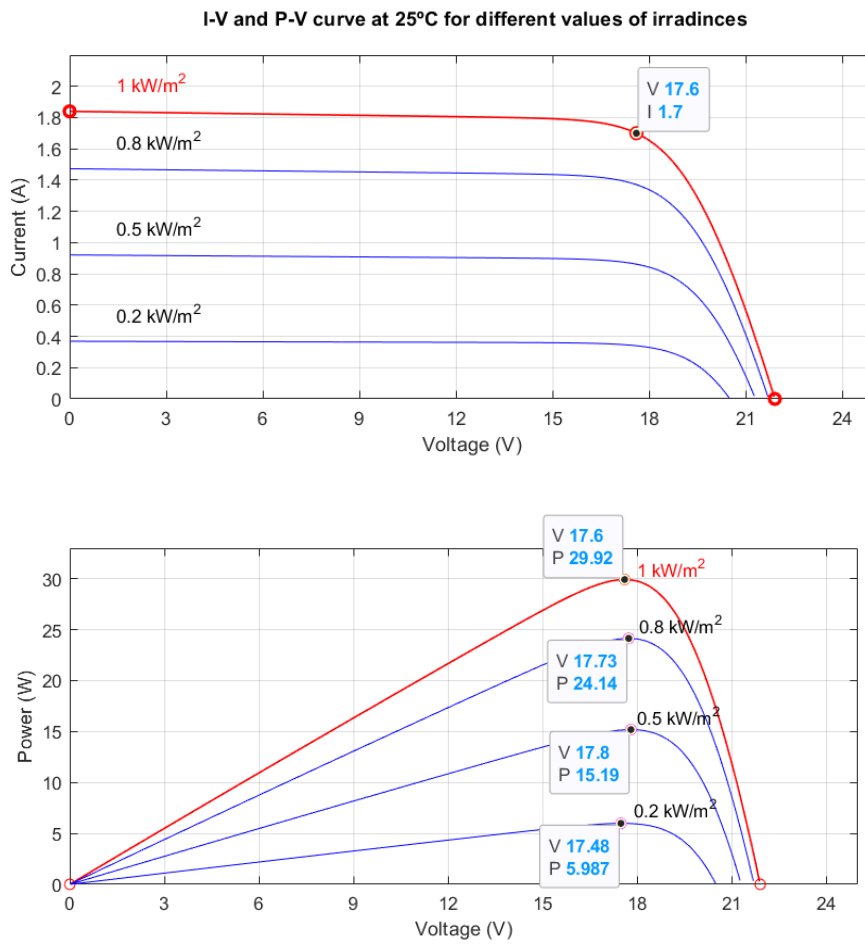
Figure 4.10 PV Simulations for constant temperature and varying irradiance levels
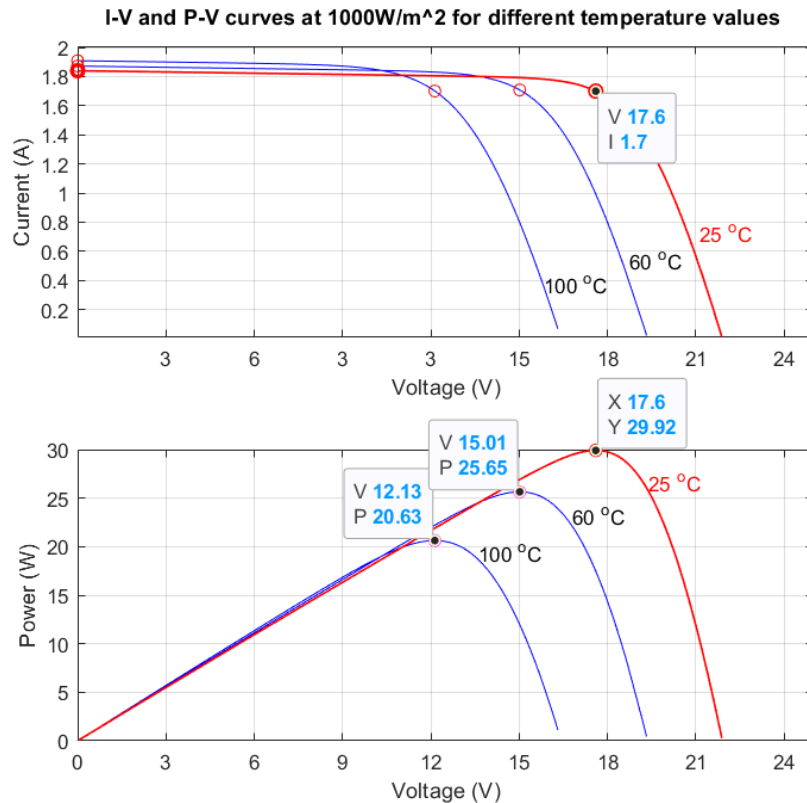
Figure 4.11 PV Simulations for constant irradiance level and varying temperature

In the figures above, we can observe how the different input conditions affect the shape and power available from the PV. In Figure 4.10, where the temperature is kept constant, the lower the solar radiation, the lower the available power is. In Figure 4.11, where the solar radiation is kept constant, the higher the temperature the lower the output power. It can also be noticed that temperature changes lead to output PV voltage changes and irradiance changes lead to output PV current changes. The case studies are based on constant temperature and varying irradiance levels. Hence, Figure 4.10 will be of more interest than Figure 4.11.

Comparing the I-V and P-V curves obtained from the ISDM with the Rs model, with the curves obtained from the PV MATLAB block, we can appreciate how for the STC, their shape is remarkably similar with just a slight change in its curvature. This is due to the fact

that the SDM with Rs model does not include the losses modeled by the shunt resistance. If we were to just simulate and test the power supply under the STC, the ISDM with Rs would have been enough for the simulations, as the precision would not have affected the MPPT control and the entire system itself. However, as the test cases require different solar radiation values, the second approach has been the one opted to use for the remaining modelings and simulations.

4.4 LINEAR MODEL

The following chapters analysis and design require a linear model of the PV module. Accordingly, in this section some ways to linearize the I-V characteristic of the PV module will be explained. Many different approaches to linearize the I-V curve exist. The PV characteristic can be linearized by joining two segments, where the first and second segment follow respectively the following generic equations:

$$I_{PV} = \frac{I_{mpp} - I_{sc}}{V_{mpp}} * V_{pv} + I_{sc} \qquad (4.20)$$

$$I_{PV} = \frac{I_{mpp}}{V_{mpp} - V_{oc}} * V_{pv} - \frac{I_{mpp} * V_{oc}}{V_{mpp} - V_{oc}} \qquad (4.21)$$

Substituting the values defined in Eq. (4.20) and Eq. (4.21), the following I-V characteristic for the PV module given is obtained:
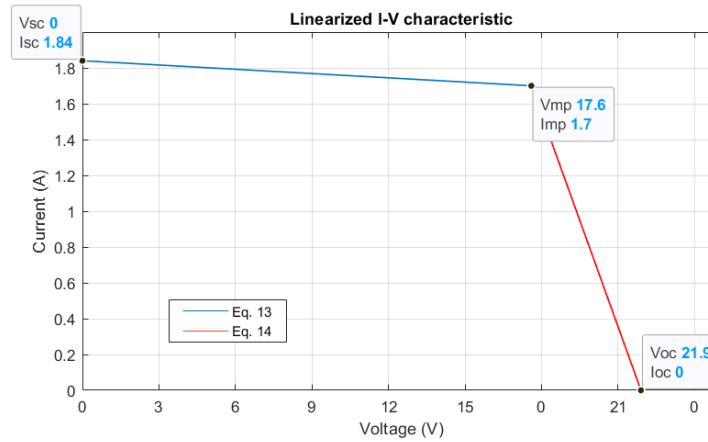
Figure 4.12 Linearized I-V curve of the PV module

Manipulations of Eq. (4.20) and Eq. (4.21), could be done in order to obtain an equivalent circuit to model that behaviour. However, it would require two different equivalent circuits, the first segment will be modeled with a current source and the second one with a voltage source [20].

A practical and more convenient way to linearize the PV model is the following [21] [22]. The linear model can be defined by the tangent line of the I-V characteristic at a general operating point (V, I):

$$i_{PV}(V, I) = (-g * V + I) + g * v_{PV} \qquad (4.22)$$

where g is the derivative of the PV characteristic I-V curve at any operating point:

$$g(V, I) = -\frac{I_o}{V_t * a_m} * e^{\frac{V + I * R_S}{V_t * a_m}} - \frac{1}{R_P} \qquad (4.23)$$

The analysis of the next sections will be based at the PV's maximum power available, hence we could particularize Eq. (4.22) and Eq. (4.23) for (V_{MPP}, I_{MPP}).

The previous equations lead to the following equivalent circuit.
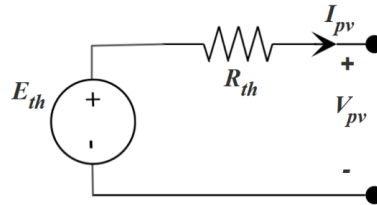
Figure 4.13 Thevenin equivalent circuit of the PV module at the MPP

where:

$$E_{th} = V_{MMP} - \frac{I_{MPP}}{g} \qquad (4.24)$$

$$R_{th} = -\frac{1}{g} \qquad (4.25)$$

The equations above were obtained by specifying Eq. (4.22) at $V = 0$ and $I = 0$ and particularizing the results at the MPP. Substituting the estimated PV model parameters obtained from the MATLAB block of Figure 4.8 in Eq. (4.24) and Eq. (4.25):

$$E_{TH} = 33.3191\,V$$

$$R_{TH} = 9.2466\,\Omega$$

This model was used to design the PV link that interfaces the PV panels with the PVSC.

To arrange the MPPT control algorithm, a more straightforward model was used. The PV was just modeled by an equivalent resistance, where:

$$R_{PV} = \left|\frac{V_{MPP}}{I_{MPP}}\right| = 10.35\,\Omega \qquad (4.26)$$

The actual value is negative, as the tangent to the I-V curve at the MPP is negative.

Chapter 5. CONTROL DESIGN

The power supply will have two control functions at the PV side, as already mentioned in the characteristics of the project. The first one regulates the power extraction of the PV panels in order to meet the load demands and the second one keeps the PV modules operating at its maximum power available. Both controls are respectively the Battery charge and the MPPT control. Moreover, this chapter will also cover the PID control of the output bucks.

5.1 MAXIMUM POWER POINT TRACKING (MPPT)

The MPPT control is in charge of maximizing the power output of the PV modules. The main challenge that any MPPT technique faces, is to correctly track the maximum power operating point of the PV system under: sudden or ramp changes in irradiance levels, sudden or ramp changes in temperature levels, partial shading, oscillations across the MPP and sudden changes at the load level. Some parameters that have to be taken into account in order to choose within all the existent MPPT techniques or in designing a new approach are the following: convergence speed, implementation complexity, the algorithm topology, and if it can be implemented in analog or digital form, circuit parameters that need to be measured and system stability amongst the most important ones [23].

Numerous MPPT techniques exist and can be classified into three categories: off-line, on-line, and artificial intelligence (AI) techniques [24]. Off-line techniques require disconnecting the PV system in order to track the MPP. On the other hand, on-line techniques can track the MPP without switching off the PV system. Within each category, the most common approaches are shown in the next figure.
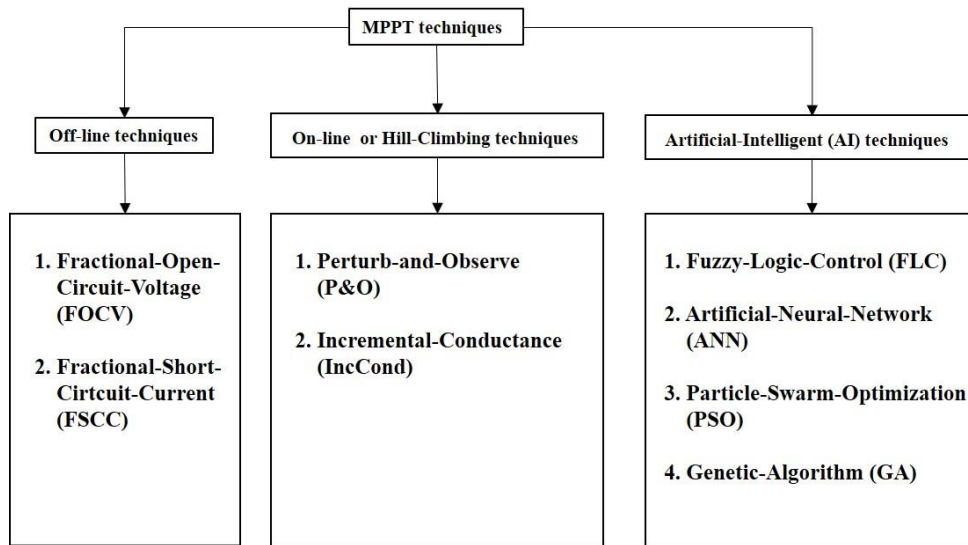
Figure 5.1 Classification of MPPT techniques [24]

Off-line techniques such as FOCV or FSCC, also known for indirect MPPT techniques, do not measure the PV system power output, they track the MPP by a reasonable approximation of where it should be located. This could lead to significant energy losses when the operating conditions differ with the supposed established operating range [13]. Even though they are quite simple and cheap to implement, they have lower efficiencies in comparison to the other existing approaches. They are usually combined with other MPPT methods to increase their tracking efficiency [24]. On the opposite side we have the Artificial-Intelligent techniques, also called, Soft Computing Methods, which are the most effective methods to track the MPP. They are based on probabilistic control strategies and present remarkably high efficiencies in steady state and under varying atmospheric conditions. However, these methods can become expensive, as they require devices that tolerate burdensome computations, and are hard to implement, as many of them require specific knowledge of the PV system, as for example, neural network strategies or advance knowledge to design correctly the parameters that each technique demands [13].

The test profile under which the power supply will be tested does not present sudden solar radiation changes or partial shading conditions, and the existent irradiance ramp change at one of the PV modules is quite slow. Therefore, the basic perturb and observe (P&O) approach will be suitable to obtain good tracking results under this testing scenario. Moreover, the Incremental-Conductance (IC) method will be developed as a second option to confirm if with this method better tracking results are obtained. However, this analysis will be carried out experimentally and will not be part of this thesis work. In theory, the IncCond technique presents better tracking results under sudden irradiance changes than the P&O technique. However, both methods can fail under severe conditions [29]. In addition, these techniques can be adjusted and improved to obtain better tracking results [25]. Further information regarding these approaches will be subsequently described. Within these techniques different implementations exist. It can be implemented in "open" or "closed loop". In "open loop" MPPT systems, the MPPT directly controls and adjusts the duty cycle without any feedback system. However, for "closed loop" MPPT systems, the MPPT can be developed in voltage-mode-based, where the control will track a reference voltage, or in current-based mode, where instead of following a voltage reference it will follow a current reference [13].

The topology presented is based on a PV battery charger system, hence the MPPT can be implemented in "open loop". "Closed loop" MPPT systems are more suitable when noise exists at the output. Therefore, both methods will be developed and implemented in "open loop".

5.1.1 PERTURB AND OBSERVE (P&O)

The P&O approach belongs to the online methods family, also known for direct MPPT techniques. It is one of the most common and popular approaches used, not only because it is simple and effective, but also because it is very flexible and can be easily modified in order to obtain better tracking results [13].

The logic behind the P&O is based on a heuristic search that can be explained with the next figure. If the operating point lies in region 1 of Figure 5.2, any increase in the voltage PV terminals will lead to an increase in the output PV power and vice versa. However, if it lies in region 2, any decrease in the PV voltage terminals will lead to an increase in the output PV power and vice versa.
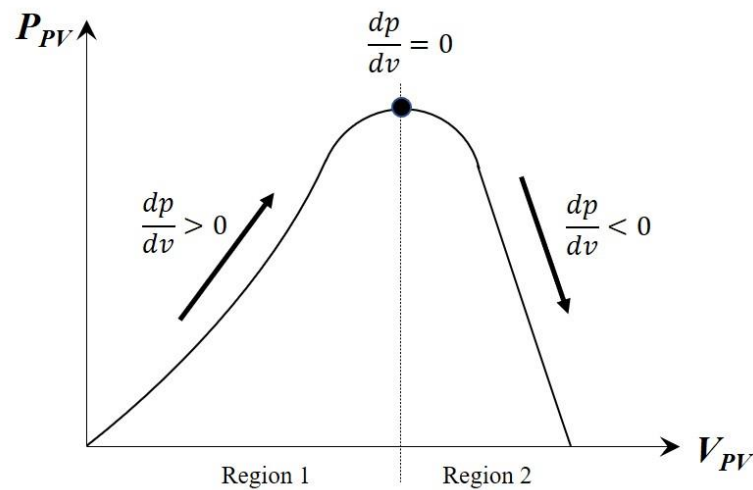
Figure 5.2 P-V curve to illustrate P&O MPPT technique

Therefore, the control will need the voltage and current measurements at the PV in order to identify the region where the PV is operating and dynamically adjust the converter duty cycle with a fixed step in order to modify the voltage at the PV terminals and be able to climb the P-V curve and reach the MPP. Another similar approach would be maximizing the PV converter output power instead of the PV output power. The only difference will be relative to the voltage and current measurements, as they will be done at the output converter terminals. This approach could lead to an overall higher system´s efficiency [13]. However, due to the topology proposed in Chapter 1, Section 1.2, this approach is unachievable, as both PVSC are connected to the same bus.

The basic flowchart of the P&O algorithm that explains the previous process is shown in the next figure.
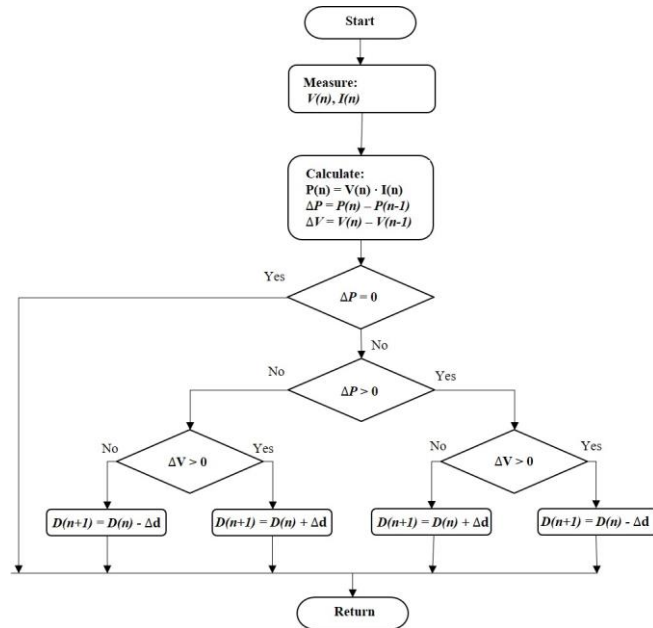
Figure 5.3 Basic P&O algorithm flowchart for Buck Converter

An equivalent and simplified version of the previous P&O flowchart is shown below.
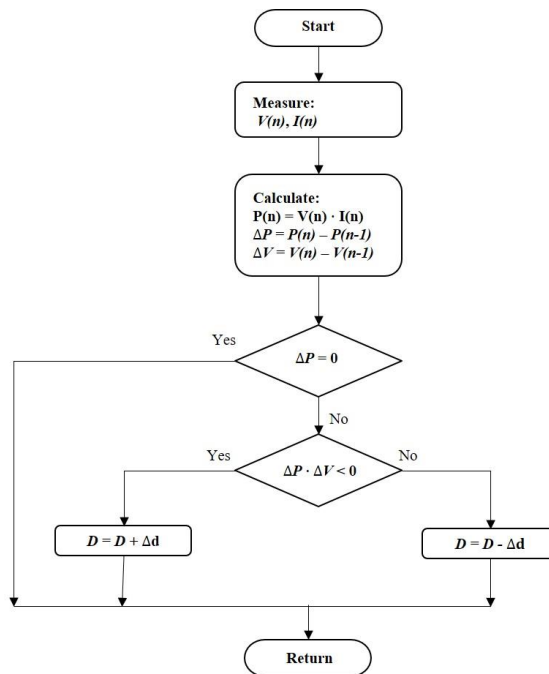
Figure 5.4 Simplified P&O algorithm flowchart

The basic P&O logic can be implanted in analog or digital domain [13]. For simplicity and flexibility purposes, the MPPT control will be implemented in a digital domain, allowing its implementation in just a simple code.

The simplified P&O algorithm can be coded in MATLAB in the following manner.

```matlab
function D  = fcn(V, V_old,P,P_old,delta_D,D_old)

    Delta_P = P - P_old;
    Delta_V = V - V_old;

    if (Delta_V*Delta_P) <= 0
        D = D_old + delta_D; %increase D by fixed step
    else
        D = D_old - delta_D; %decrease D by fixed step
    end
end
```

Figure 5.5 MATLAB code P&O implementation

The previous code was included in a Simulink block for simulation purposes as follows.
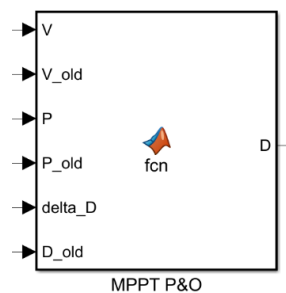
Figure 5.6 Simulink Block that calls back a MATLAB function

Parameters that will need to be considered in the design and implementation of the P&O are the perturbation frequency f_{MPPT}, that determines how often the duty cycle is updated and the fixed step size. Both will be covered in detail in Section 5.2.

53

5.1.2   *INCREMENTAL CONDUCTANCE (INCCOND)*

The IncCond is also a very commercial and common method used in MPPT tracking applications. It is based on the extreme value theorem (EVT), also called the Weierstrass theorem [13]. The EVT states that: *"if a function $f(x)$ is continuous on a closed interval $[a, b]$, $f(x)$ has both a maximum and a minimum on $[a, b]$, and if $f(x)$ has an extremum on an open interval (a, b), the extremum occurs at a critical point"* [26].

The P-V characteristic curve presents a critical point between the short circuit current and the open circuit voltage, as it has been shown in Section 4.3, where the PV module was modeled. Hence, the MPP can be found setting the P-V slope equal to zero, mathematically expressed as:

$$P_{pv} = V_{pv} * I_{pv}$$

$$\frac{dP_{pv}}{dV_{pv}} = I_{pv} + V_{pv} * \frac{dI_{pv}}{dV_{pv}} \qquad (5.1)$$

$$\frac{dP_{pv}}{dV_{pv}} = 0 \rightarrow \frac{dI_{pv}}{dV_{pv}} = -\frac{I_{PV}}{V_{PV}}$$

Therefore, the MPP is defined by Eq. (5.1). This equation will be useful to identify where the operating point is located.

$$Region\ 1\ of\ Figure\ 5.2, \quad \frac{dP_{pv}}{dV_{pv}} > 0 \rightarrow \frac{dI_{pv}}{dV_{pv}} > -\frac{I_{PV}}{V_{PV}} \qquad (5.2)$$

$$Region\ 2\ of\ Figure\ 5.2, \quad \frac{dP_{pv}}{dV_{pv}} < 0 \rightarrow \frac{dI_{pv}}{dV_{pv}} < -\frac{I_{PV}}{V_{PV}} \qquad (5.3)$$

The flowchart for implementing the incremental conductance technique is shown in the next figure. The IncCond will be implemented as a second option in MATLAB to observe if there is a qualitative improvement in regard to the P&O.
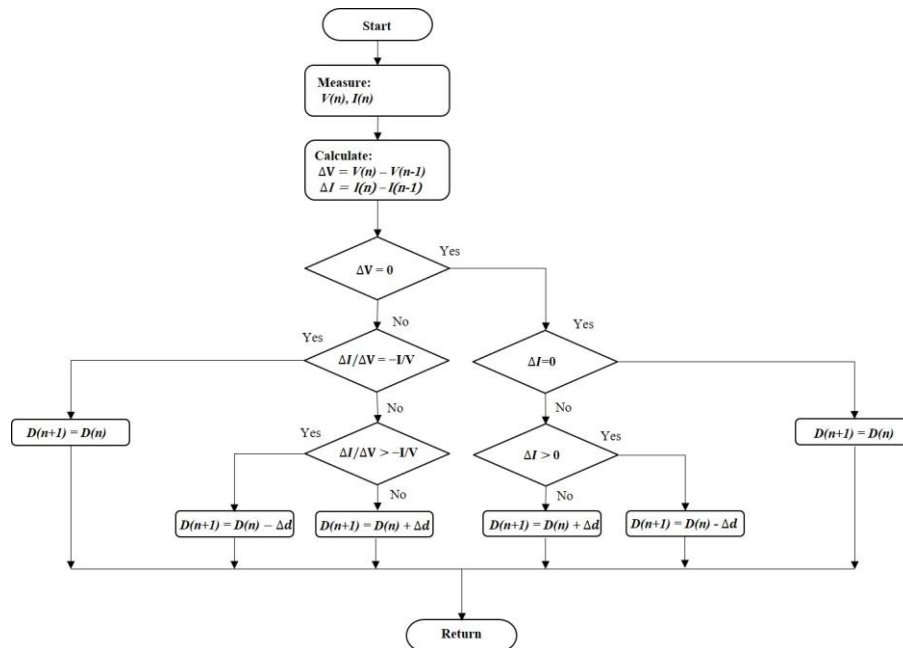
Figure 5.7 Basic flowchart of Incremental Conductance MPPT technique

The flowchart was coded in MATLAB in the following way. It was implemented in an equivalent Simulink block as shown in Figure 5.6.

```matlab
function D   = fcn(V, V_old, I, I_old, delta_D, D_old)
    Delta_I=I-I_old;
    Delta_V=V-V_old;
        if (Delta_V<0)||(Delta_V>0) %dV non zero
                if (Delta_I/Delta_V>-I/V)
                    D=D_old-delta_D;
                elseif (Delta_I/Delta_V<-I/V)
                    D=D_old+delta_D;
                else
                    D=D_old;
                end
        elseif (Delta_I<0)||(Delta_I>0) %dI non zero
                if (Delta_I>0)
                    D=D_old-delta_D;
                elseif (Delta_I<0)
                    D=D_old+delta_D;
                else
                    D=D_old;
                end
        else
            D=D_old; %dV=0 & dI=0
        end

    end
```

Figure 5.8 Incremental conductance MATLAB code implementation.

5.2 DESIGN PARAMETERS: P&O AND INCCOND

In the previous section the algorithm description of both P&O and IncCond techniques were covered. Throughout this section, the parameters that characterize them will be designed. Those parameters are the perturbation period (T_{MPPT}), defined as the time between each perturbation, and the perturbation size step or amplitude (Δd), defined as the size of each step applied to the control variable, in "open loop", the duty cycle. The MPPT control is a nonlinear control system, hence the classical approaches (frequency response techniques) used for linear regulators (PI, PD, PID,…) design cannot be used for this type of control. Consequently, the procedure used was based on a time domain analysis, this allows both (T_{MPPT}) and (Δd) to be designed independently [13].

5.2.1 PERTURBATION CONTROL FREQUENCY

To design the MPPT control parameters, a dynamic model of the topology's first stage is required. It is important to recall that the duty cycle will be dynamically adjusted by the MPPT control in order to track the maximum power available under any atmospheric condition. Hence, it will be useful to determine how duty cycle variations affect the PV output power. This can be described by the control-to-output PV voltage transfer function $G_{d\_V_{PV}}$.

The perturbation period must be higher than the system settling time in order to assure the MPPT's control stability. The system should reach a steady state operating level before applying the next duty cycle step, if not, transient oscillations could lead to inefficiencies in the tracking process. The transfer function $G_{d\_V_{PV}}$ will allow us to determine the settling time of the system (PV voltage) to a step response (duty cycle step), allowing then an optimal perturbation period design.

56

5.2.1.1   *MODELING THE CONTROL TO PV OUTPUT VOLTAGE TRANSFER FUNCTION*

In order to obtain the control to PV output voltage transfer function, an ac small-signal equivalent circuit at the nominal operating conditions (MPP) of the first stage of the power supply was done. The modeling does account for the conduction losses but not the switching losses.

Different approaches exist to construct an ac small signal equivalent circuit. The easiest and most direct one for the topology presented is the circuit averaging technique, that consists of averaging the converter waveforms directly rather than defining the state equations of the system in both operating modes and later reconstructing the averaged small-signal ac equivalent circuit. [9]

Just one of the first stage´s phases of the converter´s topology equivalent circuit is shown in the next figure. It includes all the components derived in the previous sections. The PV source, the PVSC that interfaces the PV link with the battery, and the battery model.
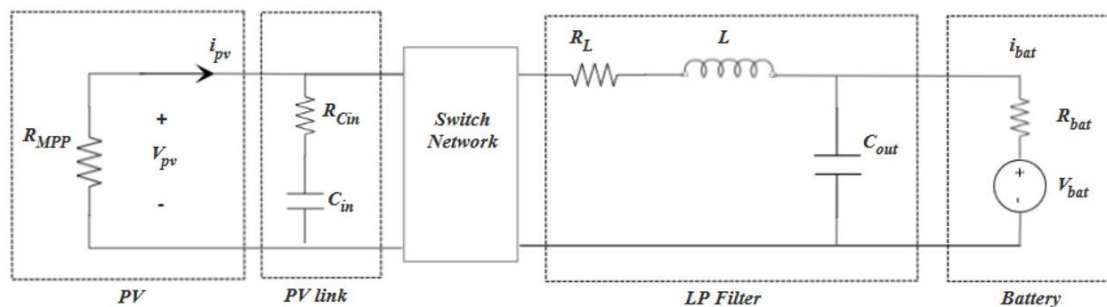
Figure 5.9 Single phase power supply first stage equivalent circuit

In Figure 5.9. we can substitute the switch network by its averaged switch average model and directly obtain the ac small signal equivalent circuit. The average switch model of the buck converter is shown in the next figure, its derivation can be found in [9].
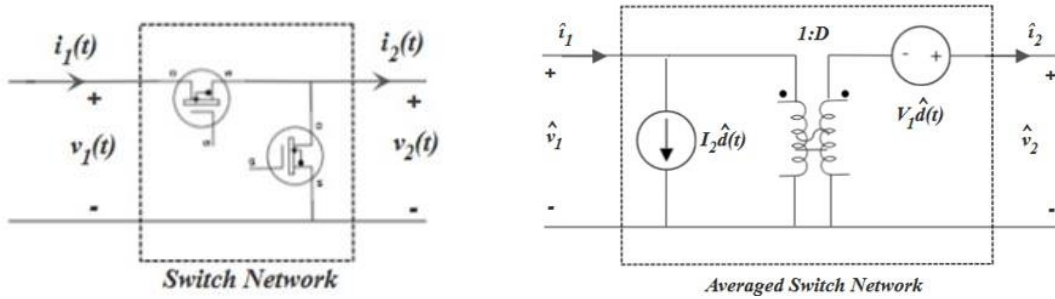
Figure 5.10 Averaged switch model of the Buck Converter for CCM

Substituting the switching network into the equivalent circuit model of Figure 5.9, we obtain the average complete model for the first phase of the PVS topology.
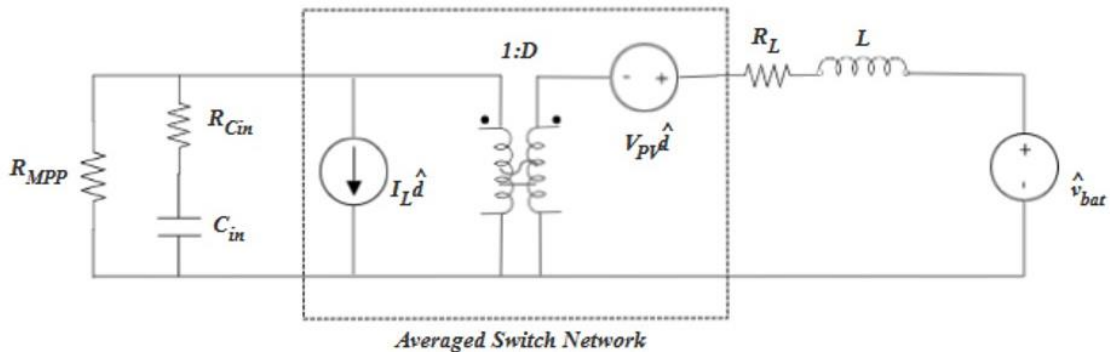
Figure 5.11 Single phase power supply first stage equivalent averaged circuit

The control to output PV voltage is defined as:

$$G_{d\_VPV} = \left. \frac{\hat{V}_{PV}}{\hat{d}} \right|_{\hat{V}_{Bat}=0} \tag{5.4}$$

To derive this equation the following manipulations were applied in Figure 5.11. All the elements in the circuit were expressed in Laplace domain and were moved to the PV side as follows.
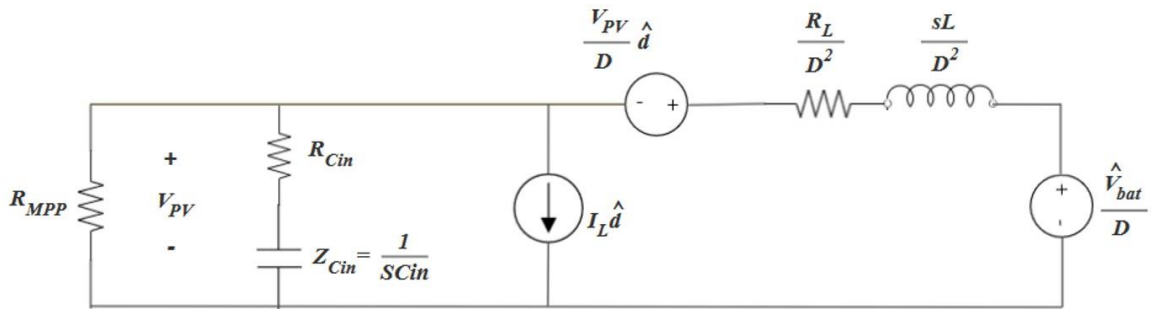
Figure 5.12 Equivalent average circuit expressed from PV side

Applying the principle of superposition, the equivalent circuit of Figure 5.12. can be expressed as the combination of the sources.
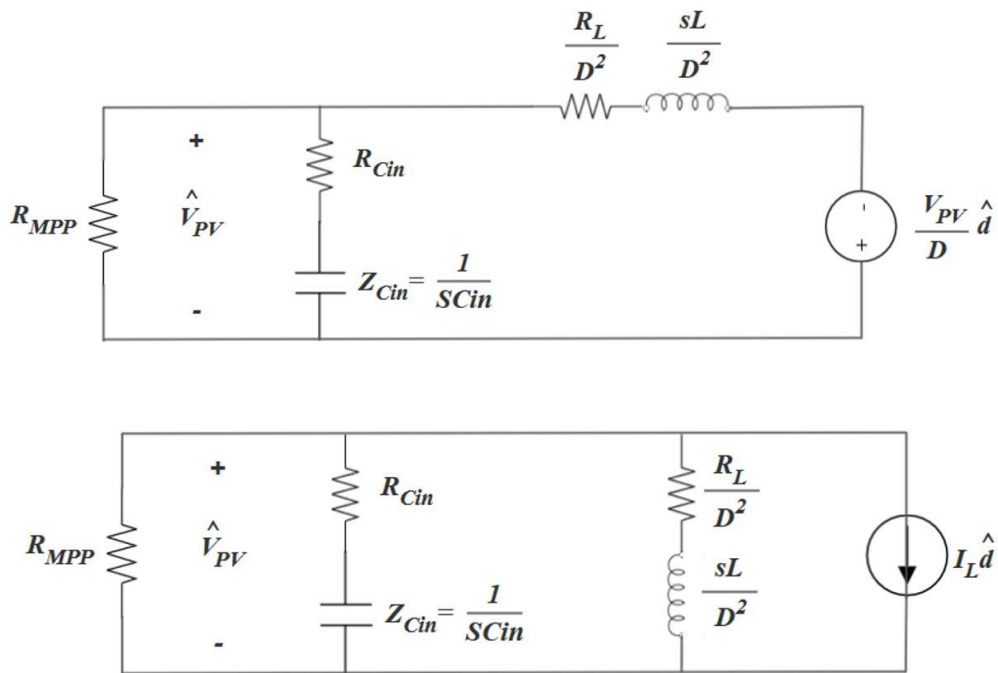
Figure 5.13 Equivalent average circuit expressed as the combination of both sources

The transfer function can then be found by the principle of superposition as:

$$G_{d\_V_{PV}} = \frac{\hat{V}_{PV}}{\hat{d}} = A_1 * (-I_L) + A_2 * \left(\frac{-V_{PV}}{D}\right) \qquad (5.5)$$

Where A_1 and A_2 are the relationship between each source $(I_L, \frac{V_{PV}}{D})$ and the PV output voltage, respectively, I_L is the DC inductor current value at the MPP, V_{PV} is the output voltage at the PV terminals when the PV source is operating at the MPP, and D is the steady state duty cycle value for the MPP condition.

Then A_1 and A_2 can be calculated as:

$$A_1 = ((Z_{MPP}//Z_{C_{in}})//Z\_L) \qquad (5.6)$$

$$A_2 = \left(\frac{(Z_{MPP}//Z_{C_{in}})}{(Z_{MPP}//Z_{C_{in}}) + Z_L}\right) \qquad (5.7)$$

where,

$$Z_{MPP} = R_{MPP} \qquad (5.8)$$

$$Z_{C_{in}} = R_{C_{in}} + \frac{1}{s * C_{in}} \qquad (5.9)$$

$$Z_L = \frac{R_L}{D^2} + \frac{s * L}{D^2} \qquad (5.10)$$

Substituting Eq. (5.6) and Eq. (5.7) in Eq. (5.5):

$$G_{d\_V_{PV}} = \frac{\hat{V}_{PV}}{\hat{d}} = -((Z_{MPP}//Z_{C_{in}})//Z\_L) * (I_L) + -\left(\frac{(Z_{MPP}//Z_{C_{in}})}{(Z_{MPP}//Z_{C_{in}}) + Z_L}\right) * \left(\frac{V_{PV}}{D}\right) \qquad (5.11)$$

where,

$$D = \frac{V_{PV@MPP}}{V_{bat}} \qquad (5.12)$$

Moreover, we will need to calculate the DC inductor as a function of the known variables. A steady state analysis will then be carried out, similar to the one carried out in Chapter 3.

The inductor voltage equation for the switch in position 1 is:

$$v_L = -v_{Bat} + v_{C_{in}} * \left(\frac{R_{MPP}}{R_{MPP} + R_{C_{in}}}\right) - i_L * \left(\frac{R_{MPP} * R_{C_{in}}}{R_{MPP} + R_{C_{in}}}\right) - i_L * R_L \qquad (5.13)$$

Applying the small-ripple approximation (SRA):

$$v_L \approx -V_{Bat} + V_{C_{in}} * \left(\frac{R_{MPP}}{R_{MPP} + R_{C_{in}}}\right) - I_L * \left(\frac{R_{MPP} * R_{C_{in}}}{R_{MPP} + R_{C_{in}}}\right) - I_L * R_L \qquad (5.14)$$

The capacitor current for the switch in position 1 is:

$$i_{C_{in}} = i_{MPP} - i_L = -\frac{v_{PV}}{R_{MPP}} - i_L = -\frac{v_{Bat} + v_L + i_L * R_L}{R_{MPP}} - i_L$$

$$= -\left(\frac{v_{C_{in}} * \left(\frac{R_{MPP}}{R_{MPP} + R_{C_{in}}}\right) - i_L * \left(\frac{R_{MPP} * R_{C_{in}}}{R_{MPP} + R_{C_{in}}}\right)}{R_{MPP}}\right) - i_L \qquad (5.15)$$

$$= -\frac{v_{C_{in}}}{R_{MPP} + R_{C_{in}}} + i_L * \frac{R_{C_{in}}}{R_{C_{in}} + R_{MPP}} - i_L$$

Applying the small-ripple approximation (SRA):

$$i_{C_{in}} \approx -\frac{V_{C_{in}}}{R_{MPP} + R_{C_{in}}} + I_L * \frac{R_{C_{in}}}{R_{C_{in}} + R_{MPP}} - I_L \qquad (5.16)$$

The inductor voltage equation for the switch in position 2 is:

61

$$v_L = -v_{Bat} - i_L * R_L \tag{5.17}$$

Applying the small-ripple approximation (SRA):

$$v_L \approx -V_{Bat} - I_L * R_L \tag{5.18}$$

The capacitor current for the switch in position 1 is:

$$i_{C_{in}} = -\frac{v_{C_{in}}}{R_{MPP} + R_{C_{in}}} \tag{5.19}$$

Applying the small-ripple approximation (SRA):

$$v_L \approx -\frac{V_{C_{in}}}{R_{MPP} + R_{C_{in}}} \tag{5.20}$$

Applying the principle of volt second balance (VSB):

$$< v_L >= 0$$

$$\left(-V_{Bat} + V_{C_{in}} * \left(\frac{R_{MPP}}{R_{MPP} + R_{C_{in}}}\right) - I_L * \left(\frac{R_{MPP} * R_{C_{in}}}{R_{MPP} + R_{C_{in}}}\right) - I_L * R_L\right) * D + (-V_{Bat} - I_L * R_L) * D' = 0 \tag{5.21}$$

$$V_{C_{in}} * \left(\frac{R_{MPP}}{R_{MPP} + R_{C_{in}}}\right) * D - I_L * \left(\frac{R_{MPP} * R_{C_{in}}}{R_{MPP} + R_{C_{in}}}\right) * D - V_{Bat} - I_L * R_L = 0$$

Solving for I_L:

$$I_L = -\frac{V_{Bat}}{R_L + \left(\frac{R_{MPP} * R_{C_{in}}}{R_{MPP} + R_{C_{in}}}\right) * D} + \frac{\left(\frac{R_{MPP}}{R_{MPP} + R_{C_{in}}}\right) * D}{R_L + \left(\frac{R_{MPP} * R_{C_{in}}}{R_{MPP} + R_{C_{in}}}\right) * D} * V_{C_{in}} \tag{5.22}$$

Applying the principle of charge balance (CB):

$$< i_{C_{in}} >= 0$$

$$\left(-\frac{V_{C_{in}}}{R_{MPP} + R_{C_{in}}} + I_L * \frac{R_{C_{in}}}{R_{C_{in}} + R_{MPP}} - I_L\right) * D + \left(-\frac{V_{C_{in}}}{R_{MPP} + R_{C_{in}}}\right) * D' = 0$$

$$-\frac{V_{C_{in}}}{R_{MPP} + R_{C_{in}}} + I_L * D * \frac{R_{C_{in}}}{R_{C_{in}} + R_{MPP}} - I_L * D = 0$$

$$-\frac{V_{C_{in}}}{R_{MPP} + R_{C_{in}}} + D * I_L * \left(\frac{R_{C_{in}}}{R_{C_{in}} + R_{MPP}} - 1\right) = 0$$

(5.23)

Solving for $V_{C_{in}}$:

$$V_{C_{in}} = -D * I_L * R_{MPP}$$

(5.24)

Substituting Eq. (5.24) into Eq. (5.22):

$$I_L = -\frac{V_{Bat}}{R_L + \left(\frac{R_{MPP} * R_{C_{in}}}{R_{MPP} + R_{C_{in}}}\right) * D} + \frac{\left(\frac{R_{MPP}}{R_{MPP} + R_{C_{in}}}\right) * D}{R_L + \left(\frac{R_{MPP} * R_{C_{in}}}{R_{MPP} + R_{C_{in}}}\right) * D} * (-D * I_L * R_{MPP})$$

(5.25)

Solving for I_L:

$$I_L \left(1 + \frac{\left(\frac{R_{MPP}}{R_{MPP} + R_{C_{in}}}\right) * D^2 * R_{MPP}}{R_L + \left(\frac{R_{MPP} * R_{C_{in}}}{R_{MPP} + R_{C_{in}}}\right) * D}\right) = -\frac{V_{Bat}}{R_L + \left(\frac{R_{MPP} * R_{C_{in}}}{R_{MPP} + R_{C_{in}}}\right) * D}$$

$$I_L = -\frac{\frac{V_{Bat}}{R_L + \left(\frac{R_{MPP} * R_{C_{in}}}{R_{MPP} + R_{C_{in}}}\right) * D}}{1 + \frac{\left(\frac{R_{MPP}}{R_{MPP} + R_{C_{in}}}\right) * D^2 * R_{MPP}}{R_L + \left(\frac{R_{MPP} * R_{C_{in}}}{R_{MPP} + R_{C_{in}}}\right) * D}}$$

(5.26)

Finally, substituting the inductor DC current into Eq. (5.6) we obtain:

$$G_{d_{V_{PV}}} = \frac{\hat{V}_{PV}}{\hat{d}}$$

$$= -((Z_{MPP}//Z_{C_{in}})//Z\_L) * \left(-\frac{\dfrac{V_{Bat}}{R_L + \left(\dfrac{R_{MPP} * R_{C_{in}}}{R_{MPP} + R_{C_{in}}}\right) * D}}{1 + \dfrac{\left(\dfrac{R_{MPP}}{R_{MPP} + R_{C_{in}}}\right) * D^2 * R_{MPP}}{R_L + \left(\dfrac{R_{MPP} * R_{C_{in}}}{R_{MPP} + R_{C_{in}}}\right) * D}} \right) - \frac{(Z_{MPP}//Z_{C_{in}})}{(Z_{MPP}//Z_{C_{in}}) + Z_L} * \left(\frac{V_{PV}}{D}\right) \tag{5.27}$$

The procedure above was implemented in MATLAB, the script can be found in the Appendix A.2. This transfer function expresses how duty cycle variations affect the output PV voltage. It was used to determine the settling time of the system under different scenarios. Furthermore, it should be noted that the switching losses were not considered as the switch network used to model the switch topology for the buck did not include them.

5.2.1.2   *THE SYSTEM'S PARAMETERS EFFECT ON THE SYSTEM'S SETTLING TIME*

First, how different solar radiations affect the system will be evaluated in order to select the level at which the settling time is higher. This value will be chosen for the next case scenarios, as to select an optimal perturbation period we will need to determine the settling time under the worst case scenario in order to assure that the system operates with stability under any condition, this will be shown in Figure 5.14. Second, the system's response under different inductance values and how the system is affected by variations in the conduction losses of the inductor will be analyzed. Finally, the system's response under different input capacitor values will be analyzed and how the system is affected by the conduction losses of the capacitor (ESR). The results obtained from analyzing these scenarios will be shown in the next figures. The corresponding MATLAB script used to plot the graphs is provided in Appendix A.3.

Note: The settling time will be assumed to be 5% of the steady state value.

In Figure 5.14, we can appreciate how the step response of the system is affected by the irradiance conditions. The different solar radiation levels affect the steady state value

and the damping factor. The results obtained look coherent, the steady state PV voltage is the highest for the highest irradiance and the lowest for the lowest irradiance level. For the next simulations, $G = 1000 \, W/m^2 \rightarrow R_{MPP} = -10.35 \, \Omega$ was assumed, as it presents the higher settling time.
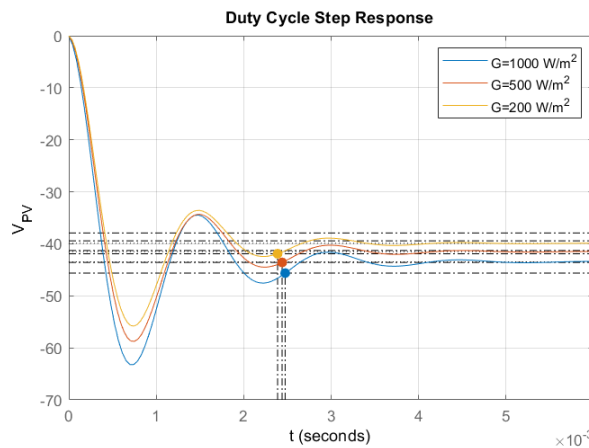
Figure 5.14 Testing the effect of different solar radiation levels

In Figure 5.15, we can see how the dynamics are affected by different inductor values, the lower the inductor, the faster and less damped the system will respond to a step change.
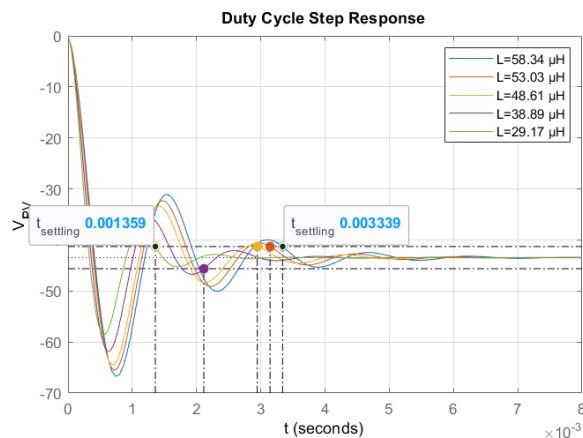
Figure 5.15 Testing the effect of different inductance values

Moreover, in Figure 5.16 we can appreciate the effect conduction losses have on the system's response, the higher the inductor resistive losses the more damped and fast the response is.
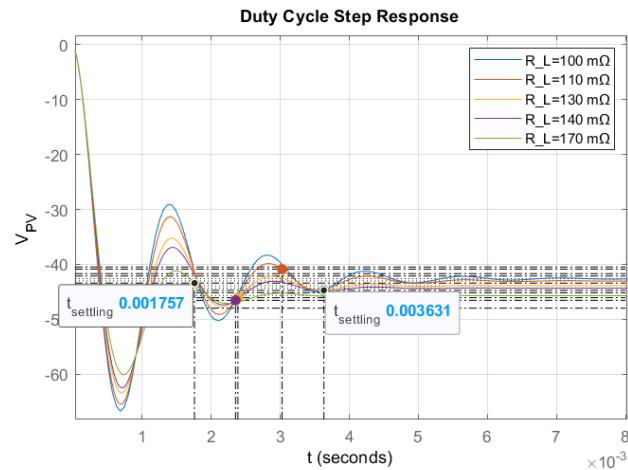
Figure 5.16 Testing the effect of different R_L values of the inductance

Furthermore, in Figure 5.17, we can appreciate how the higher the capacitor the lower and more damped the response is.
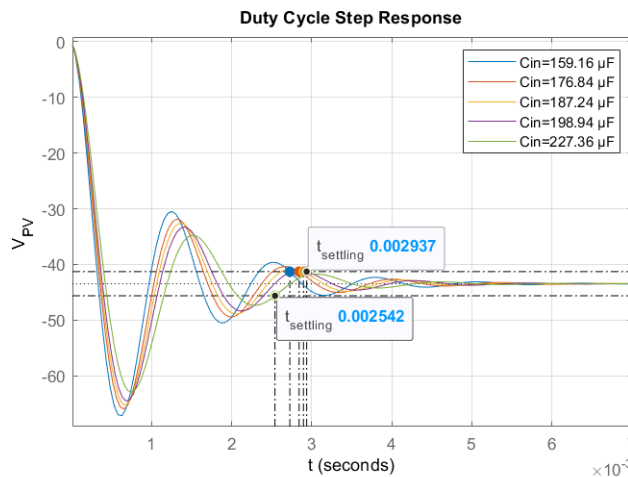
Figure 5.17 Testing the effect of different C_{in} values

Finally, in Figure 5.18 we can appreciate how higher "ESR" values lead to a faster and more damped response.
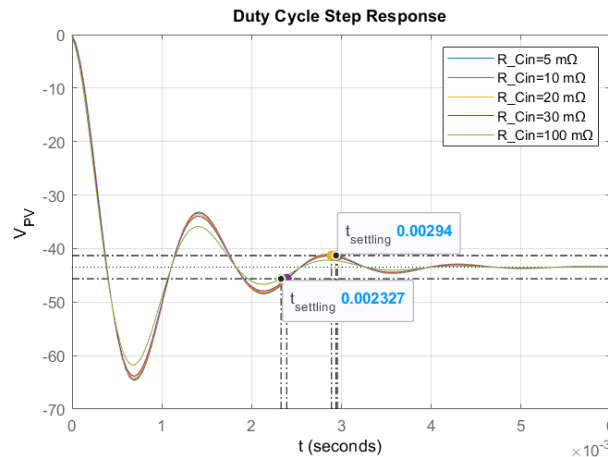
Figure 5.18 Testing the effect of different ESR values of input capacitance

From the graphs above, the following conclusions can be obtained. The higher the inductor and capacitor value the slower and more damped the system response will be and vice versa. Furthermore, the conduction losses of either components, damp the response and make the system reach a steady state operation faster. These just explained considerations must be taken into account, as having more conduction losses will affect the power supply's overall efficiency. However, it could also reduce the settling system's time response increasing the MPPT control's efficiency to an overall increase. This analysis gives an approximate perspective on how the values of the components selected will affect the system's response. This will be taken into account by the hardware team when selecting the correct components.

The final perturbation frequency value will be chosen based on simulation trial an error in order to adjust its value to a more optimal choice. As the control is going to be implemented in digital domain, additional noise sources will exist (voltage and current sensors, analog-to-digital converter (ADC), quantization resolution of the MCU,…), this could affect the MPPT performance and its tracking capability. A more detailed analysis on

how to account to MPPT performance under noisy environments can be found in [13]. From the graphs shown above, the worst case scenario occurs at $T_{settling} = 0.003339\ s$ that is equivalent in the frequency domain to $f_{loop} \approx 300\ Hz$. This perturbation frequency value will be selected as the initial stating point of the MPPT perturbation frequency design.

5.2.2 PERTURBATION SIZE STEP

The perturbation size step also has to be carefully designed. It involves a tradeoff between how fast and how precise the tracking process is. The smaller the perturbation step is the more precise the control will be, resulting in less oscillations around the MPP. However, it will worsen the control speed as it will make the tracking process slower. The perturbation's step design will be based on the expected change in the irradiance conditions, this will determine the minimum value required for the perturbation step [13]. A more detailed analysis could also include the noise effects. However, this will be considered by a reasonable approach instead of an exact design.

An expression that can be used to define the perturbation size step is the following:

$$\Delta d > \frac{1}{G_o} * \sqrt{\frac{V_{MPP} * K_{PH} * |\dot{G}| * T_{MPPT}}{H * V_{MPP} + \frac{1}{R_{MPP}}}} \tag{5.28}$$

where:

$$G_o - DC\ gain\ of\ transfer\ function\ G_{d_{V_{PV}}} \tag{5.29}$$

$$K_{PH} = \frac{\partial i_{PV}}{\partial G} - PV\ material\ constant \tag{5.30}$$

$$H = -\frac{1}{2} * \frac{\partial^2 i_{PV}}{\partial^2 v_{PV}}|_{MPP}$$

$$= \frac{1}{2} * \frac{1}{a * N_s * V_t} * \left(1 - \frac{R_S}{R_{MPP}}\right)^3 \qquad (5.31)$$

$$* \left(\frac{I_o}{a * N_s * V_t} * e^{\frac{V_{MPP} + R_S * I_{MPP}}{a * N_s * V_t}}\right)$$

$$\dot{G} - average\ rate\ of\ change\ of\ solar\ radiation\ expected\ [\frac{W}{m^2 * s}] \qquad (5.322)$$

This expression is derived and carefully explained in [13] and it is based on the following. The perturbation size step Δd applied to the converter by the P&O or IncCond will cause a shift in the PV output power ΔP_d. Similarly, a change in the solar radiation ΔG will also cause a shift on the PV output power ΔP_G. Therefore, in order to correctly track the MPP, the following condition has to be met.

$$|\Delta P_d| \geq |\Delta P_G| \quad (16) \qquad (5.33)$$

If not, the control algorithm could not distinguish between the shifts in the power produced by the perturbation size step or by the shifts in irradiance levels changes. Substituting the expressions of ΔP_d and ΔP_G in Eq. (5.33) and applying some manipulations will result in Eq. (5.28).

These equations were implemented and solved in MATLAB. The MATLAB script can be found in the Appendix.

The test cases already define the expected rate of change of the irradiance level, the MPPT control should be able to track the MPP under irradiance ramp change. While the PV module 1 will receive constant irradiance ($G = 1000W/m^2$), the PV module 2 will go from $G = 500\ W/m^2$ to $G = 1000W/m^2$ in approximately 1 min (Section 1.1.4). Therefore, the average rate of change for the test cases will be of $\dot{G} = 8.33\ W/(m^2 * s)$. For this irradiance rate of change and assuming average components parameters based on the analysis on the

69

previous sections, the minimum duty cycle perturbation step required is equal to $\Delta d_{min} = 0.00065$ ($f_{MPPT} = 300 Hz$), slightly higher if we account the noise effects. However, in order to simulate its behaviour, the irradiance ramp change will be much faster, as simulating the converter for minutes can lead to memory allocation problems as it requires burdensome computations. For simulation purposes, the ramping up was assumed to be in 1 seconds leading to an average rate of change of solar radiation of $\dot{G} = 500 \ W/(m^2 * s)$, hence $\Delta d_{min} = 0.0051$ ($f_{MPPT} = 300 Hz$). It can be seen how now the minimum duty cycle step is around 10 times higher than the test case scenario. This value obtained, indicates the minimum duty cycle step required to be able to track the MPP under irradiance ramp changes.

Moreover, it should be noted that the smaller the step, the slower a more precise the control is. As explained before, a tradeoff between accuracy and tracking speed exists. The final choice will be adjusted in the simulation environment, Chapter 6.

5.3 BATTERY CHARGE CONTROL

This section will cover the battery charge control. The battery charge controller will provide over current and over voltage protection to the battery. For the purpose of this work, the full battery charge control will be implemented in the simulation models. However, only the compensator coefficients of the voltage protection control will be designed.

Recalling the control functionalities explained in Section 1.1.3, at Mode I the PV output power should be regulated to meet the load and in Mode II the PV output power should be kept at its MPP and verifying that the battery charging limits are met. Therefore, in Mode I the battery charge control will step in limiting the bus voltage to the reference bus voltage and in Mode II the battery charge control will ensure that the battery is being charged without surpassing its maximum voltage and current limits.

This control will be digitally integrated with the MPPT control hence the sampling frequency and control loop frequency of the compensator will be tied to the MPPT perturbation frequency. To avoid this, some manipulations to the control code could be done in order to detect when the battery control is in constant voltage mode and modify its sample and loop frequency. However, for simplicity both controls were assumed tied.

The control to output voltage transfer function of the PVS Buck converter is defined as:

$$G_{vd} = \frac{\hat{V}_{bat}}{\hat{d}}\Bigg|_{\hat{V}_{PV}=0}$$

(5.34)

$$= V_{PV} * \left(\frac{C_{out} * R_{Cout} * s + 1}{C_{out} * L * s^2 + (C_{out} * R_{Cout} + C_{out} * R_L) * s + 1} \right)$$

And was obtained assuming $(\hat{V}_{PV} = 0,\ R_{Bat} = 0)$ and solving for $\frac{\hat{V}_{bat}}{\hat{d}}$ in the following small ac signal model.
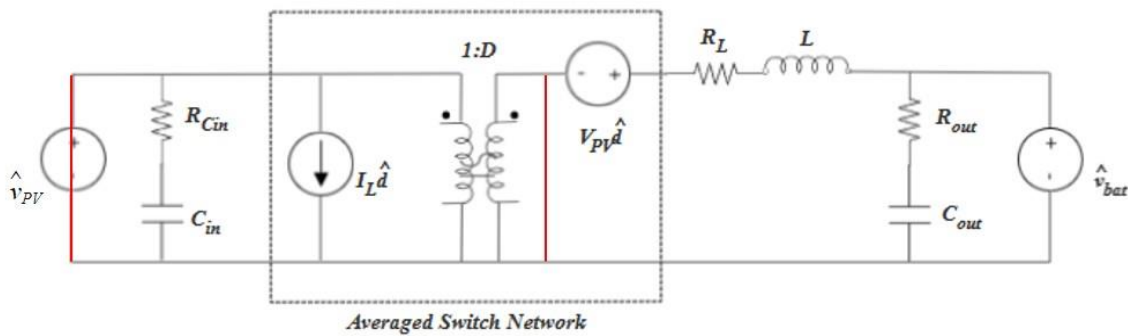
Figure 5.19 Small signal equivalent circuit of the PVS Buck converter

Substituting the final circuit parameters obtained by the hardware team shown in Chapter 3. into Eq. (5.35). will result in the following control to output voltage transfer function:

$$G_{vd} = \frac{2.704e - 06\ s\ +\ 19.85}{9.4e - 09\ s^2 +\ 6.836e - 06\ s\ +\ 1}$$

The bode plot is shown in the next figure and was done to see the frequency response of the plant system.
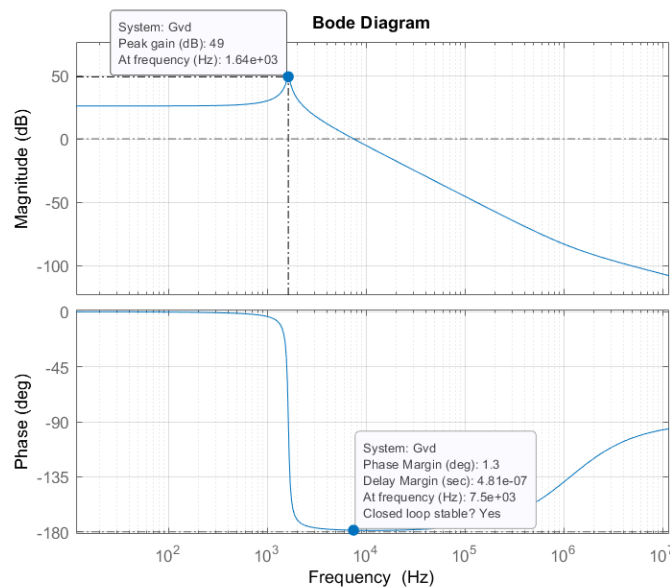
Figure 5.20 Bode plot of plant model

From the Bode plot we can see that the resonance frequency occurs at $1640\ Hz$. The sampling frequency should be 3 to 5 times lower than the resonance frequency, in order to avoid resonance. Even though the sampling frequency is determined by the MPPT control, this condition must be also taken into account. The sampling rate of the MPPT control was chosen to be around 300 Hz (Section 5.2.1), this frequency satisfies the above condition. It could possibly be increased but should remain below 700 Hz as the ADC sampling should not see resonance.

According to the Nyquist criterion the crossover frequency or system's bandwidth should be at least half of the sampling frequency. For power converters the crossover

frequency is recommended to be between $1/10^{th}$ and $1/20^{th}$ of the sampling frequency [27]. Hence, the range of the bandwidth should range between 5Hz to 30Hz approximately.

In order to reach that bandwidth range, an integral compensator will be used. The integral compensator in discrete domain can be defined as:

$$u[n] = u[n-1] + K_i * e[n] \qquad (5.36)$$

where K_I is the integral compensator coefficient.

In order to calculate the compensator gain, the Bilinear Transform Method was used, where its design flow is explained in [27]. The discrete control will be expressed in the p-domain, a continuous time domain, where the common frequency techniques can be applied to design the integral gain. Thereupon, the obtained value in the p domain will be mapped back to the discrete domain (z-domain). This results in the following process.

First, the direct Z-transform is applied to Eq. (5.37), resulting in the following transfer function:

$$G_I(z) = \frac{K_i}{1 - z^{-1}} \qquad (5.37)$$

Secondly, the Z-transform transfer function is mapped into the p-domain and expressed in its equivalent form (frequency inversion [9]):

$$G_I'(p) = \frac{K_i}{Ts} * \frac{1 + \dfrac{p}{wp}}{p} \quad \rightarrow \quad G_I'(p) = G_{PI\_inf}' * \left(1 + \frac{w_{PI}}{p}\right), \quad G_{PI\_inf}' > 0 \qquad (5.38)$$

where Ts represents the control loop/sampling frequency and w_p is defined as:

$$w_p = \frac{2}{T_s} \qquad (5.39)$$

Finally, once, G_{PI_inf}' and w_{PI} are determined, the integral gain will be calculated as:

73

$$K_i = 2 * G'_{PI\_inf} * \frac{w_{PI}}{w_p}, \quad w_p = \frac{2}{T_s} \tag{5.40}$$

The equations derived in this procedure and further details regarding the reasoning behind this process can be found in [27].

The following table shows the different K_i values obtained for different crossover frequencies, assuming 300Hz for the sampling frequency. The MATLAB script used to calculate these values is in Appendix A.5.

Calculations for: fs=300Hz	Gain Margin(dB)	Phase Margin(°)	$f_{crossover}(Hz)$	K_i
1	Inf	90.071	0.119	0.0001257
2	Inf	90.107	0.179	0.0001885
3	Inf	90.142	0.238	0.0002513
4	Inf	90.178	0.298	0.0003142
5	Inf	90.214	0.357	0.0003770
6	Inf	90.285	0.476	0.0005027
7	Inf	90.356	0.596	0.0006283
8	Inf	90.712	1.191	0.0012566
9	Inf	91.068	1.787	0.0018850
10	Inf	91.424	2.383	0.0025133
11	Inf	91.780	2.979	0.0031416
12	Inf	92.136	3.576	0.0037699
13	Inf	92.492	4.173	0.0043982
14	Inf	92.849	4.771	0.0050265
15	Inf	93.205	5.369	0.0056549

Table 5.1 Different compensator gain for different crossover frequencies

The highest possible bandwidth for the 300 Hz sample frequency is of 5.4 Hz, higher K_I values leads to several crossings at the 0 dB level making the system's response unstable. The next figure shows the Bode plot of the open loop frequency response for $K_I = 0.0038$. It can be observed that the closed loop system will be stable.
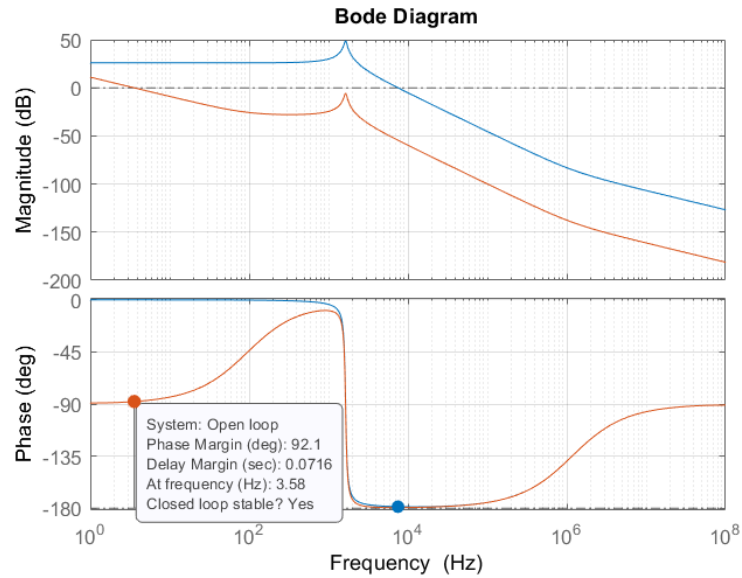
Figure 5.21 Open loop gain Bode plot

The implementation flowchart of the full battery charge control is shown in the next figure.
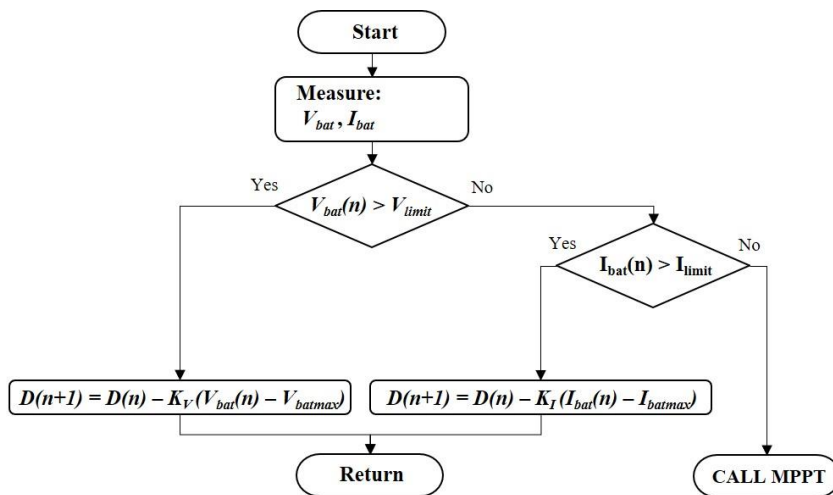
Figure 5.22 Flowchart of battery charge controlled integrated with MPPT functionality

As we see in Figure 5.22 if any of the battery limits are surpassed the control will reduce the duty cycle in order to reduce the output voltage. If not, the PVSC control will enter in the MPPT mode. Its implementation in the MATLAB will be as follows.

The integral process of Figure 5.22 when the control enters in the battery voltage protection mode is the following:

$$D(n + 1) = D(n) - K_V * (V_{bat(n)} - V_{batmax}), \ K_v = K_i \ previously \ desigend \qquad (5.41)$$

It resembles the equation that defines the integral compensator in discrete domain, Eq. (5.36). The negative sign shifts the PV operating point towards the open-circuit voltage (voltage source mode/region 2 of Figure 5.2) instead of moving into the short-circuit region (current source mode/region 1 of Figure 5.2). The reason behind this is that the damping performance is better in region 1 than in region 2 [19].

The flowchart of the Battery charge controller will be integrated with the MPPT P&O and IncCond codes of Figures 5.5 and 5.8, respectively in the way shown in the next figure. The complete code can be found in Appendix.

```
%Battery Charge Control
    if  V_batt >= V_limit    %Voltage Protection
        D = D_old - K_Vlim_1*(V_batt - V_batMax);
            %Define Sates to visualize operating mode
                BATcontrol_state_1=-3;
                state_1=2;
                MPPT_state_1=0;
    elseif abs(I_batt) >= I_limit    %Current Protection
        D = D_old - K_Ilim_1*(I_batt - I_cellMax);
            %Define Sates to visualize operating mode
                BATcontrol_state_1=-2;
                state_1=2;
                MPPT_state_1=0;
```

Figure 5.23 Battery charge control MATLAB code script

5.4 OUTPUT BUCK CONVERTERS CONTROL DESIGN

Throughout this section the 3.3V and 5V output Buck converters control will be covered. There are no requirements regarding the dynamic performance of the converters, the only specification is that the loads voltage should be met. Therefore, an integral action must be used in order to track the reference at its exact value. This could be enough for the purpose of the overall project specifications. However, to improve performance and be able to track the reference voltage faster a PID compensator will be designed. It will be implemented through the MCU.

The design processed that will be followed is the same as the one used to design the Battery charge controller. The control to output voltage transfer function of the Buck converter in its standard form, assuming is lossless, is derived in [9] and has the following form:

$$G_{vd} = \left.\frac{\hat{V}_{bat}}{\hat{d}}\right|_{\hat{V}_{PV}=0} = G_{d0} * \frac{1}{1 + \frac{s}{Q*w_o} + \left(\frac{s}{Q*w_o}\right)^2} \qquad (5.42)$$

Where:

$$G_{d0} = \frac{V_{out}}{D} \qquad (5.43)$$

$$Q = R * \sqrt{\frac{C}{L}} \qquad (5.44)$$

$$w_0 = \frac{1}{\sqrt{L*C}} \qquad (5.45)$$

Substituting the final circuit parameters obtained by the hardware team shown into Eq. 5.42 will result in the following control to output voltage transfer function (assuming 5V load)

77

$$G_{vd_{5V}} = \frac{2.263e13}{2.66e04\ s^2 + 1.064e08\ s\ +\ 2.829e12}$$

<div align="right">(5.46)</div>

The bode plot is shown in the next figure and was done to see the frequency response of the system.
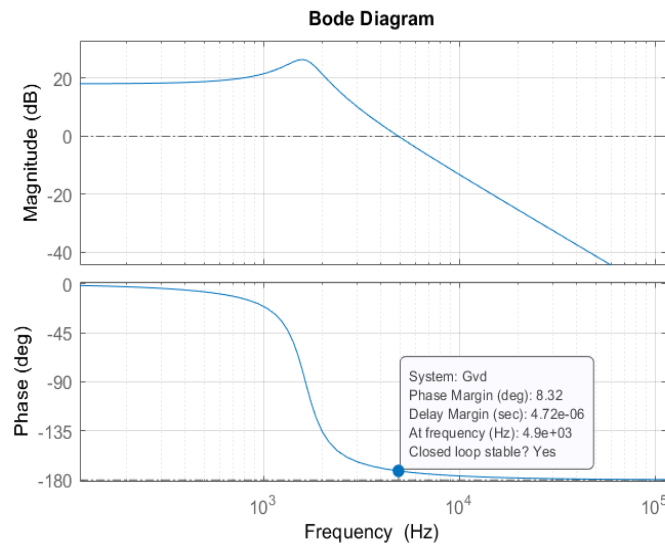
Figure 5.24 Bode plot of the plant model

The PID control is not tied to any additional control as the Battery Charge control is tied to the MPPT control. Therefore, the sampling frequency will be chosen to be equal to the switching converter frequency. This is the common choice for PWM switching converters, all the reasons are explained in [27].

$$f_{sampling} = f_{sw} = 100\ kHz$$

<div align="right">(5.47)</div>

Thereupon, the crossover frequency should be between 5 to 10 kHz, 1/20th to 1/10th of the switching converter, as explained for the battery charge control. At this bandwidth, the plant model has a very low phase margin. Hence, the compensator should increase the phase margin to 45-60º range, normal average range design [29].

The PID realization equations in its noninteracting structure are shown below [27].

78

$$u_p[n] = K_p * e[n] \tag{5.48}$$

$$u_i[n] = u_i[n-1] + K_i * e[n] \tag{5.49}$$

$$u_d[n] = K_d * (e[n] - e[n-1]) \tag{5.50}$$

$$u[k] = u_p[n] + u_i[n] + u_d[n] \tag{5.51}$$

Applying the Z-transform to the equations above and expressing them in the (p-domain) in its multiplicative form, as done for the battery charge control:

$$G'_I(p) = G'_{PI\_inf} * \left(1 + \frac{w_{PI}}{p}\right) * G'_{PD_0} * \frac{1 + \frac{p}{w_{PD}}}{1 + \frac{p}{w_P}}; \; G'_{PI\_inf}, G'_{PD_0} > 0, w_p = \frac{2}{T_{sample}} \tag{5.52}$$

Where $G'_{PI\_inf}, G'_{PD_0}, w_{PI}, w_{PD}$ will be calculated to obtain the desire system bandwidth and gain margin. Consequently, the compensator gain parameters in the discrete domain for (K_p, K_i, K_d) will be calculated with the following equations [27]:

$$K_P = G'_{PI\_inf} * G'_{PD_0} * \left(1 + \frac{w_{PI}}{w_p} - \frac{2 * w_{PI}}{w_p}\right) \tag{5.53}$$

$$K_I = 2 * G'_{PI\_inf} * G'_{PD_0} * \frac{w_{PI}}{w_p} \tag{5.54}$$

$$K_D = \frac{G'_{PI\_inf} * G'_{PD_0}}{2} * \left(1 - \frac{w_{PI}}{w_p}\right) * \left(\frac{w_p}{w_{PD}} - 1\right) \tag{5.55}$$

and would need to verify the following conditions in order to be a valid design:

$$K_P, K_I, K_D \geq 0 \tag{5.56}$$

$$0 < w_{PI} < w_p \tag{5.57}$$

$$0 < w_{PD} < w_p \tag{5.58}$$

In order to calculate G'_{PI_inf}, G'_{PD_0}, w_{PI}, and w_{PD} so that the desired phase margin and crossover frequency are obtained, the following procedure will be carried out. It will be analytically explained as it will be implemented in code so that assorted designs can be done. First, the crossover frequency and phase margin will be achieved by the design of the PD compensator. Consequently, the integral part will be introduced to increase low frequency gain and be able to achieve zero error.

5.4.1 PD COMPENSATOR DESIGN

The magnitude and phase constraints to design the PD compensator are the following:

$$\left| G'_{vd}\left(jw'_{cross_{design}} \right) \right| * \left| G'_{PD}\left(jw'_{cross_{design}} \right) \right| = 1 \tag{5.59}$$

$$\angle G'_{vd}\left(jw'_{cross_{design}} \right) + \angle G'_{PD}\left(jw'_{cross_{design}} \right) = -\pi + \varphi_{margin} \tag{5.60}$$

To obtain $w'_{cross_{design}}$ the following equation will be used:

$$w' = \frac{2}{T_{sample}} * \tan\left(w * \frac{T_{sample}}{2} \right) \tag{5.61}$$

This equation purpose is to prewarp a z-domain frequency into the corresponding p-domain frequency. At the crossover frequency:

$$w'_{cross_{design}} \approx w_{cross_{design}} \tag{5.62}$$

Therefore,

$$G'_{vd}\left(jw'_{cross_{design}}\right) = G_{vd}\left(jw_{cross_{design}}\right) \tag{5.63}$$

Solving Eq. (5.60), w_{PD} is determined as:

$$\angle G_{vd}\left(jw_{cross_{design}}\right) + \left(\arctan\left(\frac{w'_{cross_{design}}}{w_{PD}}\right) - \arctan\left(\frac{w'_{cross_{design}}}{w_{PD}}\right)\right) = -\pi + \varphi_{margin} \tag{5.64}$$

$$w_{PD} = \frac{w'_{cross_{design}}}{\tan\left(-\pi + \varphi_{margin} - \angle G_{vd}\left(jw_{cross_{design}}\right) + arctan\left(\frac{w'_{cross_{design}}}{w_{PD}}\right)\right)} \tag{5.65}$$

The maximum phase margin that can be obtained is derived from the w_{PD} condition expressed in Eq. (5.58) [28]:

$$\angle G_{vd}\left(jw_{cross_{design}}\right) < \varphi_{margin}$$

$$< \left(\angle G_{vd}\left(jw_{cross_{design}}\right) + 90° - arctan\left(\frac{w'_{cross_{design}}}{w_p}\right)\right) \tag{5.66}$$

Substituting the design specifications (fc=10000 Hz):

$$\sim 0° < \varphi_{margin} < \sim 72° \tag{5.67}$$

This shows how a phase margin between 45 to 60 degrees will be achievable.

From the magnitude constraint, Eq. (5.59), G'_{PD_0} will be determined:

$$G'_{PD_0} = \frac{1}{\left|G_{vd}\left(jw_{cross_{design}}\right)\right|} * \frac{\sqrt{1 + \left(\frac{w_{cross_{design}}}{w_p}\right)^2}}{\sqrt{1 + \left(\frac{w_{cross_{design}}}{w_P}\right)^2}} \tag{5.68}$$

Thus, once the PD compensator is determined the Integral action will be introduced.

5.4.2   I COMPENSATOR DESIGN

The integral part will allow to track the reference 5V and 3.3V load reference at null steady state error. The w_{PI} will be chosen to be 1/30$^{\text{th}}$ of the crossover frequency, this decision was based on trial and error so that the integral compensator does not alter the phase margin at the crossover frequency design. Moreover, G'_{PI_inf} will be chosen to be equal to 1 so that the loop margin is not altered by the integral compensator. The Bode plot of the PID realization in the p-domain should have a similar shape to the following figure.
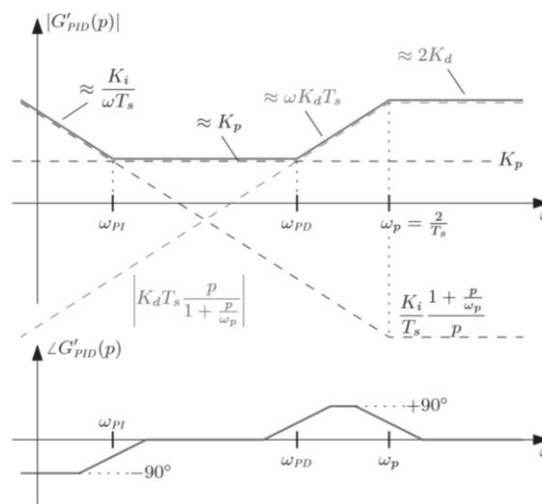
Figure 5.25 Asymptotic Bode plot of the digital PID compensator (p-domain) [27]

The expressions above used in for the PID compensator design were coded in MATLAB in order to have a direct and fast way to design the PID coefficients. The code can be found in Appendix A.6 for the 5V load, and Appendix A.7 for the 3.3V load. The following compensator parameters were obtained running the MATLAB script for different phase margins at $f_c \approx 10kHz$ and different crossover frequencies at $\varphi_m \approx 57°$, for the 5V load and the 3.3V load. The parts highlighted in blue show the chosen value towards the simulations.

PID: 5V	Gain Margin	Phase Margin	$f_{crossover}(Hz)$	Ki_5	Kp_5	Kd_5
1	Inf	45.752	9837.597	0.046	2.303	5.314
2	Inf	46.778	9832.341	0.045	2.232	5.409
3	Inf	47.806	9827.106	0.043	2.161	5.501
4	Inf	48.836	9821.904	0.042	2.088	5.592
5	Inf	49.868	9816.748	0.040	2.015	5.682
6	Inf	50.902	9811.650	0.039	1.942	5.769
7	Inf	51.939	9806.624	0.037	1.867	5.855
8	Inf	52.977	9801.685	0.035	1.793	5.939
9	Inf	54.018	9796.847	0.034	1.717	6.022
10	Inf	55.061	9792.126	0.032	1.641	6.102
11	Inf	56.105	9787.539	0.030	1.565	6.181
12	Inf	57.152	9783.100	0.029	1.488	6.257
13	Inf	58.201	9778.828	0.027	1.411	6.332
14	Inf	59.251	9774.738	0.025	1.333	6.405

Table 5.2 PID 5V Load coefficients for $f_c \approx 10kHz$ and $\varphi_m \approx [43;60]$

PID: 5V	Gain Margin	Phase Margin	$f_{crossover}(Hz)$	Ki_5	Kp_5	Kd_5
1	Inf	56.928	4981.953	0.0056	0.556	2.610
2	Inf	56.918	5228.061	0.0063	0.603	2.791
3	Inf	56.910	5473.673	0.0072	0.652	2.970
4	Inf	56.902	5718.760	0.0080	0.701	3.150
5	Inf	56.900	5966.763	0.0090	0.750	3.328
6	Inf	56.892	6453.549	0.0109	0.849	3.686
7	Inf	56.891	6696.054	0.0120	0.899	3.865
8	Inf	56.893	6937.930	0.0131	0.949	4.044
9	Inf	56.903	7419.687	0.0155	1.047	4.404
10	Inf	56.925	7898.626	0.0180	1.144	4.767
11	Inf	56.960	8374.573	0.0206	1.238	5.133
12	Inf	57.008	8847.381	0.0233	1.327	5.503
13	Inf	57.072	9316.923	0.0260	1.411	5.878
14	Inf	57.152	9783.100	0.0287	1.488	6.257

Table 5.3 PID 5V Load coefficients for $f_c \approx [5;10]kHz$ and $\varphi_m \approx 57°$

PID: 3.3V	Gain Margin	Phase Margin	$f_{crossover}(Hz)$	Ki_5	Kp_5	Kd_5
1	9869.594	42.682	9869.594	0.056	2.750	4.707
2	9864.385	43.697	9864.385	0.055	2.684	4.812
3	9859.134	44.713	9859.134	0.053	2.616	4.915
4	9853.849	45.732	9853.849	0.052	2.548	5.017
5	9848.538	46.753	9848.538	0.050	2.479	5.117
6	9843.212	47.775	9843.212	0.049	2.409	5.216
7	9837.878	48.800	9837.878	0.047	2.339	5.313
8	9832.549	49.827	9832.549	0.046	2.268	5.408
9	9827.234	50.856	9827.234	0.044	2.196	5.502
10	9821.945	51.888	9821.945	0.042	2.123	5.594
11	9816.694	52.921	9816.694	0.041	2.050	5.684
12	9811.493	53.957	9811.493	0.039	1.976	5.773
13	9806.357	54.994	9806.357	0.038	1.902	5.860
14	9801.297	56.034	9801.297	0.036	1.827	5.945

Table 5.4 PID 3.3V Load coefficients for $f_c \approx 10kHz$ and $\varphi_m \approx [44;61]$

PID: 3.3V	Gain Margin	Phase Margin	$f_{crossover}(Hz)$	Ki_3.3	Kp_3.3	Kd_3.3
1	Inf	56.887	5969.844	0.011	0.898	3.108
2	Inf	56.874	6458.121	0.013	1.011	3.465
3	Inf	56.870	6701.342	0.014	1.067	3.644
4	Inf	56.869	6943.917	0.016	1.124	3.822
5	Inf	56.872	7427.030	0.019	1.237	4.182
6	Inf	56.886	7907.269	0.021	1.348	4.543
7	Inf	56.912	8384.463	0.025	1.456	4.908
8	Inf	56.952	8858.456	0.028	1.560	5.277
9	Inf	57.006	9329.115	0.031	1.658	5.650
10	Inf	57.076	9796.328	0.034	1.751	6.028
11	Inf	60.214	9782.103	0.029	1.521	6.267
12	Inf	61.264	9777.631	0.028	1.444	6.343
13	Inf	62.315	9773.312	0.026	1.366	6.417
14	Inf	63.369	9769.153	0.024	1.287	6.489

Table 5.5 PID 3.3V Load coefficients for $f_c \approx [5;10]kHz$ and $\varphi_m \approx 57°$

These tables provide a fast and effortless way to test different system bandwidths and phase margins in the complete simulation model (Chapter 6).

In the next figures we can appreciate the Bode plots of the PID compensator and PD compensator part, and also the loop gain of the system. It can be seen, how the addition of the integral part to the PD compensator does not affect the phase margin and the crossover frequency and increase the loop gain at low frequencies.
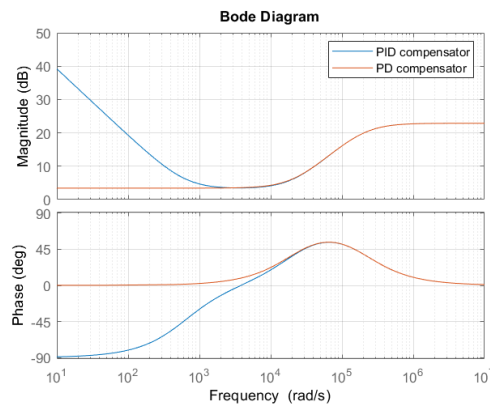
Figure 5.26 Bode plots for Output Bucks Control: PID and PD part
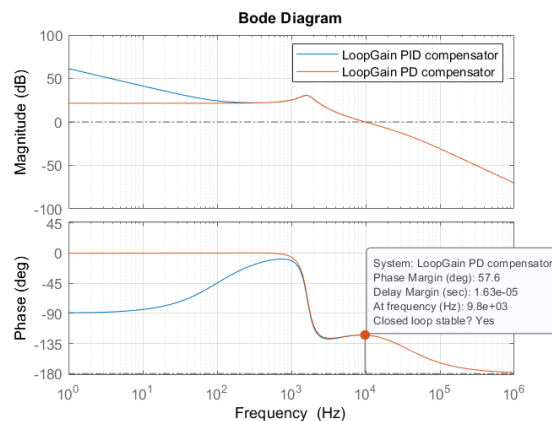
Figure 5.27 Loop gain Bode plots: PID and PD part

The bode plots were obtained for the 5V load. For the 3.3V load, the same process applies, and similar results are reached.

Chapter 6. SIMULATIONS RESULTS

Throughout this chapter the PV side and Output buck control previously designed will be implemented and tested in a simulation environment (MATLAB). Some parameters may be modified to achieve better performances or to explain design concepts. The sections of this chapter are divided in the description of the model implemented in MATLAB and such model's simulation results. The procedure followed when carrying out the simulations are the following. First, the perturbation MPPT control frequency is chosen based on the analysis of Section 5.2.2. Secondly, if ramp changes are going to be simulated, the minimum duty cycle required for the sample frequency selected must be calculated. Third, the voltage protection compensator gain is chosen based on the MPPT perturbation frequency, through the code shown in Appendix A.5. In fourth place, by the codes A.6 and A.7 of the Appendix A, the PID compensator gains of the output Buck converters are calculated and chosen. Finally, the MATLAB script will be run where all the variables of the implemented model are defined, and the model will be simulated.

6.1 FIRST STAGE OF THE POWER SUPPLY

6.1.1 SINGLE PHASE

In this section, the P&O and IncCond algorithms, modeled in Chapter 5, will be verified that work correctly and are able to find the MPP. On the other hand, the effects of the P&O control parameters in its behaviour will be shown.

6.1.1.1 MODEL DESCRIPTION
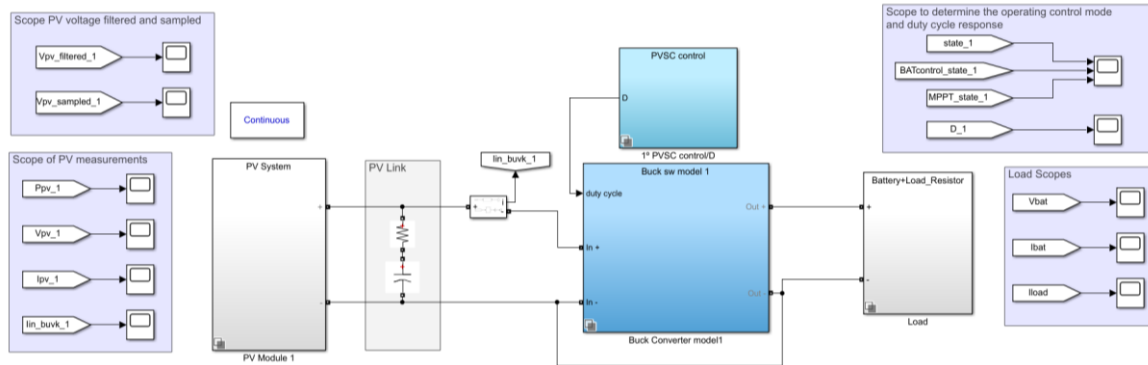
Figure 6.1 Single phase of the power supply first stage implement in MATLAB

In the "PV Module 1" subsystem block, the PV module block of Figure 4.9 can be found. In The "Buck converter model1" variant subsystem block, there are two buck converter options, one with the average model and one with the switch model of the buck converter, as shown in the next figure. However, for the simulation results only the switch model will be used. The average model was included as it allows faster simulations and at the beginning of the project gave a fast overview of the converter performance.
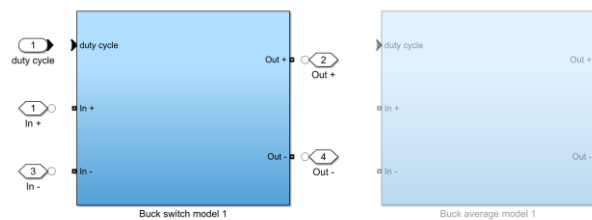
Figure 6.2 Inside the Buck Converter model 1 variant subsystem

Inside the "Buck switch model 1", we have the Buck converter model, shown in the next figure. The average model will be the same but with the average network instead of the switch network.
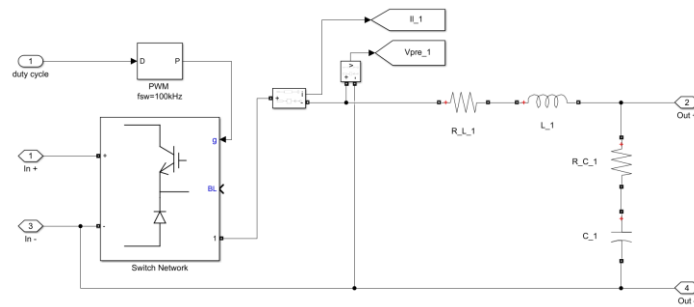
Figure 6.3 Buck converter switch model

Furthermore, inside the "PVSC control/D" variant subsystem block, there different options exist. Either the MPPT control on its own or the MPPT control integrated with the Battery charge control can be selected, shown in Figure 6.4. And within the MPPT control, both P&O and IncCond techniques described in Chapter 5, can be selected.
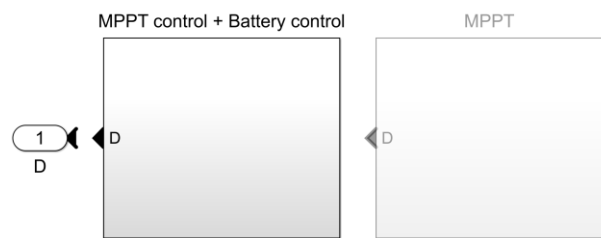
Figure 6.4 MPPT control and MPPT control integrated with the Battery charge control

As it can be appreciated in the control model of Figure 6.5, the PV voltage is measured, filtered, to attenuate switching noise, and sampled by an A/D block. Moreover, the function block that represents the MPPT algorithm can be chosen to be the P&O or the IncCond. The code of these algorithms was covered in Chapter 5. The final code that integrates the MPPT control with the Battery charge control is shown in Appendix A.9 for the IncCond and Appendix A.10 for the P&O.
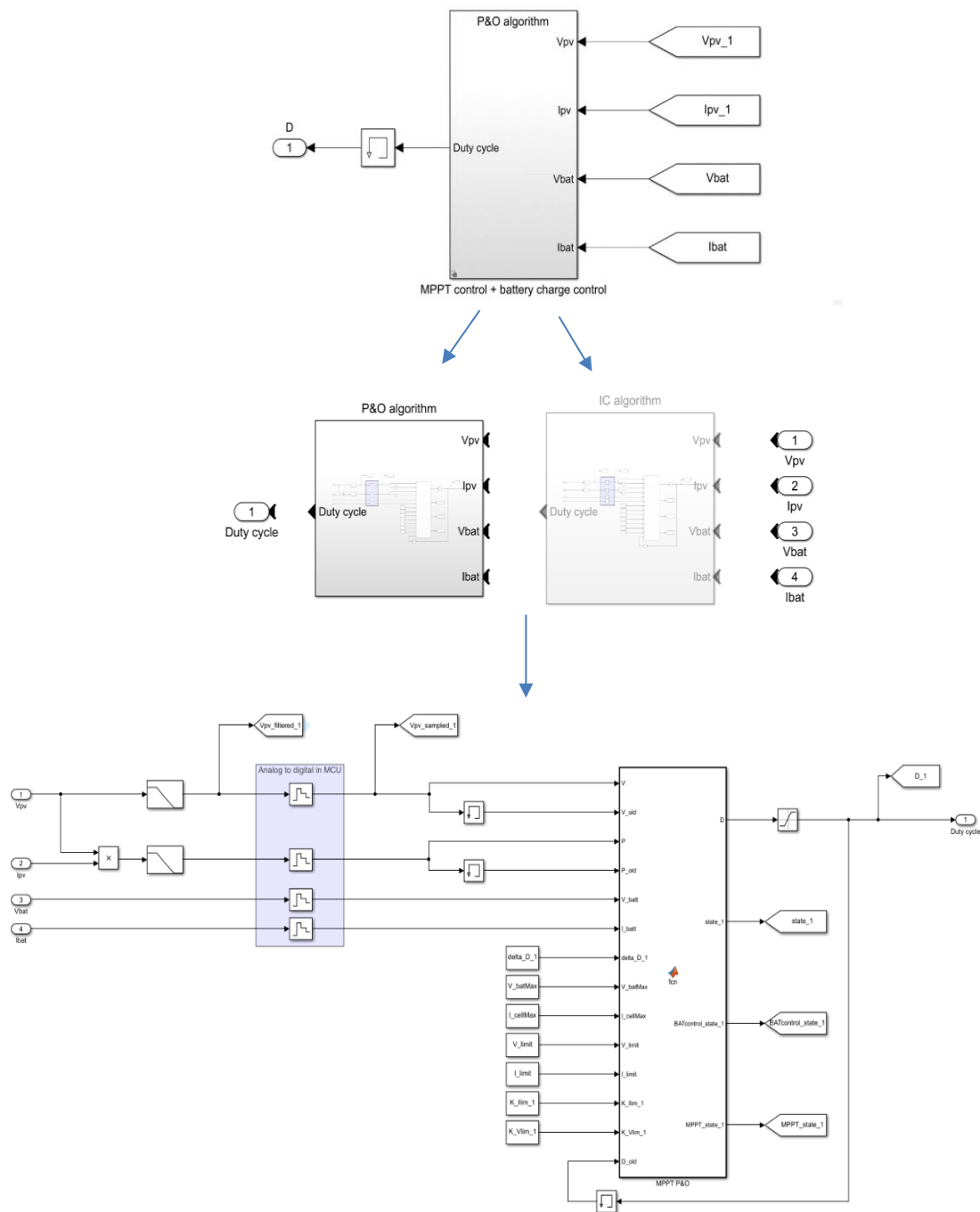
Figure 6.5 Control implementation

The "Load" variant subsystem block includes several types of load forms to simulate the control. The next figure shows what is inside the block.
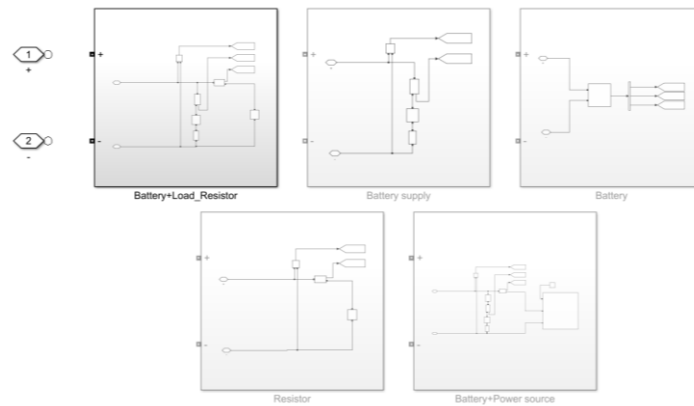
Figure 6.6 Load variant subsystem implementation

6.1.1.2   SINGLE PHASE SIMULATIONS RESULTS

For the single phase, the MPPT was tested with the P&O and IncCond algorithm under constant irradiance ($Ir = 1000 \, W/m^2$) and operating mode II (Battery connected and charging). The results obtained for the designed parameters in the previous chapters ($f_{MPPT_{perturbation}} = 300 \, Hz$, $\Delta d_{min} = 0.004$) are the following.
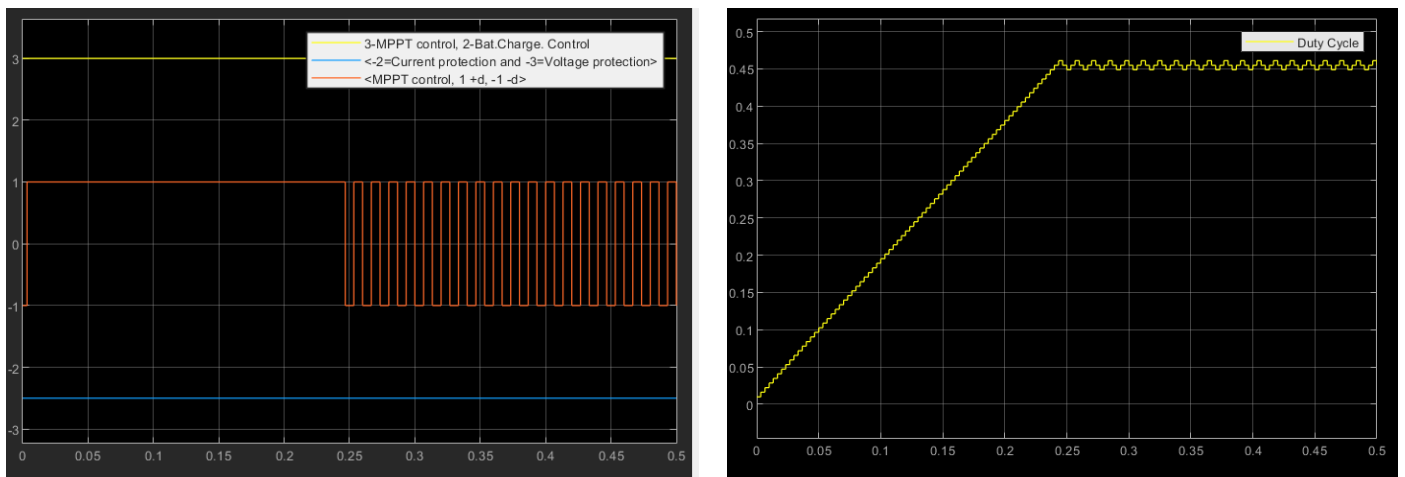
Figure 6.7 Control operating mode, Duty cycle scopes f_sample=300Hz d_min=0.004

In Figure 6.7, the Control operating mode and the duty cycle scopes are shown. It can be observed how the control is working at the MPPT control, as the yellow line is at

90

position 3 and not 2. In the duty cycle scope, it can be observed that the MPPT control is able to reach and maintain a stable and continuous oscillation around the maximum power point. It reaches the optimal operating condition as the duty cycle in steady state oscillates three times around the MPP [13].

In the following curve scope PV output power is shown.
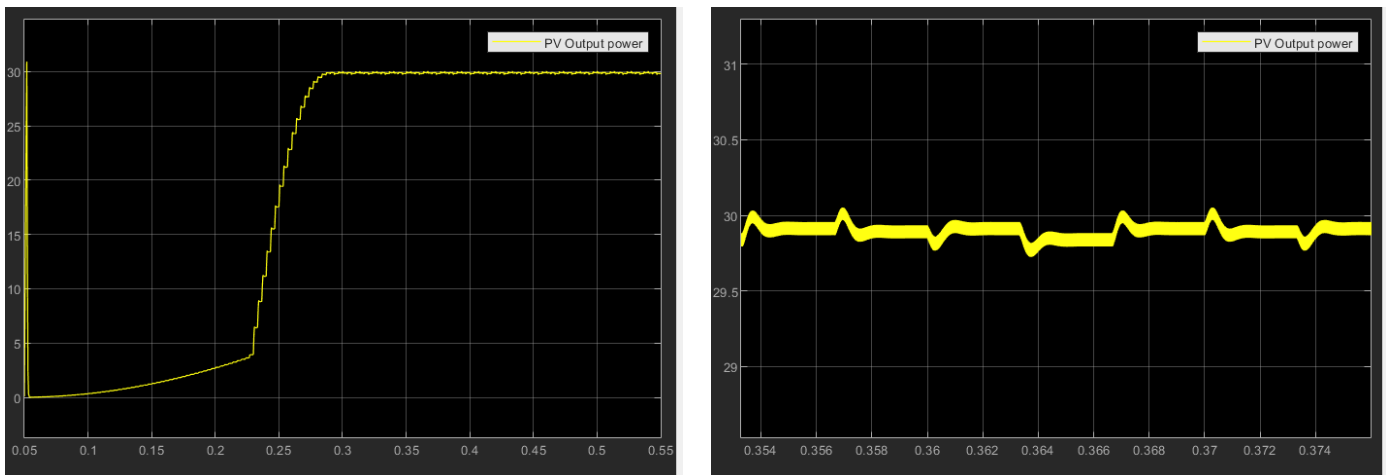
Figure 6.8 PV output power f_sample =300Hz d_min=0.004

The maximum available power of a PV module at nominal irradiance ($Ir = 1000 \, W/m^2$) is $29.92 \, W$, as it can be seen in the PV output power scope, this value is reached. Hence, the MPPT P&O algorithm is working properly and the design parameters show satisfactory performance.

In the next figure, the PV voltage scope is shown. After each duty cycle step the system reaches steady state before applying the next step, this is crucial for the correct performance of the MPPT P&O and IncCond algorithms. Therefore, the results obtained verify the initial design achieved with the control to output PV voltage transfer function of section 5.2.1. Moreover, it can be seen that the value oscillates around 17.6 V, the voltage output for the MPP.
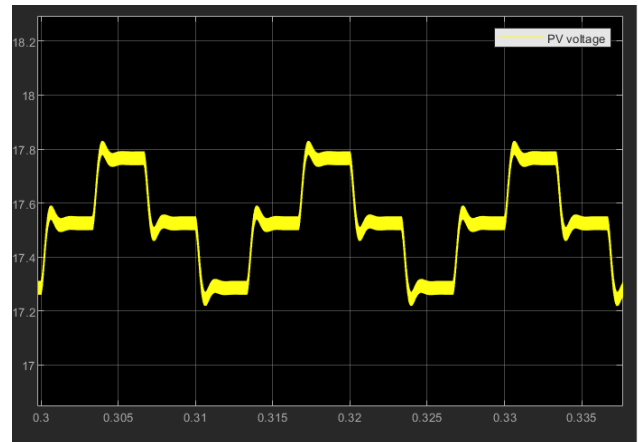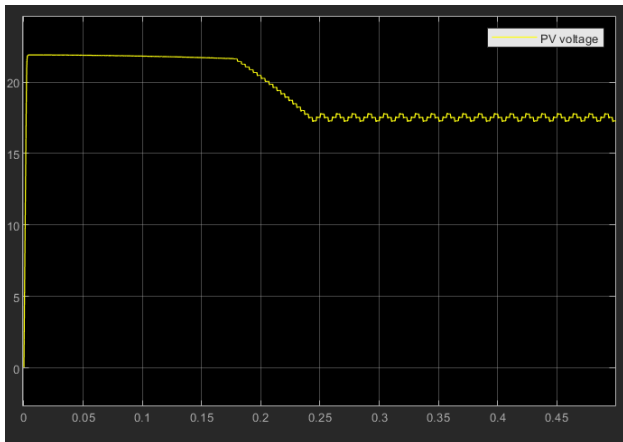
Figure 6.9 PV voltage scope f_sample=300Hz d_min=0.004

All the results presented were obtained for a sampling frequency of 300 Hz. This value could be further increased to obtain a faster performance, as the system has enough time to settle and reach steady state after each duty cycle step.

In the next figure, the PV link design is verified. The input current scope shows how the current is oscillating at the switching frequency. However, with the PV link input capacitance, the PV voltage and current at the PV terminals are constant, allowing the correct functioning of the MPPT control.
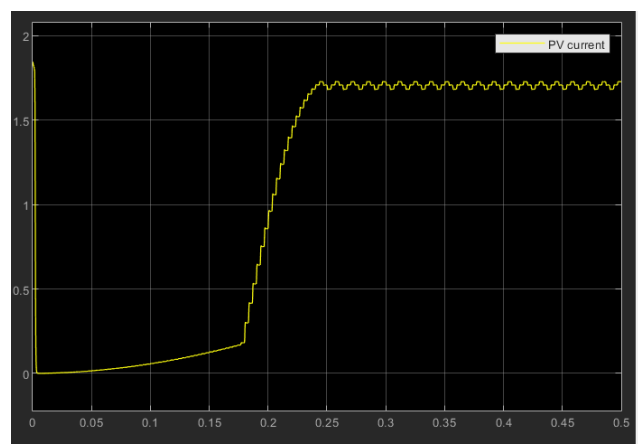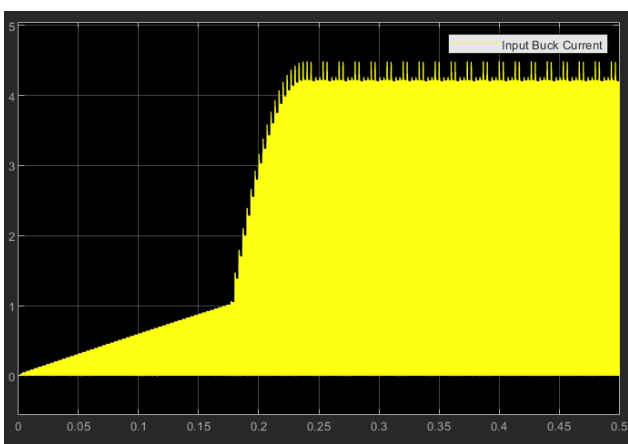
Figure 6.10 Input and PV current scopes f_sample=300Hz d_min=0.004

92

Finally, the output battery voltage scope is shown.
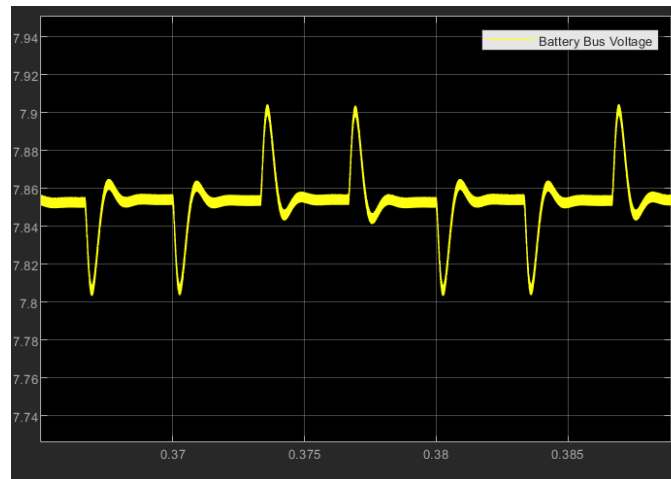
Figure 6.11 Battery bus voltage the scope f_sample=300Hz d_min=0.004

The Load used was a battery (voltage source with a resistor modeling its losses) and a resistor. It can be observed how for each duty cycle step there is a peak response at the battery voltage. This has to be considered, as the output bucks control performance could be affected by this and the load voltages could exceed the desired and specified ripple limits.

This can be adjusted by reducing the size step of the duty cycle, even though this could affect the tracking speed. The best solution to mitigate this effect is to reduce the size step enough to reduce the peaks and increase the sampling frequency to overcome the reduction in the tracking speed introduced by the reduction of the size step. This will be shown below. First, it will be shown how incrementing the sampling frequency, the system reaches the MPP faster. To further on show how a frequency increase and a reduction of the duty cycle step size, lead to an equilibrium point between precision and speed.

The next figure shows for the same model and parameters, how the increase in the sampling frequency affects the system's response. It was increased from 300 Hz to 600 Hz. At this control loop frequency, it can be appreciated how the system reaches the MPP much faster than before. It takes around 0.12 s instead of 0.22 s. However, the voltage has less time to settle. Increasing more the sampling frequency could make the control loop unstable.
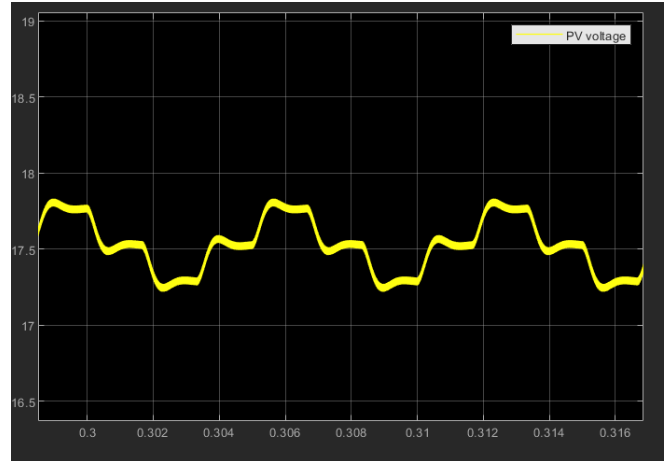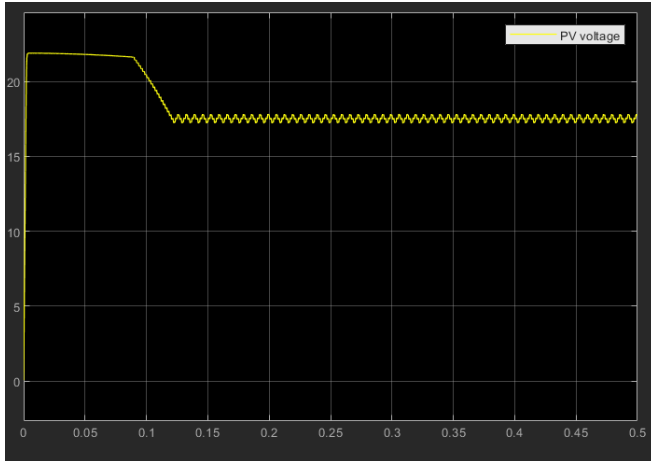
Figure 6.12 PV voltage Scope f_sample=600Hz d_min=0.004

The next scope shows how having the perturbation frequency at 600 Hz and reducing the size step to half its value, the battery bus voltage peaks are reduced from 0.1V peak to peak to less than 0.05V peak to peak, and the system reaches steady state at a reasonable time, around 0.34s. This situation qualitatively improves the voltage ripple at the battery bus. However, it is on the verge of becoming unstable. With regards to the experimental results, this should be considered.
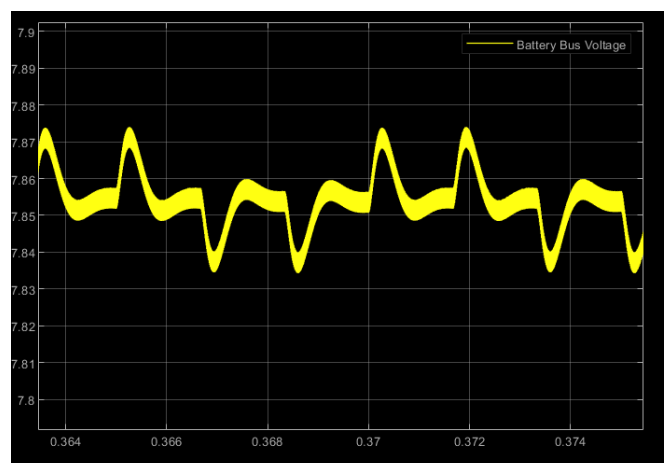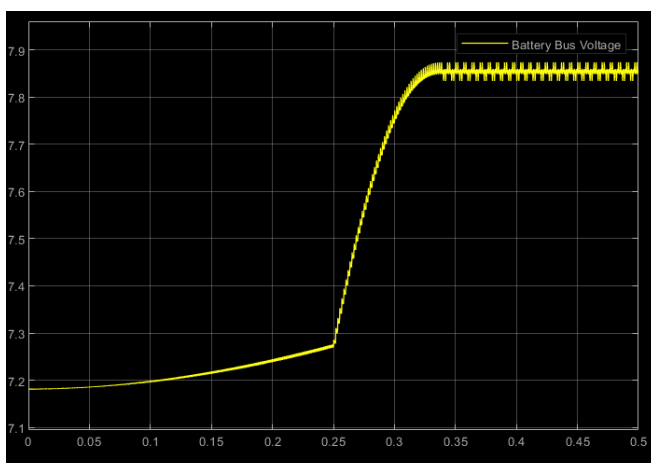
Figure 6.13 Battery Bus Voltage Scope f_sample=600Hz d_min=0.002

94

The results when the IncCond algorithm is used instead of the P&O, are almost identical as barely any differences can be seen. Therefore, it is not worth pointing out and showing its comparative.

6.1.2   DOUBLE PHASE

In this section, the test cases described in Section 1.1.4 will be simulated. It will be verified that the PVS control works correctly.

6.1.2.1   MODEL DESCRIPTION

The model used is shown below, it includes the other PV module and the buck converter connected to the common bus. The variant subsystems blocks are the same to the ones described for the single phase model.
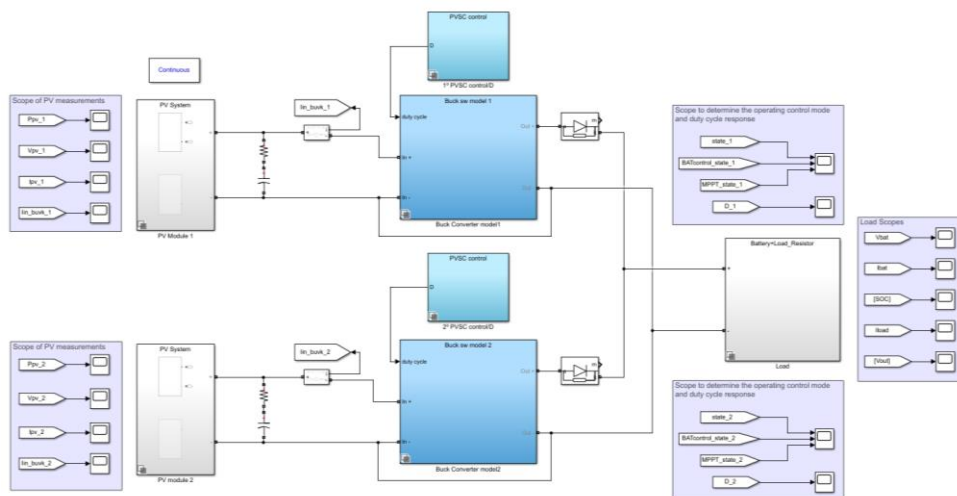
Figure 6.14 Complete power supply first stage MATLAB model implementation

6.1.2.2   DOUBLE PHASE SIMULATIONS RESULTS

The results in this section, were obtained for the following model parameters. The sampling frequency was set to 300 Hz and the perturbation size step was set to be 0.005.

With the full first stage of the power supply implemented in MATLAB, the first two test cases simulations of Figure 1.2, will be carried out. The cases will be tested in the following way:

Operating Mode	*Mode I: 1st part*		*Mode I: 2nd part*	*Mode II*	
Time (s)	0	1	2	3	4
PV module 1:Ir=[W/m^2]	1000	1000	1000	1000	1000
PV module 2:Ir=[W/m^2]	500	500	1000	1000	1000
Battery (0-OFF, 1-ON)	0	0	0	1	1

Table 6.1 Simulations operating modes

It should be expected at "Mode I: First part" and "Mode II: Second part" that the Battery charge control is able to regulate the Output voltage to 8.4V. Once the battery is connected, the Control should enter in the MPPT mode. With regards of this to happen, the following was carried out. The battery voltage reference was set to 8.4 V and the V_{batmax} of the Eq. (5.41), will be defined to be 99% of the 8.4 V. This way, at operation Mode I, $V_{refbat} > V_{batmax}$. Once the battery is connected to the power supply, the voltage at the common bus will be defined by the battery ($V_{battery-bus} = V_{bat} + I_{bat} * R_{bat_s} \approx 8 + 2 * 0.12 \approx 8.24$). Therefore, $V_{battery-bus} < 99\% * V_{batmax}$, forcing the control to operate in the MPPT mode and charging the battery at the maximum power available as specified at the specifications.

In the following scope the operating control modes are shown, for both converters. It can be appreciated how initially the control operates in MPPT (yellow line at 3) and the duty cycle is being constantly increased to track the MPP (red line at 1). Once, the battery bus voltage goes above its limit, the voltage is regulated by the Battery charge control

(yellow line in 2) in the voltage protection mode (blue line in -3). Finally, when the battery is connected (t=3s), the control enters again in MPPT mode, and oscillates around the MPP (red line from 1 to -1, meaning that the duty cycle is being increased and decreased.
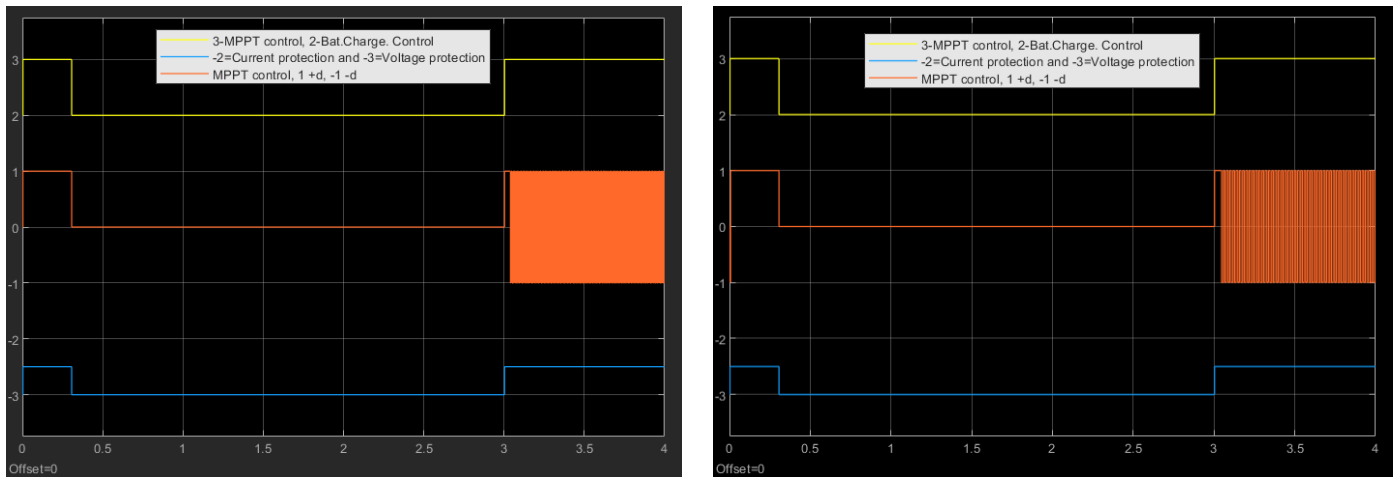
Figure 6.15 Operating modes of the PV module 1 and PV module 2 control

This behaviour is reflected in the duty cycle in the following way. The next scope shows the full duty cycle of the PV module 1 scope and a zoomed version at the steady state when the battery is connected.
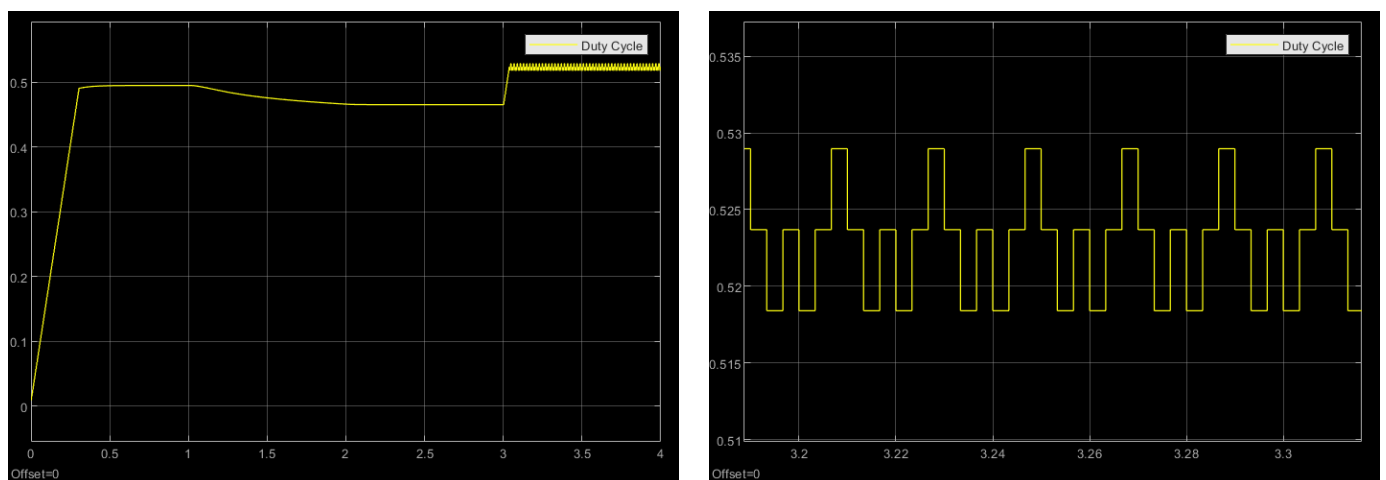
Figure 6.16 Double phase Duty Cycle Step Scope

97

It can be appreciated how at the beginning, the duty cycle is being increased step by step (MPPT control) until the voltage protection steps in. When the battery is connected, the duty cycle oscillates around the MPP as shown in the zoomed version.

In the next figure, both the PV module 1 and PV module 2 output power scopes will be shown. To recall the simulation operating modes of the Table 6.1, the PV module 1 will be constantly under 1000 W/m^2 irradiance and the PV module will suffer a step change from 500 to 1000 W/m^2.
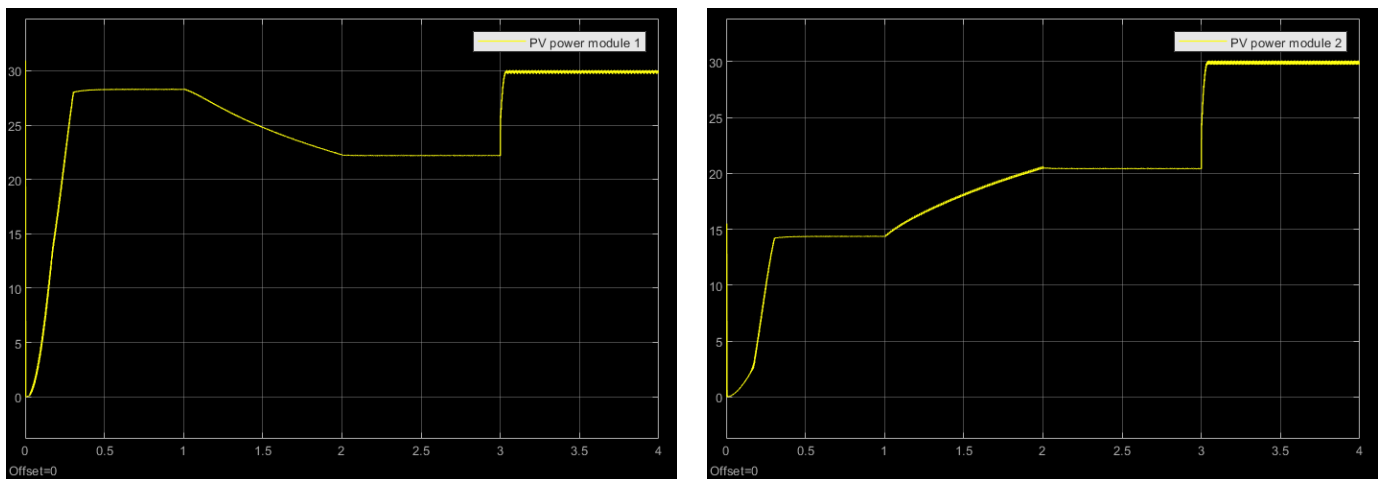
Figure 6.17 PV module 1 and PV module 2 output power scopes

The results obtained verified the expected behaviour. PV module 1 available power is limited by the battery charge control and when the PV power module 2 irradiance level increases, it reduces its power to compensate the PV module 2 power increase. Finally, once the battery is connected, the MPPT correctly tracks the MPP ($\sim 29.92\ W$). On the other hand, PV module 2, at 500 W/m^2 reaches almost the MPP and at t=1s it suffers a ramp change due to irradiance ramp change and once the battery is connected the MPPT control correctly tracks the MPP.

Furthermore, the performance of the battery charge control can be seen more properly at the battery bus voltage scope, shown in the next figure

98
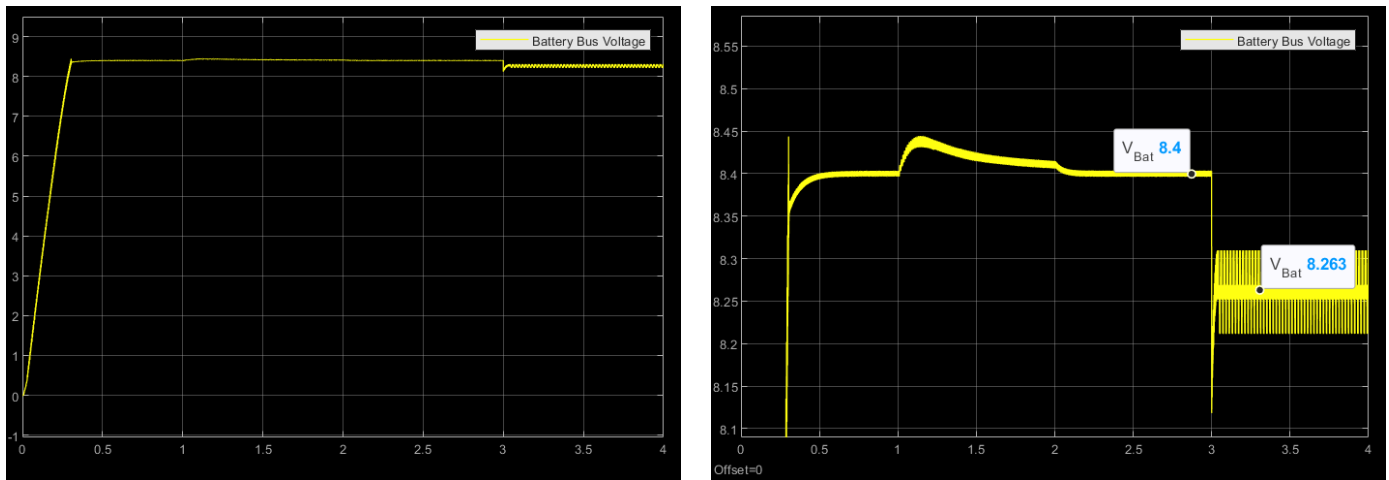
Figure 6.18 Battery Bus voltage scope

When the battery is not connected, the Battery Bus voltage is regulated to 8.4V (maximum battery voltage), and once it is connected, the voltage is set by the battery voltage as it can be seen in Figure 6.18. The dynamics of the voltage protection control are more visible in the zoomed scope, it can be seen that it is slow but stable. Making the response faster could lead to instability problems. As explained in Section 5.3., this control is tied to the MPPT, in order to make the response faster, the control should be independent of the MPPT control loop frequency. This could be achieved by identifying the operating control mode and changing its sampling frequency. However, as there are no requirements regarding the voltage protection control dynamics the solution achieved is good enough.

Finally, the battery's current scope will be shown. It can be appreciated how the battery current charging limits are met (less than 2.6A) and that its charging, as it has a positive current value. The ripple requirements are not met as the duty cycle step size is too big. However, a higher step size value was chosen to obtain faster simulations and present that the control performance is working in the correct way.

99
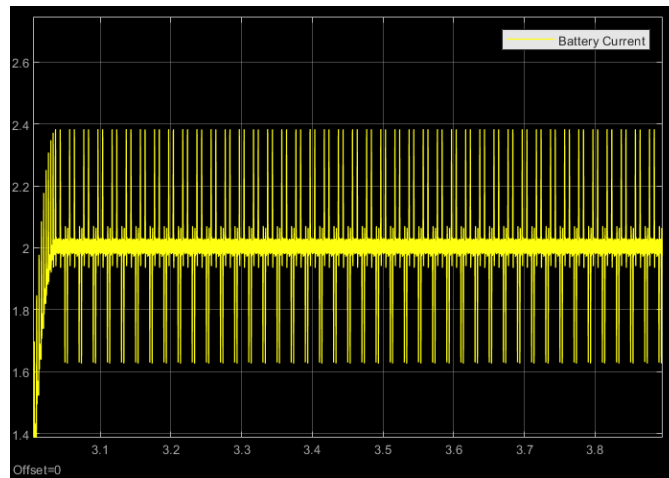
Figure 6.19 Battery current scope

All the results obtained, verify the expected behaviour, as it presents a stable and a correct performance.

6.2   SECOND STAGE OF THE POWER SUPPLY

The following model was implemented in MATLAB to test the PID compensator design of Section 5.4. Both 3.3V and 5V will be tested individually and together. The simulations in this section do not only verify the design of the PID control, but also represent a similar behaviour the power supply should have when all the power is supplied by the battery source.

6.2.1   SINGLE PHASE: 5V AND 3.3V LOADS

6.2.1.1   MODEL DESCRIPTION

The model for the 5V load is shown below. It includes an ideal voltage source set to the nominal battery voltage (8V) and the output buck converter for the 5V load regulated with the PID control.
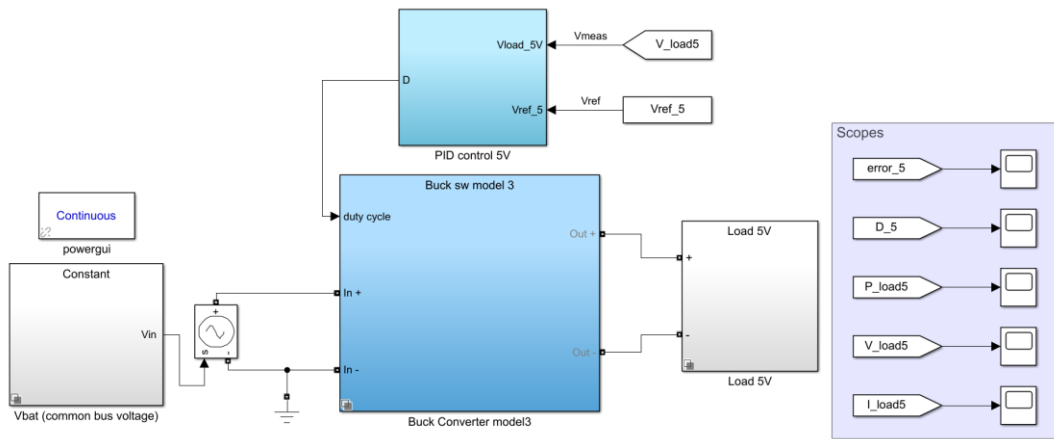
Figure 6.20 Single phase MATLAB model implementation for Output 5V Load
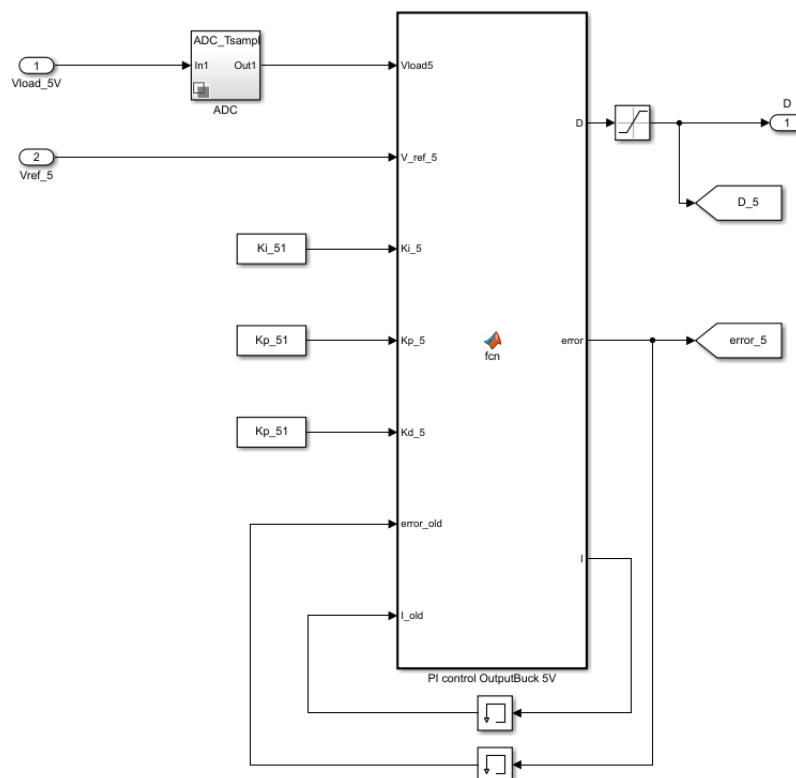
Figure 6.21 PID implementation for Output Buck converter

The PID function code was described in Section 5.4.

SIMULATION RESULTS

To verify the control's performance, a reference step change was introduced to simulate the system's ability to track the reference voltage. The results obtained for the design parameters in Section 5.4, are shown in the following figures. The compensator gains used are the following: Ki_5=0.038, Kp_5=1.3947, Kd_5=6.3711, Ki_3.3=0.0098, Kp_3.3=1.5959, Kd_3.3=6.1552
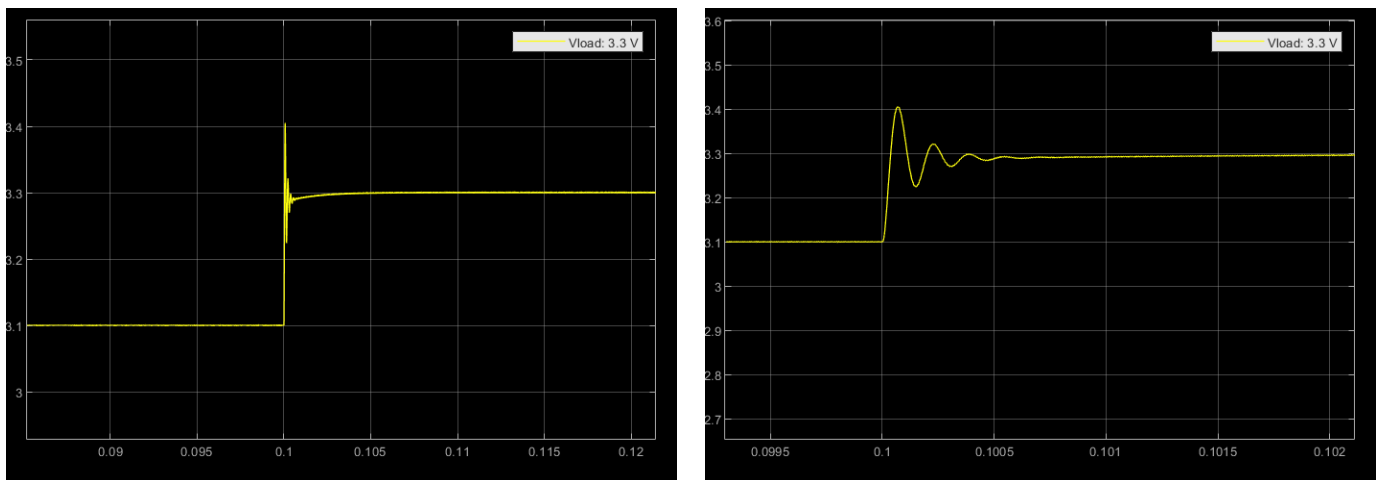
Figure 6.22 Output Voltage scope for the 5V Load
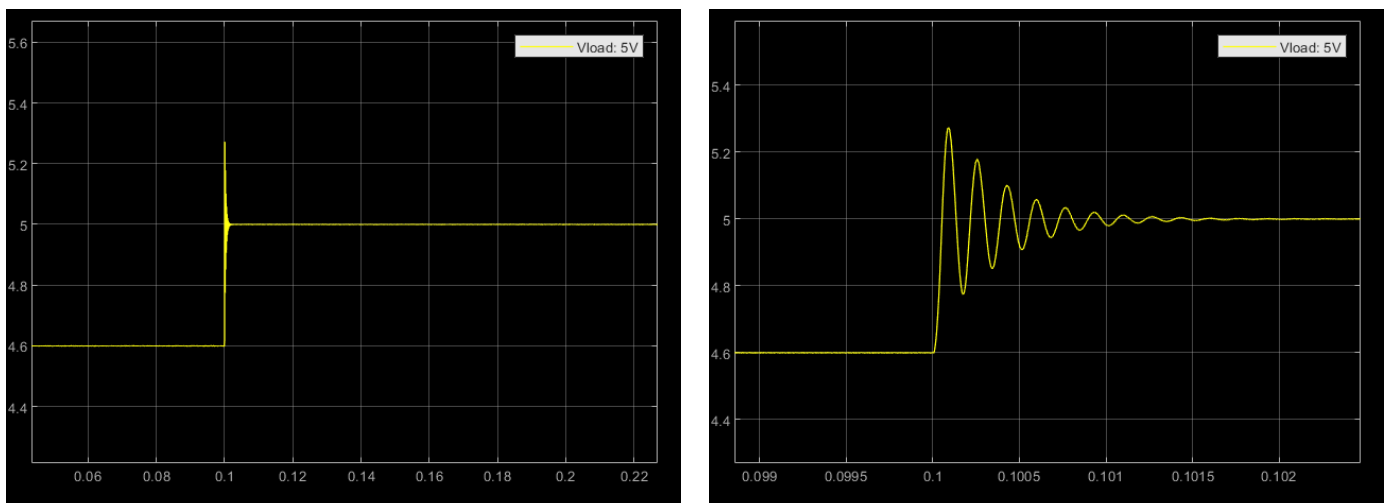
Figure 6.23 Output Voltage scope for the 3.3V Load

The results show that the system is able to track the reference voltage and presents a stable response. It also can be seen that the voltage ripple limits are met for both loads.

Moreover, the expected system settling time is verified, as for a system bandwidth of 10 kHz, the expected settle time should be around 0.3 ms (as a rough estimate).

6.2.2 DOUBLE PHASE: 5V AND 3.3V LOADS

6.2.2.1 MODEL DESCRIPTION

The following model shows the second stage of the power supply implemented in MATLAB. It includes both output bucks and its corresponding PID regulators. The subsystems models were already shown in the single phase.
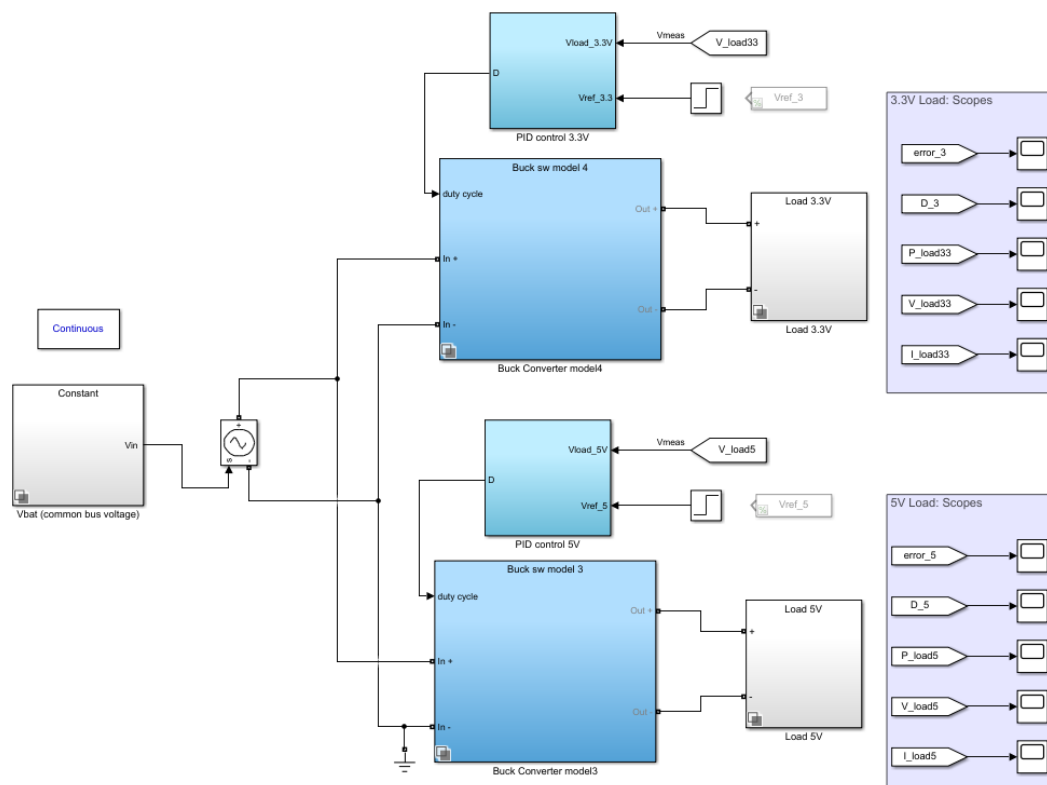
Figure 6.24 MATLAB implementation of the second stage of the power supply

6.2.2.2 SIMULATION RESULTS

The results obtained show stable tracking performance. The results are equivalent to the one obtained for the single phase, as it has been simulated with an ideal voltage source. The voltage ripple at both loads are met ($\Delta V_{load} < 2\%$ for both loads)
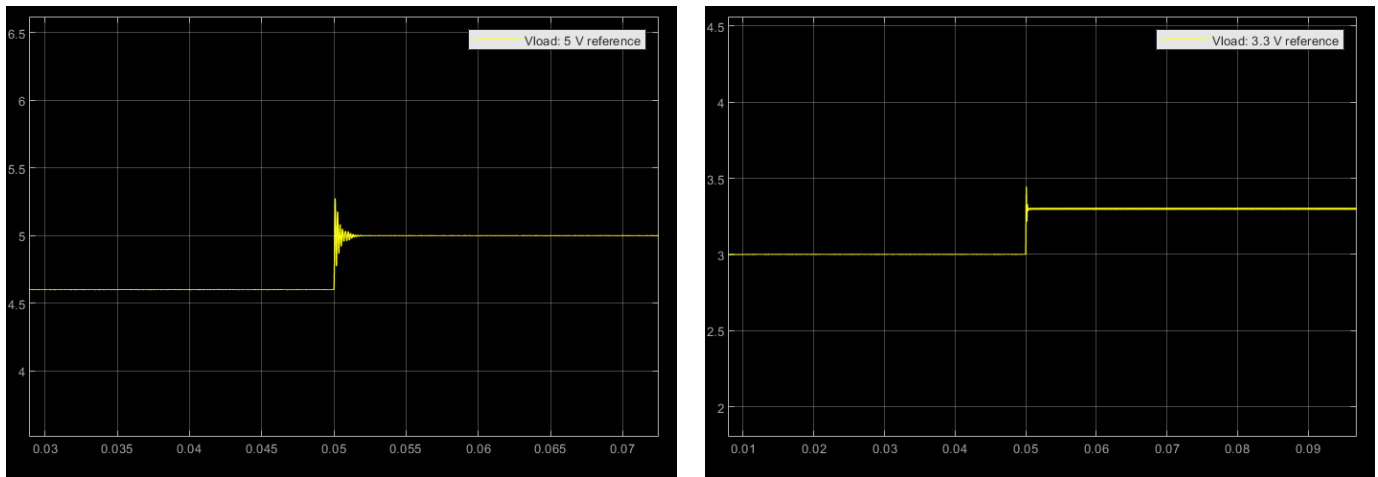
Figure 6.25 Second stage simulation results

6.3 FULL POWER SUPPLY

Throughout this section, the full power supply model was implemented in MATLAB.

6.3.1 MODEL DESCRIPTION

Each block´s content has already been described in the previous sections. The process followed towards the simulation is the following. It is similar to the previous one used, but it includes all steps. First, the code of Appendix A.4 will be run, whether the power supply in the MPPT operation is simulated under ramp irradiance changes and the necessity of determining the minimum duty cycle. In addition, the codes of Appendix A.5-A.7, through these codes, the voltage regulation compensator gain is designed and the two output

104

Buck compensator gains. Once chosen, they will be introduced in the codes of Appendix A.8, that includes all the parameters of the model that will be shown further on. Lastly, such code is run, and the model implemented in MATLAB is run.
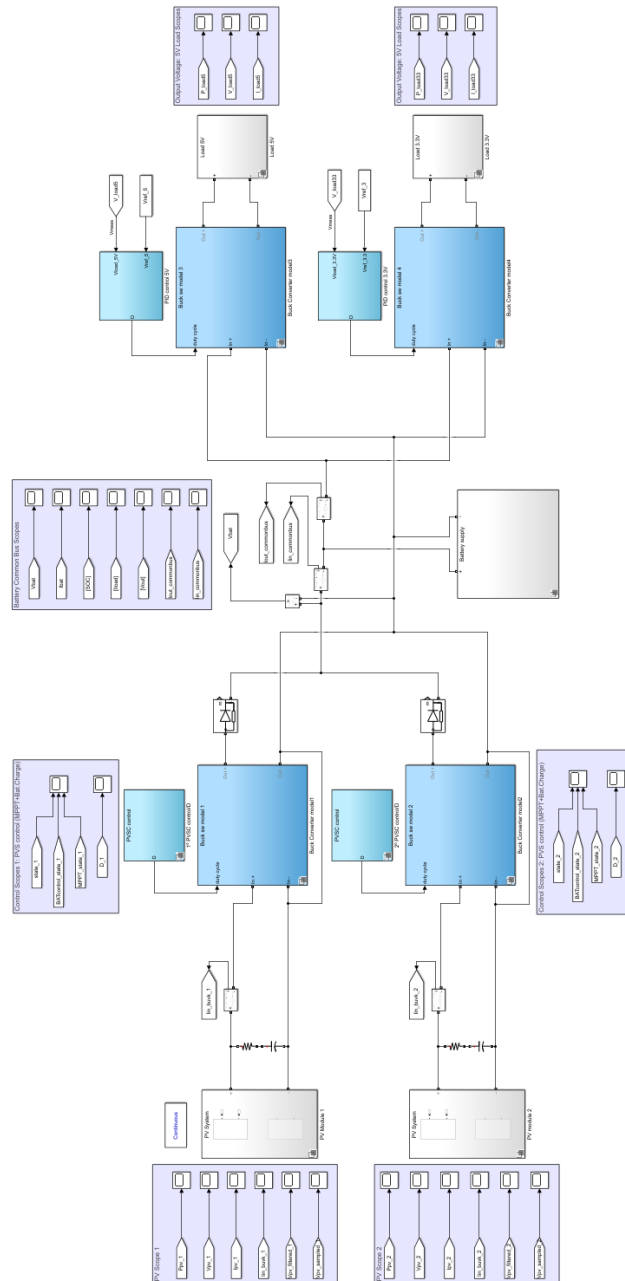
Figure 6.26 Full Power Supply MATLAB implementation

6.3.2   SIMULATION RESULTS

The following results were obtained, from simulating operating Mode II (Battery connected and both PV modules with $1000W/m^2$ irradiance. The MPPT perturbation frequency was adjusted from the previous simulations, as at f_sample=300Hz and d_min=0.004, the control performance showed instability problems. The MPPT perturbation frequency was further reduced to 200 Hz, and the duty cycle step was maintained to 0.004.

The next figures show the output voltage scope of each load type.
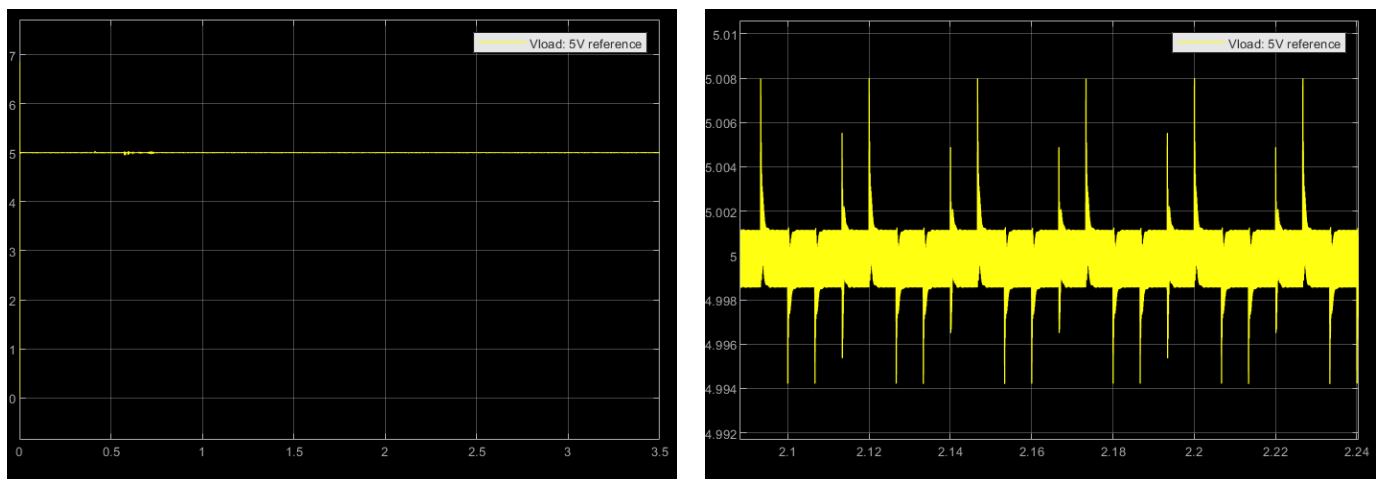
Figure 6.27 Output Voltage Scopes: 5V load
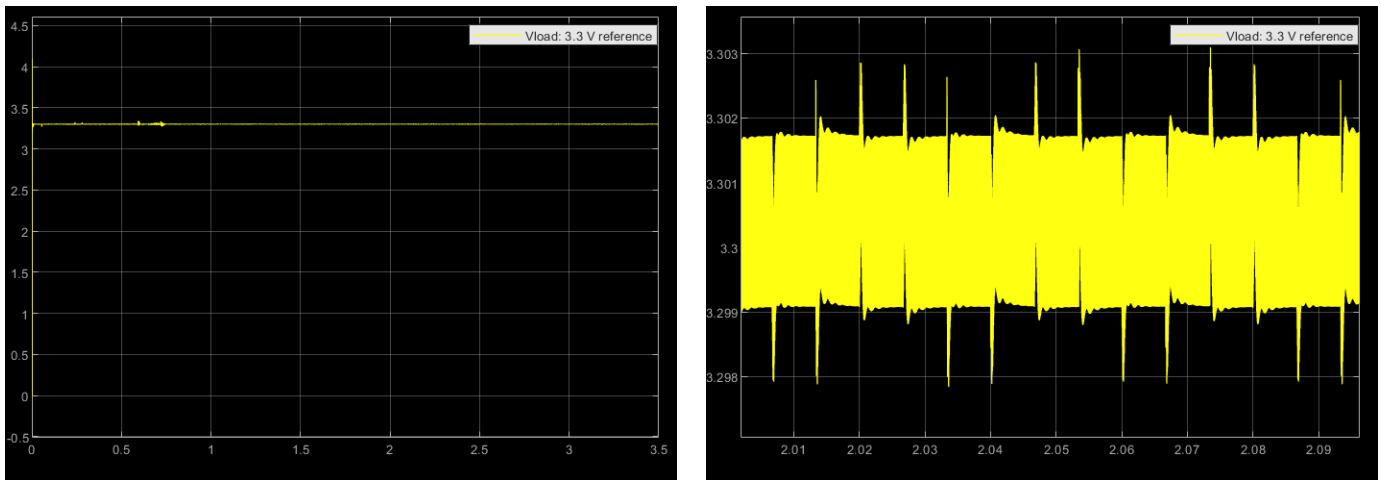
Figure 6.28 Output Voltage Scope: 3.3V load

It can be seen how the PID compensator for the output buck is stable and correctly tracks the voltage reference. The peaks of the zoomed version are the result of the battery voltage peaks. Moreover, the results obtained satisfy the ripple requirements:

$$V_{load:5V_{peak\,to\,peak}} \approx 0.014\,V < V_{ripple} = 2\% * 5 = 0.1\,V \qquad (6.1)$$

$$V_{load:3.3V_{peak\,to\,peak}} \approx 0.005\,V < V_{ripple} = 2\% * 3.3 = 0.066\,V \qquad (6.2)$$

The next figure shows the output power at each load type. It can be seen how for the 5V load type, P=20W and for the 3V load type, P=16.5W, as shown in the inputs and outputs characteristics. This figure verifies that the current ripple at both loads is also met.

107
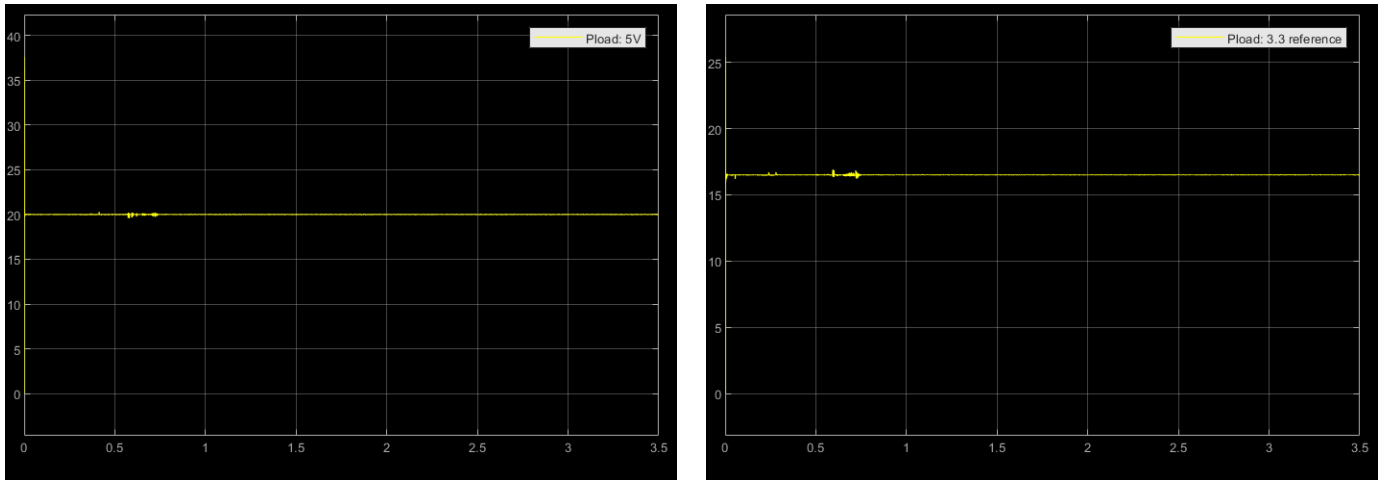
Figure 6.29 Output power at each load type

Furthermore, the control mode and performance are shown in the next figure. It can be appreciated how the control mode is in MPPT operation mode. Also, it can be appreciated how the duty cycle reaches the optimal operating condition as the duty cycle in steady state oscillates three times around the MPP, as explained previously. As the sample frequency is now 200 Hz, it can be appreciated how it takes more time to reach the MPP than in the previous simulations.
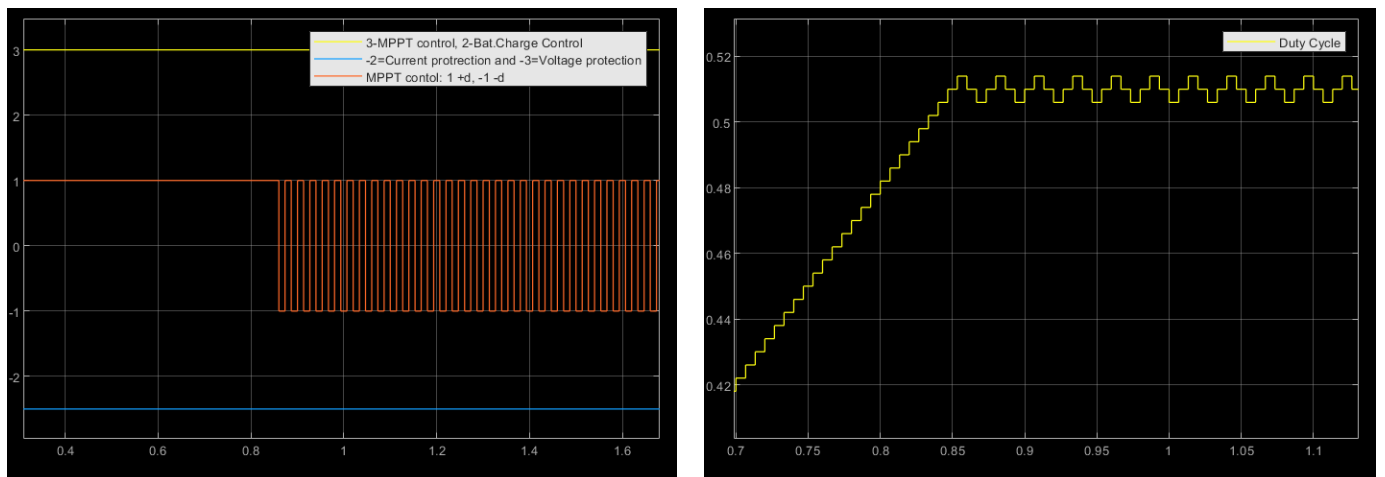
Figure 6.30 Operating control mode and Duty cycle scopes

Finally, the PV module 1 output power scope will be shown. It can be seen how the MPP is reached ($P \approx 30\,W$).
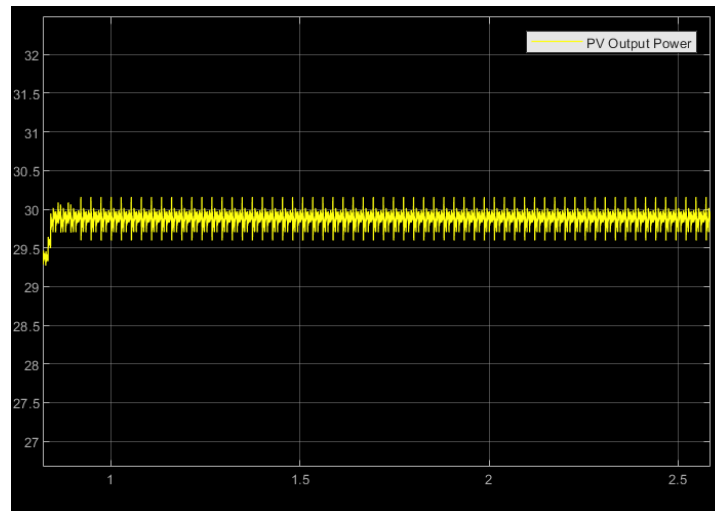
Figure 6.31 PV Output power scope

All the results attained are satisfactory. The MATLAB model runs correctly. The PVS control identifies that it has to enter in the MPPT mode, the MPPT mode correctly tracks the MPP and output buck PID control properly tracks the voltage reference meeting the ripple requirements. This model could be modified and include more functionalities as needed.

Chapter 7. CONCLUSIONS

To sum up, a description of what has been done is carried out to successively state the most relevant conclusions.

First, some mild contributions were done to the hardware team, calculating the value range that the LC filter of the input Buck converter should have according to the topology agreed by all team members so that the ripple requirements specified at the battery (Section 1.1.1.4) can be reached, such as the necessary value the input capacitance must have for it to attenuate the converter switching at the PV input terminals and the MPPT control is able to efficiently track the maximum power point.

Moreover, the PV modules based on the available datasheet were modeled, and such model was implemented in MATLAB, that will be used to simulate the power supply.

Consecutively, the control of the PV side input buck converters (MPPT control + Voltage protection part of Battery charge control) design was done. The approaches carried out for the MPPT control were the P&O and the IncCond. From the simulations and results obtained, no significant difference that is worth mentioning was found. However, both algorithms will be evaluated in the experimental testing to verify the results attained, as in theory the IncCond presents better results than the P&O, especially when facing sudden irradiance changes. Furthermore, it was opted to integrate the MPPT and the integral voltage action protection part in the same control loop. This limits the speed when following the battery charge control reference, however, the proposed solution is stable and enough for this project´s specifications. In regard to the output Buck converters control, the PID compensator gains were designed to stop each output Buck control for it to be a control that presents void tracking error and that is stable.

Towards testing the power supply experimentally, the values obtained for the control parameters final design can be considered a good starting point because of the results achieved after the simulations. It can be concluded that the MPPT control frequency should be between 100 and 500 Hz. Once this value is chosen through the code in Appendix A.4, a minimum necessary value that must have a perturbation step can be obtained. Although, towards the practical simulations, as the ramp changes are smooth it will not be of greater importance, the range should be between 0.002 and 0.008. The battery charge control´s integral compensator gain that presents the best results in the simulation is Kv=0.0038. Such parameter will be able to be modified with the tables provided in Chapter 5, Section 5.3.

The compensator gain used and that present the best results are: for the PID of the 5V output Buck converter: Ki_5=0.0287, Kp_5=1.4883, Kd_5=6.2574 and for the PID of the 3.3 output Buck converter: Ki_3.3=0.0344, Kp_3.3=1.7510, Kd_3.3=6.0285. Nevertheless, such parameters can be possibly modified using the tables provided in Chapter 5.4, Section 5.4.2. as for each perturbation frequency and duty cycle values of the MPPT control must be adjusted.

One of the possible solutions that gives an optimal result in the simulation of the complete power system MATLAB model has been achieved for f_{MPPT}=200Hz y Δd=0.004. With these values and the previous ones mentioned for the battery charge control and PID compensators, the optimal operating condition is reached. The duty cycle in steady state oscillates only three times around the MPP, and the output voltage ripple and current ripple are satisfactory met.

Additionally, to the proposed Project, improvements can be made, and more functionalities could be included. The MPPT control and the Battery charge control can be untied from each other. This way, the speed when regulating the voltage or the current at the battery bus can be increased. On another hand, another topology could be laid out. This project is based on a specific topology, so other topologies could be suggested and each of

their results could be compared between them. Moreover, all the designed parameters must be verified through experimental results.

Chapter 8. BIBLIOGRAPHY

[1]   IEEE International Future Energy Challenge (2020). *IFEC 2020 - Power Supply for Nano Satellites*. http://energychallenge.weebly.com/ifec-2020.html

[2]   IEEE International Future Energy Challenge (2020). *IFEC 2020 - Power Supply for Nano Satellites : Preliminary Specifications*. http://energychallenge.weebly.com/uploads/6/4/2/8/6428791/editor/ifec2020-blockdiagram.png?1574586039

[3]   Phaesun. (2016). *Solar Modules Sun Plus*. https://docs-emea.rs-online.com/webdocs/171c/0900766b8171c20b.pdf

[4]   Samsung SDI Co.,Ltd. (2009, May). *Specification of Product for Lithium-ion Rechargeable Cell Model : ICR18650-26F*. https://www.batteryspace.com/prod-specs/ICR18650-26F.pdf

[5]   The 2020 International Future Energy Challenge (IFEC2020). (2020, July 13). *Request for Proposals (RFP)*. http://energychallenge.weeby.com/uploads/6/4/2/8/6428791/ifec_2020_rfp_13_july_2020.pdf

[6]   Xiao, W. (2017). *Photovoltaic power system: Modeling, design, and control*. John Wiley & Sons Ltd.

[7]   Kalyan Kumar, K., Bhaskar, R., Hemanth, K. (2014*). Implementation of MPPT Algorithm for Solar Photovoltaic Cell by Comparing Short-circuit Method and Incremental Conductance Method.* Procedia Technology. https://doi.org/10.1016/j.protcy.2013.12.553

[8]   Keim, R. (2018, June 13). *How to Choose the Frequency of Your Switching Regulator*. ALL ABOUT CIRCUITS. https://www.allaboutcircuits.com/technical-articles/how-to-choose-the-frequency-of-your-switching-regulator/

[9]   Erickson, R. W., Maksimović, D. (2001). *Fundamentals of Power Electronics*. Norwell, Mass: Kluwer Academic.

[10]   Kemet. *Ceramic capacitors KEMET C1210C106K5RACTU*. https://www.digikey.com/product-detail/en/kemet/C1210C106K5RACTU/399-11629-1-ND/4918885

[11]   Würth Elektronik. *Fixed inductors Würth Elektronik 74435574700*. https://www.digikey.com/product-detail/en/w-rth-elektronik/74435574700/732-2179-1-ND/2175694

[12]   Kemet. *Ceramic capacitors KEMET C1210X225K1RAC7800*. https://www.digikey.com/product-detail/en/kemet/C1210X225K1RAC7800/399-16357-1-ND/7652885

[13]   Femia, M., Petrone, G., Spagnuolo, G., Vitelli, M. (2013). *PowerElectronics and Control Techniques for Maximum Energy Harvesting in Photovoltaic Systems*. CRC Press Taylor & Francis Group.

[14]   Rezaee, A. (2016). *Parameter estimation of solar photovoltaic (PV) cells: A Review. Elsevier.* https://doi.org/10.1016/j.rser.2016.03.049

[15]   Anandhraj, P. Mohana, K. (2019, June 1). *Extraction of Solar PV Module Parameters Using Back Search Optimization Algorithm.* Springer. https://doi-org.colorado.idm.oclc.org/10.1007/978-981-13-6772-4_113

[16]   Cubas, J., Pindado, S., De Manuel, C. (2014, March 14). *Explicit Expressions for Solar Panel Equivalent Circuit Parameters Based on Analytical Formulation and the Lambert W-Function.* Instituto Universitario de Microgravedad "Ignacio Da Riva" (IDR/UPM). Escuela Técnica Superior de Ingeniería Aeronáutica y del Espacio (ETSIAE). Universidad Politécnica Madrid.

[17]   Cubas, J., Pindado, S., Farrahi, A. (2013). *New Method for Analytical Photovoltaic Parameter Extraction. ICRERA 2013.* Instituto Universitario de Microgravedad "Ignacio Da Riva" (IDR/UPM). Escuela Técnica Superior de Ingeniería Aeronáutica y del Espacio (ETSIAE). Universidad Politécnica Madrid.

[18]   Yatimi, H., Aroudam, E. (2014). *Renewable Energy in the Service of Mankind Vol II.* In A. Sayigh (Ed). *Select Topics from the World Renewable Energy Congress WREC 2014. Evaluation of the Characteristics of the PV Module Considering Effects of Real Climatic Conditions* (pp. 459-467). Springer. https://link.springer.com/book/10.1007/978-3-319-18215-5

[19]   *Petrone, G., Spagnuolo G., Ramos-Paja, C.A., Spagnuolo, G., Vitelli, M., Xiao, W. (2017, Mar 20). Photovoltaic Sources Modeling.* IEEE Press.

[20]   Gradella Villalba, M., Ruppert Filho, E. (2008, Oct 10). *Dynamic analysis of the input-controlled buck converter fed by a photovoltaic array.* University of Campinas - UNICAMP - Brazil (Original work published 2007, Sep 3). http://dx.doi.org/10.1590/S0103-17592008000400009

[21]   Villalba G.M., Ruppert, E. (2009). *Analysis and Simulation of the P&O MPPT Algortithm using a Linearized PV Array Model.* 35th Annual Conference of IEEE Industrial Electronics, Porto, 2009, pp. 231-236, doi: 10.1109/IECON.2009.5414780.

[22]   Gradella, M., Gama de Siqueira, T., Ruppert, E. (2010, Jan 27). *Voltage Regulation of Photovoltaic Arrays: Small-Signal Analysis and Control Design.* IET Power Electronics (Original work published 2008, Dec 16).

[23]   Pandey, S. Kumar Jena, P. (2017, June). *A Review on Maximum Power Point Tracking Techniques for Photovoltaic Systems.* International Research Journal of Engineering and Technology (IRJET) Volume 4 Issue 6.

[24]   Eltamaly, A.M., Abdelaziz, A.Y. (2020). *Modern Maximum Power Point Tracking Techniques for Photovoltaic Energy Systems*. Springer. https://doi.org/10.1007/978-3-030-05578-3

[25]   MazenAbdel-Salam, M.,Mohamed-Tharwat,E., Goda,M. (2018). *An improved perturb-and-observe based MPPT method for PV systems under varying irradiation levels.* Elsevier. https://doi.org/10.1016/j.solener.2018.06.080

[26]   Wolfram   MathWorld.   (n.d.).   *Extreme   Value   Theorem.* https://mathworld.wolfram.com/ExtremeValueTheorem.html

115

[27]   Corradini, L., Maksimovic´,D., Mattavelli, P., Zane, R. (2015). *Digital Control of High-Frecuency Switched-Mode Power Converters.* IEEE Press.

[28]   Pagola, F.L. (2006). *Regulación Automática*. Universidad Pontificia Comillas de Madrid.

[29]   Deng, W., Gehan A. J. Amaratunga, G.A.J. (2014, Oct 16). *Limits of Incremental Conductance for Determining the Maximum Power Point under Rapidly Changing Irradiance and an Alternative Technique based on Fast Scanning. IEEE. 40th Photovoltaic Specialist Conference (PVSC), Denver, CO, 2014, pp. 3690-3694, doi: 10.1109/PVSC.2014.6924908.*

[30]   United Nations Office for Outer Space Affairs. (2015). *Space Supporting the Sustainable Development Goals.* United Nations. https://www.unoosa.org/oosa/en/ourwork/space4sdgs/index.html

[31]   Zivkovic, O. (2019, Dec 5). *A new generation of 'hyper' satellites to prevent a climate catastrophe.* DW Made for Minds. https://www.dw.com/en/a-new-generation-of-hyper-satellites-to-prevent-a-climate-catastrophe/a-51535184

[32]   Välimäki, M. (2017, Jul). *Los satélites finlandeses Aalto nos saludan desde el espacio.* This is Finland. https://finland.fi/es/neegocios-amp-innovacion/los-satelites-finlandeses-aalto-nos-saludan-desde-el-espacio/

APPENDIX A. MATLAB SCRIPTS

This appendix includes all the MATLAB scripts used in this Bachelor's thesis.

A.1   SCRIPT USED TO SOLVE SYSTEM OF CHAPTER 4, SECTION 4.2

```matlab
%% Solving for the unknown parameters of the single diode
with Rs circuit

%Defining manufacture data
Isc=1.84; %short circuit current
Voc=21.9; %open circuit voltage
Vmp=17.6; %voltage @MPP
Imp=1.7;  %current @MPP

%Defining thermal voltage
k=1.38065*10^(-23); %Boltzmann constant
q=1.60217*10^(-19); %Electron charge
T=25+273;            %T=25° in Kelvin
Vt=k*T/q;            %thermal voltage of the PV module

%Defining symbolic variables (unknown parameters to be
solved)
syms Ipv Io am Rs

%Defining system of equations
eq1=Ipv-Io*(exp(Voc/(am*Vt))-1)==0;
eq2=Ipv==Isc;
eq3=Ipv-Io*(exp((Vmp+Imp*Rs)/(am*Vt))-1)==Imp;
eq4=Ipv-Io*(exp((Vmp+Imp*Rs)/(Vt*am))-1)-
(Io*Vmp*exp((Vmp+Imp*Rs)/(Vt*am)))/(Vt*am)==0;

%Solving the system
eq=[eq1 eq2 eq3 eq4];
var=[Ipv Io am Rs];
[Ipv Io am Rs]=vpasolve(eq,var);
```

A.2 S*CRIPT USED TO OBTAIN CONTROL TO* PV *VOLTAGE TRANSFER FUNCTION,* C*HAPTER* 5, S*ECTION* 5.2.1.

```
%%
syms I_L R_mp R_L V_Bat R_Cin C_in V_Cin D s d V_pv L IL
%Value of R_mp<0
%R_Cin=0;
%R_L=0;
%% Define steady state equations
%Switch position 1
Eeq=V_Cin*(R_mp/(R_mp+R_Cin)); %thevenin
Req=(R_mp*R_Cin)/(R_mp+R_Cin); %thevenin

eq_V_L_1=-V_Bat+Eeq-I_L*Req-I_L*R_L; %%V_L pos1
eq_I_Cin_1=-(V_Bat+eq_V_L_1+I_L*R_L)/R_mp-I_L; %%I_Cin I_L
pos1

%Switch position 2
eq_V_L_2=-V_Bat-I_L*R_L; %%V_L pos2
eq_I_Cin_2=-V_Cin/(R_mp+R_Cin); %%I_Cin pos2

%% VSB and CB
VSB=simplify(eq_V_L_1*D+eq_V_L_2*(1-D)); %Volt second
Balance ==0
CB=simplify(eq_I_Cin_1*D+eq_I_Cin_2*(1-D)); %Charge Balance
==0

%VSB solve for I_L(V_Cin)
I_L_V_Cin=(isolate(VSB==0,I_L)); %solves for I_L(V_Cin)
%CB solve for V_Cin(I_L)
V_Cin_I_L=(isolate(CB==0,V_Cin)); %solves for V_Cin(I_L)

%% DC value for I_L
%substitute V_Cin_I_L in I_L_V_Cin --> isolate variable I_L
I_L_1=(isolate(I_L==-(R_Cin*V_Bat + R_mp*V_Bat - D*R_mp*-
D*I_L*R_mp)/(R_Cin*R_L + R_L*R_mp + D*R_Cin*R_mp),I_L));

%verify the procedure manually (was obtained by my own
calculations)
I_L_manual=simplify(((-
V_Bat)/(R_L+((D*R_mp*R_Cin)/(R_mp+R_Cin))))/(1+(D^2*R_mp*(R_
mp/(R_mp+R_Cin))/(R_L+(D*R_mp*R_Cin)/(R_mp+R_Cin)))));
```

118

```matlab
%% Small signal model to find transfer function
V_d_Vpv=Vpv/d;
Z_Cin=R_Cin+1/(s*C_in);
Z_mp=R_mp;
Z_L=R_L/D^2+(s*L)/D^2;

%Superposition
%%%%Current Source
Za=(Z_mp*Z_Cin)/(Z_mp+Z_Cin); %Z_mp//Z_Cin
Z_t1=simplify((Za*Z_L)/(Za+Z_L));% (Z_mp//Z_Cin)//Z_L

vpv_currentsource=simplify(-Z_t1*I_L_manual*d);

%%%%Voltage Source
Z_t2=(Za/(Za+Z_L));
vpv_voltagesource=simplify(Z_t2*(-V_pv/D)*d);

vpv_tot=simplify(vpv_currentsource+vpv_voltagesource);

%% Transfer function
vpv_cs=simplify(-Z_t1*I_L_manual); % without d
vpv_vs=simplify(Z_t2*(-V_pv/D)); % without d

vpv_d=simplify(vpv_cs+vpv_vs); %transfer function-->control
to Vpv substituting I_L previously calculated

%%Transfer function w/out simplifying IL
vpv_cs=simplify(-Z_t1*IL); % without d
vpv_vs=simplify(Z_t2*(-V_pv/D)); % without d

vpv_d_IL=simplify(vpv_cs+vpv_vs); %transfer function--
>control to Vpv w/out substituting I_L previously calculated
```

A.3 S*CRIPT USED TO OBTAIN THE FIGURES OF* C*HAPTER* 5,
S*ECTION* 5.2.1.

```matlab
%% Testing settling times for different irradiance levels
G=1000,500,200W/m^2
R_mp1=[-10.35,-20.86,-51.77]; %G=1000,500,200, 17.6/1.7,
17.8/0.8533, 17.73/0.3425
D_1=[0.454545,0.44943,0.45121];
for i=1:3
    R_mp=R_mp1(i);
    L=48.5e-6;
    D=D_1(i);
    V_Bat=8;
    V_pv=17.6;
    R_L=120e-3;
    C_in=215.15e-6;
    R_Cin=20e-3;
    s=tf('s');
    T(i)=-(R_mp*(C_in*R_Cin*s + 1)*(D^3*R_mp^2*V_pv -
R_Cin*R_L*V_Bat - R_L*R_mp*V_Bat + D*R_Cin*R_L*V_pv +
D*R_L*R_mp*V_pv - L*R_Cin*V_Bat*s - L*R_mp*V_Bat*s +
D^2*R_Cin*R_mp*V_pv))/((D^2*R_mp^2 + R_Cin*D*R_mp + R_L*R_mp
+ R_Cin*R_L)*(R_L + L*s + D^2*R_mp + C_in*L*R_Cin*s^2 +
C_in*L*R_mp*s^2 + C_in*R_Cin*R_L*s + C_in*R_L*R_mp*s +
C_in*D^2*R_Cin*R_mp*s));
end
linearSystemAnalyzer(T(1),T(2),T(3));

R_mp=-10.35;
%% Testing effect of different values of R_L on the step
response for G=1000W/m^2
R_L1=[100e-3,110e-3,130e-3,140e-3,170e-3]; %% Value chosen
R_L=120e-3
for i=1:5
    R_L=R_L1(i);
    L=48.5e-6;
    D=0.454545;
    V_Bat=8;
    V_pv=17.6;
    C_in=200e-6;
    R_Cin=10e-3;
    s=tf('s');
```

```matlab
    T(i)=-(R_mp*(C_in*R_Cin*s + 1)*(D^3*R_mp^2*V_pv -
R_Cin*R_L*V_Bat - R_L*R_mp*V_Bat + D*R_Cin*R_L*V_pv +
D*R_L*R_mp*V_pv - L*R_Cin*V_Bat*s - L*R_mp*V_Bat*s +
D^2*R_Cin*R_mp*V_pv))/((D^2*R_mp^2 + R_Cin*D*R_mp + R_L*R_mp
+ R_Cin*R_L)*(R_L + L*s + D^2*R_mp + C_in*L*R_Cin*s^2 +
C_in*L*R_mp*s^2 + C_in*R_Cin*R_L*s + C_in*R_L*R_mp*s +
C_in*D^2*R_Cin*R_mp*s));
end
linearSystemAnalyzer(T(1),T(2),T(3),T(4),T(5));

%% Testing effect of different values of R_Cin on the step
response for G=1000W/m^2
R_Cin1=[5e-3,10e-3,20e-3,30e-3,100e-3]; %% Value chosen
R_Cin=20e-3
for i=1:5
    R_Cin=R_Cin1(i);
    L=48.5e-6;
    D=0.454545;
    V_Bat=8;
    V_pv=17.6;
    R_L=120e-3;
    C_in=200e-6;
    s=tf('s');
    T(i)=-(R_mp*(C_in*R_Cin*s + 1)*(D^3*R_mp^2*V_pv -
R_Cin*R_L*V_Bat - R_L*R_mp*V_Bat + D*R_Cin*R_L*V_pv +
D*R_L*R_mp*V_pv - L*R_Cin*V_Bat*s - L*R_mp*V_Bat*s +
D^2*R_Cin*R_mp*V_pv))/((D^2*R_mp^2 + R_Cin*D*R_mp + R_L*R_mp
+ R_Cin*R_L)*(R_L + L*s + D^2*R_mp + C_in*L*R_Cin*s^2 +
C_in*L*R_mp*s^2 + C_in*R_Cin*R_L*s + C_in*R_L*R_mp*s +
C_in*D^2*R_Cin*R_mp*s));
end
linearSystemAnalyzer(T(1),T(2),T(3),T(4),T(5));

%% Testing effect of different values of Cin on the step
response for G=1000W/m^2
Cin1=[159.16e-6,176.84e-6,187.24e-6,198.94e-6,227.36e-6]; %%
Value chosen R_Cin=20e-3
for i=1:5
    R_Cin=10e-3;
    L=48.5e-6;
    D=0.454545;
    V_Bat=8;
    V_pv=17.6;
    R_L=120e-3;
```

```matlab
    C_in=Cin1(i);
    s=tf('s');
    T(i)=-(R_mp*(C_in*R_Cin*s + 1)*(D^3*R_mp^2*V_pv -
R_Cin*R_L*V_Bat - R_L*R_mp*V_Bat + D*R_Cin*R_L*V_pv +
D*R_L*R_mp*V_pv - L*R_Cin*V_Bat*s - L*R_mp*V_Bat*s +
D^2*R_Cin*R_mp*V_pv))/((D^2*R_mp^2 + R_Cin*D*R_mp + R_L*R_mp
+ R_Cin*R_L)*(R_L + L*s + D^2*R_mp + C_in*L*R_Cin*s^2 +
C_in*L*R_mp*s^2 + C_in*R_Cin*R_L*s + C_in*R_L*R_mp*s +
C_in*D^2*R_Cin*R_mp*s));
end
linearSystemAnalyzer(T(1),T(2),T(3),T(4),T(5));

%% Testing effect of different values of L on the step
response for G=1000W/m^2
L1=[58.34e-6,53.03e-6,48.61e-6,38.89e-6,29.17e-6]; %% Value
chosen R_Cin=20e-3
for i=1:5
    R_Cin=10e-3;
    L=L1(i);
    D=0.454545;
    V_Bat=8;
    V_pv=17.6;
    R_L=120e-3;
    C_in=200e-6;
    s=tf('s');
    T(i)=-(R_mp*(C_in*R_Cin*s + 1)*(D^3*R_mp^2*V_pv -
R_Cin*R_L*V_Bat - R_L*R_mp*V_Bat + D*R_Cin*R_L*V_pv +
D*R_L*R_mp*V_pv - L*R_Cin*V_Bat*s - L*R_mp*V_Bat*s +
D^2*R_Cin*R_mp*V_pv))/((D^2*R_mp^2 + R_Cin*D*R_mp + R_L*R_mp
+ R_Cin*R_L)*(R_L + L*s + D^2*R_mp + C_in*L*R_Cin*s^2 +
C_in*L*R_mp*s^2 + C_in*R_Cin*R_L*s + C_in*R_L*R_mp*s +
C_in*D^2*R_Cin*R_mp*s));
end
linearSystemAnalyzer(T(1),T(2),T(3),T(4),T(5));

%% Final response substituting parameters
    R_mp=-10.35;
    R_L=33.5e-3; %inductance resistance
    L=47e-6; %inductance
%     R_C_1=(13.621e-3)/20;
%     C_1=20*10e-6; %capacitance
    V_pv=17.6;
    R_Cin=(13.621e-3); %esr
    C_in=190e-6+2.2e-6; %capacitance
```

122

```
    D=0.4545;
    V_Bat=8;

    s=tf('s');
    G_v_p_v_d=-(R_mp*(C_in*R_Cin*s + 1)*(D^3*R_mp^2*V_pv -
R_Cin*R_L*V_Bat - R_L*R_mp*V_Bat + D*R_Cin*R_L*V_pv +
D*R_L*R_mp*V_pv - L*R_Cin*V_Bat*s - L*R_mp*V_Bat*s +
D^2*R_Cin*R_mp*V_pv))/((D^2*R_mp^2 + R_Cin*D*R_mp + R_L*R_mp
+ R_Cin*R_L)*(R_L + L*s + D^2*R_mp + C_in*L*R_Cin*s^2 +
C_in*L*R_mp*s^2 + C_in*R_Cin*R_L*s + C_in*R_L*R_mp*s +
C_in*D^2*R_Cin*R_mp*s));
    linearSystemAnalyzer(G_v_p_v_d);
```

A.4 SCRIPT USED TO OBTAIN THE MINIMUM DUTY CYCLE REQUIRED TO TRACK THE MPP UNDER IRRADIANCE RAMP CHANGES

```
%% Determine G^' and perturbation step->run the code and
obtain minimum size step
G_p=500/2; %W/m^2/s 250 ,%G average rate of change of solar
radiation average rate of change of solar radiation
f_loop=300;
T_p=(1/f_loop)*1.5; %period of the MPPT
perturbation=settling time worst case*extra percentage(extra
margin to assure stability)


%% Minimum Perturbation Size Step
%%%%Defining converter and model parameters
    %%%DC gain
        R_mp=-10.35; %G=1000 W/m^2
        D=0.4545;
        V_Bat=8;
        V_pv=17.6;
        L=47e-6;
        R_L=33.5e-3;
        C_in=190e-6+2.2e-6;
        R_Cin=(13.621e-3)/19;
        s=tf('s');
```

```
        Gvp_d=-(R_mp*(C_in*R_Cin*s + 1)*(D^3*R_mp^2*V_pv -
R_Cin*R_L*V_Bat - R_L*R_mp*V_Bat + D*R_Cin*R_L*V_pv +
D*R_L*R_mp*V_pv - L*R_Cin*V_Bat*s - L*R_mp*V_Bat*s +
D^2*R_Cin*R_mp*V_pv))/((D^2*R_mp^2 + R_Cin*D*R_mp + R_L*R_mp
+ R_Cin*R_L)*(R_L + L*s + D^2*R_mp + C_in*L*R_Cin*s^2 +
C_in*L*R_mp*s^2 + C_in*R_Cin*R_L*s + C_in*R_L*R_mp*s +
C_in*D^2*R_Cin*R_mp*s)); %transfer function od equation x.
        Go=dcgain(Gvp_d); %DC gain of Gvp

%%% Defying H
    %%Defying PV model parameters
        Io=2.0527e-11; %diode saturation current
        a=0.94005;     %ideality factor
        R_s=1.0051;    %series resistance
        Ns=36;         %cells per module
        V_mp=17.6;     %PV voltage at MPP
        I_mp=1.7;      %PV current at MPP
        k=1.38065*10^(-23); %Boltzmann constant
        q=1.60217*10^(-19); %Electron charge
        T=25+273;          %T=25° in Kelvin
        V_t=k*T/q;         %thermal voltage of the PV
module
     %%H
        H=(1/2)*(1/(a*Ns*V_t))*(1-
R_s/R_mp)^3*((Io/(a*Ns*V_t))*exp((V_mp+R_s*I_mp)/(a*Ns*V_t))
);

%%% Defying material constant K_ph
    syms G
    alfa_I=0.05;      %Temperature coefficient of Isc
    G_stc=1000;       %Nominal irradiance level
    T_stc=25;         %Nominal temperature level
    T=25;             %Actual operating temperature
    Iph_stc=1.8452;   %PV current at MPP approximated to PV
short circuit current
    Iph=Iph_stc*(G/G_stc)*(1+alfa_I*(T-T_stc)); %Equation
that defines the PV current based on changing atmospheric
conditions
% K_ph calculation
    K_ph_syms=diff(Iph,G);
    K_ph=double(K_ph_syms);


%Minimum perturbation size step required
```

```
d_min=double(vpa(abs((1/Go))*sqrt((V_mp*K_ph*G_p*T_p)/(H*V_m
p+1/R_mp))),6));

display(d_min);
```

A.5 SCRIPT USED TO DETERMINE THE VOLTAGE PROTECTION GAIN OF THE BATTERY CHARGE CONTROL

```
s=tf('s');

%Select the sampling frequency based on the MPPT
perturbation frequency
%Run the script
%Choose value of Ki based on system's bandwidth
%Values already shown in Excel tables for
fs=[100,200,300,400,500]Hz

%%% PLANT MODEL
  %%%BUCK CONVERTER PARAMETERS
    R_Cout=(13.621e-3)/20;
    C_out=200e-6;
    R_L=33.5e-3;
    L=47e-6;
    V_PV=19.85;
    R_Load_total=(8/(4*5+3.3*5));

  %%% CONTROL TO OUTPUT VOLTAGE TF
    Gvd=V_PV*((C_out*R_Cout*s + 1)/(C_out*L*s^2 +
(C_out*R_Cout + C_out*R_L)*s + 1));

    %%%Bode plot of Gvd
    % h1=bodeplot(Gvd);
    % setoptions(h1,'FreqUnits','Hz');
    % grid on;

for i=1:29
    % Define system bandwidth
        fc_bat=[60];
        wc = 2*pi*fc_bat;
```

125

```matlab
    % Sampling ADC frequency
        fsample=300;%Hz
        Tsample=1/fsample; %s
        wsample=2*pi*fsample; %rad/s
        wp = wsample/pi; %rad/s

    % PI zero and high-frequency gain
        w_PI = wc/20;
        GPIinf = [0.002 0.003 0.004 0.005 0.006 0.008 0.01
0.02 0.03 0.04 0.05 0.06 0.07 0.08 0.09 0.15 0.2 0.22 0.25
0.3 0.4 0.5 0.6 0.7 0.8 0.9 1.1 1.2 1.3];

    % Integral Gain
        Ki_bat(i)=2*GPIinf(i)*w_PI/wp; %Ki compensator gain
in Z-domain

    % Defining Battery charge voltage protection control (I)
        Control_I=(Ki_bat(i)/Tsample)*((1+s/wp)/s);

    % Loop gain Bode plots
        figure(i);
        h1=bodeplot(Gvd);
        setoptions(h1,'FreqUnits','Hz');
        hold on;
        h2=bodeplot(Control_I*Gvd);
        setoptions(h2,'FreqUnits','Hz');
        grid on;

     % Phase margin and crossover frequency loop gain bode
plots
        [Gm(i),Pm(i),Wgm(i),Wcross(i)] =
margin(Control_I*Gvd);
        fgm(i)=Wgm(i)/(2*pi); % frequency of Gain margin in
Hz
        fcross(i)=Wcross(i)/(2*pi); %crossover frequency in
Hz
end

Kd_3=zeros(40);
Kp_3=zeros(40);
```

A.6 SCRIPT USED TO DESIGN THE PID 5V LOAD COMPENSATOR PARAMETERS

```matlab
s=tf('s');
%%% PLANT MODEL
    %%%Parameters
        C=120e-6;
        L=47e-6;
        V=5;
        D=5/8; %5/8
        Rload_5=5/4;
    %%%Gvd(control to output transfer function of Buck
converter)
        Qo=Rload_5*sqrt(C/L);
        wo=1/sqrt(L*C);
        Gdo=(V/D);
        Gvd=Gdo/(1+s/(Qo*wo)+(s/wo)^2);

for i=1:21
    % Specify crossover frequency (fc) and phase margin (pm)
        fc_5=10000; %Hz
        wc = 2*pi*fc_5; %rad/s
        phase_margin_design=[45 46 47 48 49 50 51 52 53 54
55 56 57 58 59 60 61 62 63 64 65];
        phase_margin(i) = (pi/180)*phase_margin_design(i);%
In radians
    % Sampling ADC frequency
        fsample=100e3; %fsw=f_sample (Hz)
        Tsample=1/fsample; %(seconds)
        wsample=2*pi*fsample; %rad/s

    % Design of PID control (p-domain)
        % Magnitude and phase of Gvd at specify crossover
frequency
            [mag_Gvd,phase_Gvd] = bode(Gvd,wc);
            phase_wc = (pi/180)*phase_Gvd; %phase at wc in
radians

        % Prewarping wc
            wc_prime = (2/Tsample)*tan(wc*Tsample/2);
%wc~wc_prime
```

```matlab
        [mag_prew,phase_prew] = bode(Gvd,wc_prime); %mag
and pha at wc_prime

        % PD Compensator Design
            wp = wsample/pi;
            w_PD = (1/(tan(-pi+phase_margin(i)-
phase_wc+atan(wc_prime/wp))))*wc_prime;
            GPD_0 =
sqrt(1+(wc_prime/wp)^2)/(mag_Gvd*(sqrt(1+(wc_prime/w_PD)^2))
);
        % PI Design part
            w_PI = wc/30;
            GPI_inf = 1;
        % P,I and D Gains
            Kp_5(i) = GPI_inf*GPD_0*(1+w_PI/w_PD-2*w_PI/wp);
            Ki_5(i) = 2*GPI_inf*GPD_0*w_PI/wp;
            Kd_5(i) = GPI_inf*GPD_0/2*(1-w_PI/wp)*(wp/w_PD-
1);
        % Defining Control based on PID gains obtained

PID_compensator(i)=Kp_5(i)+(Ki_5(i)/Tsample)*((1+s/wp)/s)+Kd
_5(i)*Tsample*(s/(1+s/wp));

PD_compensator(i)=Kp_5(i)+Kd_5(i)*Tsample*(s/(1+s/wp));
        % Bode Plots to verify open loop gain stability
%           figure(i);
% %             h1=bodeplot(Gvd); %% Gvd Plant
% %             setoptions(h1,'FreqUnits','Hz');
% %             hold on;
% %             h2=bodeplot(Control*Gvd); %% Open loop gain
% %             setoptions(h2,'FreqUnits','Hz');
% %             grid on;
        [Gm(i),Pm(i),Wgm(i),Wcross(i)] =
margin(PID_compensator(i)*Gvd);
        fgm(i)=Wgm(i)/(2*pi);
        fcross(i)=Wcross(i)/(2*pi);

        % LinearSystemAnlayzer
%           open_loop=Control*Gvd;
%           linearSystemAnalyzer(open_loop);

end
```

A.7 Script used to design the *PID* 3.3V Load compensator parameters

```matlab
s=tf('s');
%%% PLANT MODEL
    %%%Parameters
        C=120e-6;
        L=47e-6;
        V=3.3;
        D=3.3/8; %5/8
        Rload_5=3.3/5;
    %%%Gvd(control to output transfer function of Buck
converter)
        Qo=Rload_5*sqrt(C/L);
        wo=1/sqrt(L*C);
        Gdo=(V/D);
        Gvd=Gdo/(1+s/(Qo*wo)+(s/wo)^2);

for i=1:21
    % Specify crossover frequency (fc) and phase margin (pm)
        fc_3=10000; %Hz
        wc = 2*pi*fc_3; %rad/s
        phase_margin_design=[45 46 47 48 49 50 51 52 53 54
55 56 57 58 59 60 61 62 63 64 65];
        phase_margin(i) = (pi/180)*phase_margin_design(i);%
In radians
    % Sampling ADC frequency
        fsample=100e3; %fsw=f_sample (Hz)
        Tsample=1/fsample; %(seconds)
        wsample=2*pi*fsample; %rad/s

    % Design of PID control (p-domain)
        % Magnitude and phase of Gvd at specify crossover
frequency
            [mag_Gvd,phase_Gvd] = bode(Gvd,wc);
            phase_wc = (pi/180)*phase_Gvd; %phase at wc in
radians

        % Prewarping wc
            wc_prime = (2/Tsample)*tan(wc*Tsample/2);
%wc~wc_prime
```

```matlab
        [mag_prew,phase_prew] = bode(Gvd,wc_prime); %mag
and pha at wc_prime

        % PD Compensator Design
            wp = wsample/pi;
            w_PD = (1/(tan(-pi+phase_margin(i)-
phase_wc+atan(wc_prime/wp))))*wc_prime;
            GPD_0 =
sqrt(1+(wc_prime/wp)^2)/(mag_Gvd*(sqrt(1+(wc_prime/w_PD)^2))
);
        % PI Design part
            w_PI = wc/30;
            GPI_inf = 1;
        % P,I and D Gains
            Kp_3(i) = GPI_inf*GPD_0*(1+w_PI/w_PD-2*w_PI/wp);
            Ki_3(i) = 2*GPI_inf*GPD_0*w_PI/wp;
            Kd_3(i) = GPI_inf*GPD_0/2*(1-w_PI/wp)*(wp/w_PD-
1);
        % Defining Control based on PID gains obtained

PID_compensator(i)=Kp_3(i)+(Ki_3(i)/Tsample)*((1+s/wp)/s)+Kd
_3(i)*Tsample*(s/(1+s/wp));

PD_compensator(i)=Kp_3(i)+Kd_3(i)*Tsample*(s/(1+s/wp));
        % Bode Plots to verify open loop gain stability
%           figure(i);
% %             h1=bodeplot(Gvd); %% Gvd Plant
% %             setoptions(h1,'FreqUnits','Hz');
% %             hold on;
% %             h2=bodeplot(Control*Gvd); %% Open loop gain
% %             setoptions(h2,'FreqUnits','Hz');
% %             grid on;
        [Gm(i),Pm(i),Wgm(i),Wcross(i)] =
margin(PID_compensator(i)*Gvd);
        fgm(i)=Wgm(i)/(2*pi);
        fcross(i)=Wcross(i)/(2*pi);

end
```

A.8   Script where the MATLAB model values are defined

```matlab
%%%MATLAB script of the power supply full model
%Define Irradiance Step Change
outv1=[1000 1000  0      0      ];
outt1=[0     2.5   4      5.5    ];
outv2=[1000 1000  0      0      ];
outt2=[0     2.5   4      5.5    ];
k_5=17;
k_3=16;
k=12;
%Power Supply Inputs
    %PV module 1
        Ir_1=1000; %Irradiance
        T_1=25; %Temperature
    %PV module 2
        Ir_2=1000; %Irradiance
        T_2=25; %Temperature

% PV link
    %PV link 1
        R_Cin_1=(13.621e-3)/19; %esr
        Cin_1=190e-6+2.2e-6; %capacitance
    %PV link 2
        R_Cin_2=(13.621e-3)/19+10e-3; %esr
        Cin_2=190e-6+2.2e-6; %capacitance

%PVSC: Buck Converter
    %Buck converter 1
        %Low pass filter 1
        R_L_1=33.5e-3; %inductance resistance
        L_1=47e-6; %inductance
        R_C_1=(13.621e-3)/20;
        C_1=100e-6; %capacitance
        %PWM_1
        fsw_1=100e3;

    %Buck converter 2
        %Low pass filter 2
        R_L_2=33.5e-3; %inductance resistance
```

```matlab
        L_2=47e-6; %inductance
        R_C_2=(13.621e-3)/20;
        C_2=100e-6; %capacitance
        %PWM_2
        fsw_2=100e3;

% Battery parameters
    %https://www.batteryspace.com/prod-specs/ICR18650-
26F.pdf
    Ampere_hr=2.6;
    R_Cell = 0.033;
    R_bat= 0.12;
    V_CellNom = 3.7;
    V_CellMax = 4.2;
    V_bat=8;
    V_batMax = 2*V_CellMax;
    I_cellMax = 2.6;


    %MPPT control
    %P&O and IC
        %%% MCU ADC Sampling frequency
            f_sample_1=200; %Hz
            T_sample_1=1/f_sample_1; %
            f_analog_filter_1=fsw_1/20; % analog filter to
attenuate swithcing noise

        %%% Duty Cycle step
            delta_D_1=d_min*1.1; % incremental duty cycle
          Duty_initial_1=0;% found inside memory block

    % Controler paramters regarding battery charge control
        V_limit = 8.6;
        I_limit = I_cellMax;
        K_Vlim_1 = Ki_bat(k); % Run script:design CCCV
control coeficcients
        K_Ilim_1 = 0; %assuming no current protection


%MPPT control
    %P&O and IC
        %%% MCU ADC Sampling frequency
            f_sample_2=200; %Hz
            T_sample_2=1/f_sample_2; %
```

```matlab
            f_analog_filter_2=fsw_2/20; % analog filter to
attenuate swithcing noise

        %%% Duty Cycle step
            delta_D_2=d_min*1.1; % incremental duty cycle
            Duty_initial_2=0;% found inside memory block

    % Controler paramters regarding battery charge control
        V_limit = V_CellMax*0.99;
        I_limit = I_cellMax;
        K_Vlim_2 = Ki_bat(k); % Run script:design CCCV
control coeficcients
        K_Ilim_2 = 0; %assuming no current protection

%OUTPUT Converter: Buck Converter
    %Buck converter 3
        %Low pass filter 3
        R_L_3=19.2e-3; %inductance resistance
        L_3=47e-6; %inductance
        R_C_3=(13.621e-3)/12;
        C_3=120e-6; %capacitance
        %PWM_1
        fsw_3=100e3;

%OUTPUT BUCK CONTROL 5
    %Micro-controler ADC sampling, should not see resonance
        %fc1=fc_5(3);
        f_sample_after_5=100e3;%fc1*10;
        fcontrol_loop_5=f_sample_after_5;
    %PID control parameters
        Vref_5=5; %reference load voltage

        Ki_51=Ki_5(k_5);
        Kp_51=Kp_5(k_5);
        Kd_51=Kd_5(k_5);

%Rload
    R_load5=5/4;

%OUTPUT Converter: Buck Converter 3
    %Buck converter 4
        %Low pass filter 4
        R_L_4=19.2e-3; %inductance resistance
        L_4=47e-6; %inductance
```

133

```
        R_C_4=(13.621e-3)/12;
        C_4=120e-6; %capacitance
        %PWM_1
        fsw_4=100e3;

%OUTPUT BUCK CONTROL
    %Micro-controler ADC sampling, should not see resonance
        f_sample_33=100e3;
        fcontrol_loop_3=f_sample_33;
    %PID control parameters
        Vref_3=3.3; %reference load voltage

        Ki_33=Ki_3(k_3);
        Kp_33=Kp_3(k_3);
        Kd_33=Kd_3(k_3);

%Rload
    %3
    R_load33=3.3/5;
```

A.9 MPPT CONTROL (INCCOND) INTEGRATED WITH BATTERY CHARGE CONTROL

```
function [D,state_1,BATcontrol_state_1, MPPT_state_1]   =
fcn(V, V_old, I, I_old, V_batt, I_batt,delta_D_1,V_batMax,
I_cellMax, V_limit, I_limit,K_Ilim_1, K_Vlim_1,D_old)
    if I_batt >= I_limit   %Current Protection
        D = D_old - K_Ilim_1*(I_batt - I_cellMax);
        BATcontrol_state_1=-2;
        state_1=2;
        MPPT_state_1=0;

    elseif V_batt >= V_limit   %Voltage Protection
        D = D_old - K_Vlim_1*(V_batt - V_batMax);
        BATcontrol_state_1=-3;
        state_1=2;
        MPPT_state_1=0;
    else   %MPPT IC
        BATcontrol_state_1=-2.5;
```

```matlab
        state_1=3;
        Delta_I=I-I_old;
        Delta_V=V-V_old;
            if (Delta_V<0)||(Delta_V>0) %dV non zero
                if (Delta_I/Delta_V>-I/V)
                    MPPT_state_1=-1;
                    D=D_old-delta_D_1;
                elseif (Delta_I/Delta_V<-I/V)
                    MPPT_state_1=1;
                    D=D_old+delta_D_1;
                else
                    MPPT_state_1=0;
                    D=D_old;
                end
            elseif (Delta_I<0)||(Delta_I>0) %dI non zero
                if (Delta_I>0)
                    MPPT_state_1=-1;
                    D=D_old-delta_D_1;
                elseif (Delta_I<0)
                    MPPT_state_1=1;
                    D=D_old+delta_D_1;
                else
                    MPPT_state_1=0;
                    D=D_old;
                end
            else
                MPPT_state_1=0;
                D=D_old; %dV=0 & dI=0
            end
    end
end
```

A.10 MPPT CONTROL (P&O) INTEGRATED WITH BATTERY CHARGE CONTROL

```matlab
function [D,state_1,BATcontrol_state_1, MPPT_state_1]  =
fcn(V, V_old,P,P_old,V_batt, I_batt,delta_D_1,V_batMax,
I_cellMax, V_limit, I_limit,K_Ilim_1, K_Vlim_1, D_old)
```

```matlab
if I_batt >= I_limit    %Current Protection
    D = D_old - K_Ilim_1*(I_batt - I_cellMax);
    BATcontrol_state_1=-2;
    state_1=2;
    MPPT_state_1=0;
if (V_batt >= V_limit)    %Voltage Protection
    D = D_old - K_Vlim_1*(V_batt - V_batMax);
    BATcontrol_state_1=-3;
    state_1=2;
    MPPT_state_1=0;
else   %MPPT
    BATcontrol_state_1=-2.5;
    state_1=3;
    Delta_P = P - P_old;
    Delta_V = V - V_old;

    if (Delta_V*Delta_P) <= 0
        MPPT_state_1=1;
        D = D_old + delta_D_1; %increase D by fixed step
    else
        MPPT_state_1=-1;
        D = D_old - delta_D_1; %decrease D by fixed step
    end
end
```

APPENDIX B. SUSTAINABLE DEVELOPMENT GOALS

This project is aligned with the development of space tools that are helping the world to improve in the areas of telecommunication, global navigation and earth observation.

Space knowledge is critical for the world´s improvement and it fits within the sustainable development goals. Its research and application is a key objective to transform our world, in fact The United Nations is supporting the Sustainable Development Goals through the European Global Navigation Satellite Systems Agency [30].

From the 17 Sustainable Development goals, two can be outlined within the nanosatellites industry: "Climate Action" and "Industry, Innovation & Infrastructure". Climate change is constantly being evaluated by satellites. These permit a global perspective and evaluation in order to carry out optimal decisions to benefit our climate. Satellites also allow us to track several phenomena like for example the atmospheric gases, the glaciers actual situacion, floodings and much more [31] [32]. In regards to the "Industry, Innovation & Infrastructure" goal, satellites provide many different uses that contribute and optimize many different aspects such as the construction of buildings and city infrastructure, automating building activities by controlling equipment through 3D design information, speed incrementation in relation to non-automated machines, tarmac consumption reduction and topographic surveys of construction sites and infrastructure monitoring [30].